SECURITY CLASSIFICATION

REPOR

AD-A245 372

READ INSTRUCTIONS BEFORE COMPLETING FORM

1. REPORT NUMBER
GRL/9101

3. RECIPIENT'S CATALOG NUMBER

4. TITLE (and Subtitle)
PROOF OF THE FEASIBILITY OF COHERENT AND INCOHERENT SCHEMES FOR PUMPING A GAMMA-RAY LASER

5. TYPE OF REPORT & PERIOD COVERED
Annual Letter Report
12/24/90 - 12/23/91

6. PERFORMING ORG. REPORT NUMBER

7. AUTHOR(s)
C. B. Collins

8. CONTRACT OR GRANT NUMBER(s)
N00014-90-K-2001

9. PERFORMING ORGANIZATION NAME AND ADDRESS
University of Texas at Dallas
Center for Quantum Electronics
P.O. Box 830688
Richardson, TX 75083-0688

10. PROGRAM ELEMENT, PROJECT, TASK AREA & WORK UNIT NUMBERS

11. CONTROLLING OFFICE NAME AND ADDRESS
INNOVATIVE SCIENCE AND TECHNOLOGY DIRECTORATE
OF STRATEGIC DEFENSE INITIATIVE ORGANIZATION

12. REPORT DATE
12/31/91

13. NUMBER OF PAGES
103

14. MONITORING AGENCY NAME & ADDRESS(if different from Controlling Office)
Dr. Paul Kepple
Naval Research Laboratory
4555 Overlook Ave., S.W.
Washington, D.C. 20375-5000
Attn: Code 4720

15. SECURITY CLASS. (of this report)
Unclassified

15a. DECLASSIFICATION/DOWNGRADING SCHEDULE

16. DISTRIBUTION STATEMENT (of this Report)

This document has been approved for public release and sale; its distribution is unlimited.

17. DISTRIBUTION STATEMENT (of the abstract entered in Block 20, if different from Report)

DTIC ELECTE JAN 31 1992 S D

18. SUPPLEMENTARY NOTES

19. KEY WORDS (Continue on reverse side if necessary and identify by block number)

Gamma-ray laser, Ultrashort wavelength laser

20. ABSTRACT (Continue on reverse side if necessary and identify by block number)

The most productive approaches to the problem of the gamma-ray laser have focused upon upconversion techniques in which metastable nuclei are pumped with long wavelength radiation. At the nuclear level the storage of energy can approach tera-Joules (10^{12}J) per liter for thousands of years. However, any plan to use such a resource for a gamma-ray laser poses problems of a broad interdisciplinary nature requiring the fusion of concepts taken from relatively unrelated fields of physics. Our research group has described

(continued on next page)

DD FORM 1 JAN 73 1473 EDITION OF 1 NOV 65 IS OBSOLETE
S/N 0102-LF-014-6601

SECURITY CLASSIFICATION OF THIS PAGE (When Data Entered)

20. Abstract (continued)

several means through which this energy might be coupled to radiation fields with cross sections for stimulated emission that could reach 10^{-17} cm^2. Such a stimulated release could lead to output powers as great as 3 x 10^{21} Watts/liter. Since 1978 we have pursued an approach for the upconversion of longer wavelength radiation incident upon isomeric nuclear populations that can avoid many of the difficulties encountered with traditional concepts of single photon pumping. Experiments have confirmed the general theory and have indicated that a gamma-ray laser is feasible if the right combination of energy levels and branching ratios exists in some real material. Of the 1,886 distinguishable nuclear materials, the present state-of-the-art has been adequate to identify 29 first-class candidates, but further evaluation cannot proceed without remeasurements of nuclear properties with higher precision. A laser-grade database of nuclear properties does not yet exist, but the techniques for constructing one have been developed and utilized under this contract. Resolution of the question of the feasibility of a gamma-ray laser now rests upon the determination of: 1) the identity of the best candidate, 2) the threshold level of laser output, and 3) the upconversion driver for that material.

This annual report focuses upon our approach that is the nuclear analog to the ruby laser. It embodies the simplest concepts for a gamma-ray laser and not surprisingly, the greatest rate of achievement in the quest for a subAngstrom laser was realized in that direction. For ruby the identification and exploitation of a bandwidth funnel were the critical keys in the development of the first laser. There was a broad absorption band linked through efficient cascading to the narrow laser level.

In 1987 we reported a major milestone which showed that comparable structure existed at the nuclear scale in the first of the 29 candidate isomers available for testing, $^{180}Ta^m$. Populations of the isomer were successfully pumped down with flashes of x-rays absorbed through an astonishingly large cross section of 40,000 on the usual scale (10^{-29} cm^2 keV) where 10 describes a fully allowed process. This corresponded to a partial width for useful absorption of 0.5 eV, even better than what had been assumed for idealized nuclei. Subsequently, we discovered that the giant pumping resonances occurred with a gratifying frequency throughout the table of nuclides, reaching optimal size and strength in the mass region where the better candidates lie. Nineteen isomers were successfully pumped with the bremsstrahlung from both a 4 MeV linac and a 6 MeV linac. The giant resonances for pumping the candidate isomers $^{180}Ta^m$ and $^{123}Te^m$ were found to open at gateway energies well below 4 MeV. These candidates have the largest integrated cross sections for pumping with x-rays ever found below 4 MeV in any nuclei. These two poorest of the 29 candidates are the only ones available for testing and they continue to outperform even the most optimistic expectations. The likelihood for the full feasibility of one of the better candidates continues to be raised by the successes enjoyed with the least attractive of the 29 candidates.

During the current reporting period we focused upon three issues. The first concerned the identification of the type of nuclear state responsible for such favorable pumping characteristics. For the test case of ^{115}In our photoexcitation experiments, scattering measurements, and nuclear structure calculations all agreed upon the identity and characteristics of the giant pumping resonance as detailed in the attached reprint. The second emphasis fell upon a study of the systematics of the excitation energies of these resonances in the mass-180 region of nuclei, where lie the better candidates for a gamma-ray laser. As described in the attached preprint excitation energies were found to vary little from 2.5 MeV across this region. Finally, emphasis was focused upon the design and construction of a resonance fluorescence detector for use in the presence of large amounts of scattered pump radiation to support future experiments planned for pumping prelasing levels of fluorescence from the types of nuclear levels suitable for use in an actual device. Results continued to be extremely favorable as described in the following.

CRC Handbook of Laser Science and Technology

Supplement 1: Lasers

Editor

Marvin J. Weber, Ph.D.
Lawrence Livermore National Laboratory
University of California
Livermore, California

CRC Press
Boca Raton Ann Arbor Boston

Library of Congress Cataloging-in-Publication Data

Lasers/editors, Marvin J. Weber.
p cm — (CRC handbook of laser science and technology
Supplement ; 1)
Includes bibliographical references and index.
ISBN 0-8493-3506-X
1. Lasers I. Weber, Marvin J., 1932- II. Series.
TA1675.L378 1991
621.36'6—dc20

90-2333
CIP

Direct all inquiries to CRC Press, Inc., 2000 Corporate Blvd., N.W., Boca Raton, Florida, 33431

International Standard Book Number 0-8493-3506-X

Library of Congress Card Number 90-2333
Printed in the United States

HANDBOOK OF LASER SCIENCE AND TECHNOLOGY

VOLUME I: LASERS AND MASERS

VOLUME II: GAS LASERS

VOLUME III: OPTICAL MATERIALS
PART 1: NONLINEAR OPTICAL PROPERTIES/RADIATION DAMAGE

SECTION 1: NONLINEAR OPTICAL PROPERTIES

1.1 Nonlinear and Harmonic Generation Materials — Shohba Singh
1.2 Two-Photon Absorption — Walter L. Smith
1.3 Nonlinear Refractive Index — Walter L. Smith
1.4 Stimulated Raman Scattering — Fred Milanovich

SECTION 2: RADIATION DAMAGE

2.1 Introduction — Richard T. Williams and E. Joseph Friebele
2.2 Crystals — Richard T. Williams
2.3 Glasses — E. Joseph Friebele

VOLUME IV: OPTICAL MATERIALS
PART 2: PROPERTIES

SECTION 1: FUNDAMENTAL PROPERTIES

1.1 Transmitting Materials
  1.1.1 Crystals — Perry A. Miles, Marilyn J. Dodge, Stanley S. Ballard, James S. Browder, Albert Feldman, and Marvin J. Weber
  1.1.2 Glasses — James W. Fleming
  1.1.3 Plastics — Monis Manning
1.2 Filter Materials — Lee M. Cook and Stanley E. Stokowski
1.3 Mirror and Reflector Materials — David W. Lynch
1.4 Polarizer Materials — Jean M. Bennett and Ann T. Glassman

SECTION 2: SPECIAL PROPERTIES

2.1 Linear Electro-Optic Materials — Ivan P. Kaminow
2.2 Magneto-Optic Materials — Di Chen
2.3 Elasto-Optic Materials — Milton Gottlieb
2.4 Photorefractive Materials — Peter Günter
2.5 Liquid Crystals — Stephen D. Jacobs

VOLUME V: OPTICAL MATERIALS
PART 3: APPLICATIONS, COATINGS, AND FABRICATION

SECTION 1: APPLICATIONS

1.1 Optical Waveguide Materials — Peter L. Bocko and John R. Gannon
1.2 Materials for HIgh Density Optical Data Storage — Alan E. Bell
1.3 Holographic Parameters and Recording Materials — K. S. Pennington
1.4 Phase Conjugation Materials — Robert A. Fisher
1.5 Laser Crystals — L. G. DeShazer, S. C. Rand, and B. A. Wechsler
1.6 Laser Glasses — Charles F. Rapp
1.7 Infrared Quantum Counter Materials — Leon Esterowitz

SECTION 2: THIN FILMS AND COATINGS

2.1 Multilayer Dielectric Coatings — Verne R. Costich
2.2 Graded-Index Surfaces and Films — W. Howard Lowdermilk

SECTION 3: OPTICAL MATERIALS FABRICATION

3.1 Fabrications Techniques — G. M. Sanger and S. D. Fantone
3.2 Fabrication Prodedures for Specific Materials — G. M. Sanger and S. D. Fantone

HANDBOOK OF LASER SCIENCE AND TECHNOLOGY

SUPPLEMENT 1: LASERS

TABLE OF CONTENTS

Chapter 4.5

GAMMA-RAY LASERS

Carl B. Collins

UPCONVERSION IN THE NUCLEUS

At the nuclear level, the storage of excitation energies in the Mössbauer range of 1 to 1000 keV can approach tera-Joules (10^{12} J) per liter for thousands of years. If successfully coupled to the radiation field the stimulated release of such nuclear energies would occur at the rate at which resonant electromagnetic radiation passed through the laser medium and could lead to output powers as great as 3×10^{21} W/l. This is an astronomical level of intensity and has not been approached to within orders of magnitude on earth by any means previously. The peak power from a one liter device would represent about 0.03% of the total power output from the sun.

Unfortunately, the quest for a gamma-ray laser has been one of the longest unfruitful efforts in the field of laser science. Virtually all of the sustained pioneering work was done by relatively few groups in the U.S. and in the U.S.S.R. and focused upon the single photon, brute force approach to pumping. That work dealt extensively with concepts involving the use of a neutron flux for pumping the laser medium, either in situ in real-time or as a preparatory step to be followed by a rapid separation of isotopes within their natural lifetimes. All proposals were concluded to require infeasibly high levels of particle fluxes to pump the inversions, exceeding even those available from nuclear explosions, and to require neutron moderators having virtually infinite thermal capacities. By 1980, all conceivable variants of the single photon approach had been characterized as hopeless. In 1981 this traditional approach to a gamma-ray laser was virtually abandoned with the publication of Baldwin's splendid review of all classical efforts.[1]

A renaissance in feasibility studies was launched with the modernization of concepts for the upconversion in the nucleus of lower energy input radiation. In the early 1980s, processes such as the stimulated anti-Stokes scattering of intense but conventional laser radiation were introduced.[2] The theoretical implications of this renaissance were reviewed[3] in 1982. If strengthened by recent infusions of nuclear phase modulation theory,[4] that article still provides the most convenient review of the basic concepts and requirements for a viable gamma-ray laser scheme. By involving two distinct steps, the upconversion techniques for pumping a gamma-ray laser avoid the severe relationships between storage times and spontaneous powers wasted at threshold that were imposed on the single-step processes.[1] Replacement power that is required falls within a technically accessible range avoiding damage to the laser medium.

These two-step, upconversion processes can be divided further into two basic categories that correspond to the type of pumping employed: coherent and incoherent, as shown in Figure 4.5.1. The critical concept here is that both transfer the stored population to a state at the head of a cascade leading to the upper laser level. To be effective the pumping processes cannot transfer too many quanta of angular momenta from the fields, and the cascade provides a mechanism for further changes that may be necessary to reach the laser levels. Then the ultimate viability of these pump schemes will depend upon:

1. Spectroscopic studies locating a suitable configuration of nuclear energy levels, and
2. "kinetic" studies providing an efficient path of cascading from the intermediate or dressed state to the upper laser level.

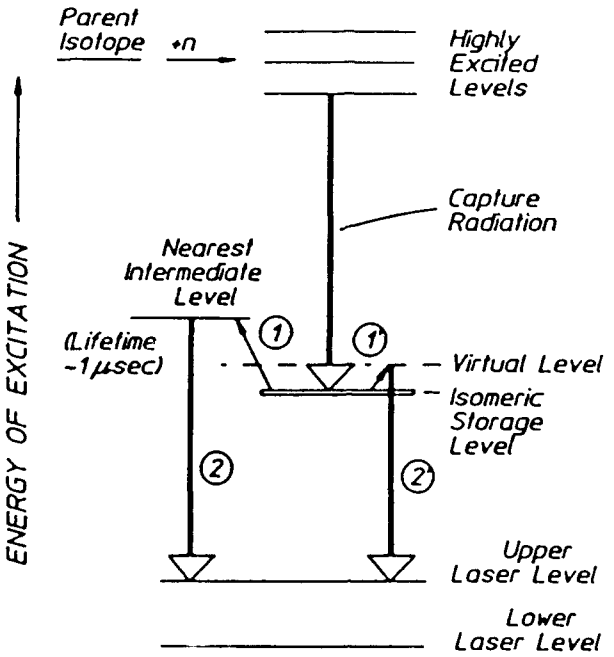

FIGURE 4.5.1 Schematic diagram showing the energetically excited levels of a typical nucleus of interest to the development of a gamma-ray laser. Life-times of the stored energies in the isomeric level produced by the initial capture can range from days to hundreds of years. The first phase of the two-step process for the stimulated release of the stored energy is shown in the figure by the solid arrows. Both subsequent alternatives correspond to the use of longer wave-length radiation to lift a nucleus from the storage level to a higher level of excitation that has a much shorter lifetime. The arrow marked (1) illustrates the incoherent pumping of the storage level through the absorption of an x-ray that is resonant with the energy separation between the storage level and the next higher level of proper symmetry. The arrow marked (1') represents the alternative process of coherent pumping through the nonresonant absorption of a photon from the radiation field in order to create a virtual or dressed state of excitation shown by the dashed level in the figure. In either case the gamma-ray output ultimately results from the upper laser level populated by a cascade occurring as a second step, as shown in the figure by either of the double arrows, (2) and (2').

Because of the interdisciplinary nature of the problem, even for an idealized nuclear material, computations of threshold levels of pumping are not without difficulty. However, under idealized conditions, the part of the pump energy which must be supplied in situ would not be large enough to represent a major impediment to the realization of a gamma-ray laser.[3] The real difficulties take peculiar forms. The use of coherent upconversion would require the location of nearly degenerate levels which could not be resolved by conventional techniques of nuclear spectroscopy. The use of incoherent pumping with X-rays would require a level of knowledge about branching ratios and transition probabilities beyond that available from current methodology. Despite the many applications of beautiful and involved techniques of nuclear spectroscopy, the current data base is inadequate in both coverage and resolution either to answer the question of whether an acceptable isotope exists or to guide in the selection of a possible candidate medium for a gamma-ray laser. In fact, the paucity of laser-grade data describing nuclear properties is so severe that one cannot say which real isotope represents the best approximation to the ideal.

For lifetimes ranging from seconds to infinity there are 1886 real nuclei to consider as candidates for a gamma-ray laser. Computer based searches of the existing data base have served to identify 29 first class candidates. Of these, 10 are known to have the necessary

(but not necessarily sufficient) arrangement of levels in which there is an isomeric storage level and at lower energies: (1) an upper laser level with lifetime between 1 nsec and 10 μs, and (2) a lower laser level of even less energy. Unfortunately, all ten are exotics having no other utility and, hence, there is no supply of samples for experimentation.

CRITICAL EXPERIMENTS

Incoherent Pumping of Nuclei

Levels of nuclear excitation which might be efficiently stimulated in a gamma-ray laser are very difficult to pump directly. To have lifetimes long enough to integrate the rates of inversion of population that can be pumped at reasonably accessible levels of input power, such levels must have very narrow widths for interaction with the radiation field. This is a fundamental attribute that has led to the general concern that absorption widths in nuclei are too narrow to permit effective pumping with X-rays. Precisely the same concerns were voiced in atomic physics before Maiman's great discovery and it is useful to pursue this analogy between ruby and gamma-ray lasers.

The nuclear analog of the ruby laser embodies the simplest concepts for a gamma-ray laser. Not surprisingly, the greatest rate of achievement in the quest for a sub-Angstrom laser has developed in that direction. For ruby the identification and exploitation of a bandwidth funnel were the critical keys in the development of the first laser. There was a broad absorption band linked through efficient cascading to the narrow laser level. Nuclei to be used in the analog of the ruby laser can start in either ground or isomeric states. However, with the latter, most of the output power can be derived from the energy stored in the isomeric state at its creation.

Whether or not the initial state being pumped is isomeric, the principal figure of merit for bandwidth funneling is the partial width for the transfer, $b_a b_o \Gamma$. The Γ is the total width of the intermediate level shown to the left of Figure 4.5.1 and the branching ratios b_a and b_o specify the probabilities that a population pumped by absorption into the broad level will decay back into the initial or fluorescent levels, respectively. It is not often that the sum of branching ratios is unity, as channels of decay to other levels are likely. However, the maximum value of partial width for a particular level occurs when $b_a = b_o = 0.5$.

The actual measurement of partial width involves the correlation of fluorescence yields excited by a pulse of continuous X-rays with those expected from the expression[5,6]

$$N_f = N_o \sum_i \xi_i \frac{\varphi_i}{A} \tag{1}$$

where No_o and N_f are the numbers of initial and fluorescent nuclei, respectively, (φ_i/A) is the spectral intensity of the bremsstrahlung in keV/keV/cm^2 at the energy E_i of the i-th pump band, and the summation is taken over all of the possible pump bands capable of cascading to the same fluorescence level of interest. The ξ_i is a combination of nuclear parameters including the partial width $b_a b_o \Gamma$ in keV,

$$\xi_i = \frac{(\pi b_a b_o \Gamma \sigma/2)_i}{E_i} \tag{2}$$

where σ is the peak of the Breit-Wigner cross section for the absorption step. The combination of parameters in the numerator of Equation 2 is termed the integrated cross section for the transfer of population in the incoherent scheme of pumping.

Of the many potential systems for a test of the formulations of Equations 1 and 2, the literature[7] supports the calculation of integrated cross sections for very few. Table 4.5.1

Table 4.5.1
SUMMARY OF NUCLIDES, ABSORPTION LINES, AND INTEGRATED CROSS SECTIONS $\pi b_a b_o \Gamma\sigma/2$ FOR THE EXCITATION OF DELAYED FLUORESCENCE SUITABLE FOR USE AS CALIBRATION STANDARDS OF X-RAY PUMP SOURCES

	Pump line (keV)	Cross section (10^{-29} cm²keV)
^{79}Br	761	6 2
^{77}Se	250	0 20
	480	0 87
	818	0 7
	1005	30 0
^{115}In	1078	18 7

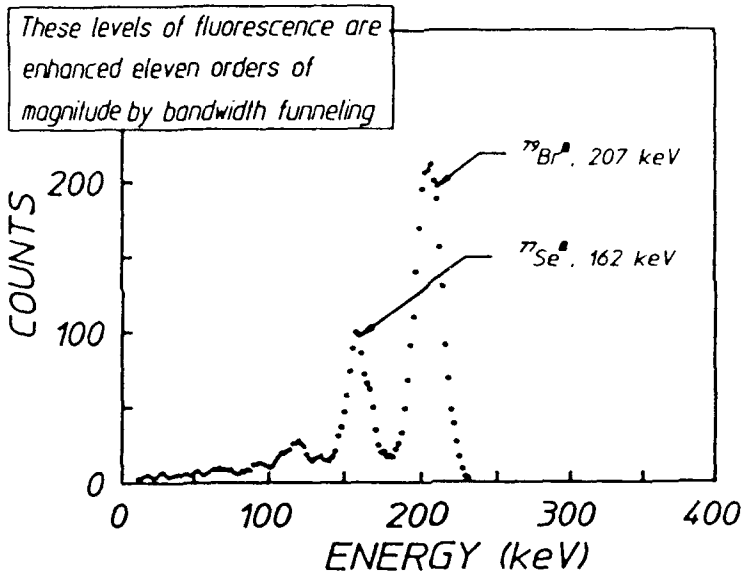

FIGURE 4 5 2 Fluorescence spectrum from a target containing 1.25 g LiBr and 1.20 g of elemental Se, both in natural abundances, excited with a single irradiation by the bremsstrahlung produced by the DNA/PITHON electron beam device Acquisition time of this data was 80 s Prominent lines are contributed by the isomeric transitions indicated

summarized those which are known with sufficient accuracy to serve as standards In the convenient units of 10^{-29} cm² keV, values range from the order of unity to a few tens for bandwidth funnels that are sufficient for demonstrations of nuclear fluorescence from reasonable amounts of material at readily accessible levels of input.

In a recently reported[5,6,8] series of experiments it was shown that bandwidth funneling works as well at the nuclear level as it had at the molecular level. In order to validate the optical pumping model of Equations 1 and 2, samples of the standard nuclei of Table 4.5.1 were pumped with intense pulses of bremsstrahlung from the DNA nuclear simulator, PITHON. The clear signal-to-noise ratios that typified subsequent measurements of nuclear fluorescence exited through the pump bands of Table 4.5.1 are shown in Figure 4.5.2 The quality of such data enabled us to "invert" Equations 1 and 2 so that the spectral intensities of the pump could be obtained at three energies from the measured values of fluorescence

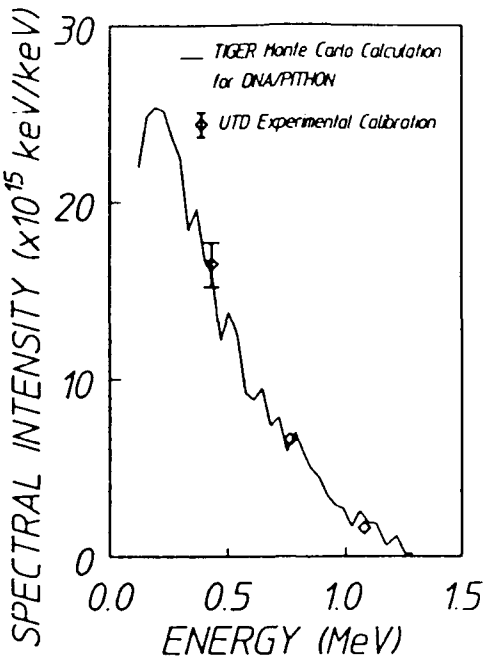

FIGURE 4.5.3 Data points plot the spectral intensities measured directly with nuclear activation techniques using the parameters of Table 4.4.1 in comparison to the spectrum computed with a coupled electron, photon transport code for a typical PITHON shot. Vertical bars show uncertainty in the measurement at the one point for which that uncertainty was larger than the plotted size of the symbol.

excited from a single pulse. Figure 4.5.3 shows a typical result[6] in comparison with a calculation of the bremsstrahlung spectrum from that particular source on that particular shot. Both measurement and calculation are absolutes with no free parameters to adjust. Such a direct measurement of the spectrum from a single intense pulse of X-ray continua had not been previously possible because of the lack of any dispersive media at these energies and the agreement with expectations is striking. The type of selective excitation of calibration nuclei is now used to establish the intensity of pump sources used to excite actual laser candidates so that fluorescence efficiencies can be determined from data with Equations 1 and 2.

Tempering expectations that these successes might be readily extended to the pumping of actual isomeric candidates for a gamma-ray laser was a concern for the conservation of various projections of the angular momenta of the nuclei. Many of the interesting isomers belong to the class of nuclei deformed from the normally spherical shape. For those systems there is a quantum number of dominant importance, K, which is the projection of individual nucleonic angular momenta upon the axis of elongation. To this is added the collective rotation of the nucleus to obtain the total angular momentum J. The resulting system of energy levels resembles those of a diatomic molecule for which

$$E_x(K,J) = E_x(K) + B_xJ(J+1) \tag{3}$$

where $J \geq K \geq 0$ and J takes values $|K|, |K|+1, |K|+2, \ldots$ In this expression B_x is a rotational constant and $E_x(K)$ is the lowest value for any level in the resulting "band" of energies identified by other quantum numbers x. In such systems the selection rules for

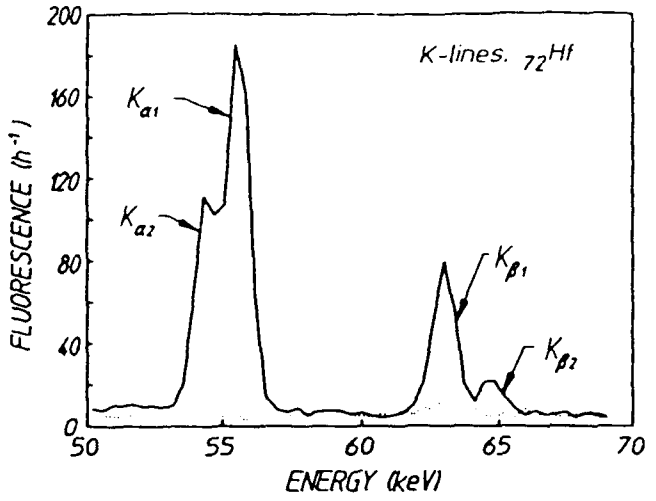

FIGURE 4.5.4 Dotted and solid curves show, respectively, the spectra obtained before and after dumping some of the isomeric ^{180m}Ta contained in a target sample enriched to 5%. An HPGe detector was used to obtain the dotted spectrum before irradiation. The feature at 63 keV is from traces of natural activity in the counting shield. The solid curve is the spectral signature of the radioactive debris accumulated by cascading from the levels into which the isomeric population was dumped. The actual lines are the K-lines of hafnium arising from electron capture by the ^{180}Ta ground debris.

electromagnetic transitions require both $|\Delta J| \leq M$ and $|\Delta K| \leq M$, where M is the multipolarity of the transition.

In most cases of interest, the lifetime of the isomeric state is large because it has a value of K differing considerably from those of lower levels to which it would, otherwise, be radiatively connected. As a consequence, bandwidth funneling processes such as shown to the left of Figure 4.5.1 must span substantial changes in ΔK and component transitions have been expected to have large, and hence unlikely, multipolarities.

Attempts to test these rather negative expectations have generally been confounded by the rarity of the 29 candidates for a gamma-ray laser. However, very recently there has been reported[9] a major success in dumping some of the isomeric population of one of the actual candidates for a gamma-ray laser.

Not a particularly attractive candidate, *a priori*, ^{180}Ta^m was the only one for which a macroscopic sample was available in 1987. The need to span a formidably large $\Delta K = 8$ between isomer and fluorescence level supported little initial enthusiasm for this nucleus. When actually pumped, however, it showed the largest integrated cross section ever reported for interband transfer in any material, 4×10^{-22} cm^2 eV. This is an enormous value for bandwidth funneling, being about 10,000 times greater than what is characteristic of an efficient nucleus which starts in the ground state and transfers to the isomer (see, for example ^{77}Se or ^{79}Br in Table 4.5.1). The optical pumping of any isomer had never been previously reported, so nothing was available for a more direct comparison with these results.[9]

The partial width for absorption from ^{180}Ta^m isomer to fluorescence was measured to be about 0.5 eV, a value far exceeding the 1 μeV usually offered as a rule of thumb that would limit the interband transfer of nuclear population. It is a current speculation that collective oscillations of the core nucleons break the symmetries of the nuclei and provide this major windfall making it easier to dump isomers by mixing single particle states needed in the transfer process. Much more experimentation will be needed to identify whether this is the actual mechanism responsible and to understand if the lessons taught by ^{180}Ta^m are generally applicable in the pool of candidate isomers. Now, such experiments are facilitated by the

widths themselves, which have reduced the level of effort to practical dimensions. The experiments with $^{180}Ta^{m}$ have shown that clear fluorescence signals can be obtained on a scale of illuminating milligrams of material with intensities which peak in time at only a few W/cm^2, even when integrated over all wavelengths. At this level, meaningful experiments can be performed on other candidate isomers when samples become physically available.

Coherent Pumping of Nuclei

Coherent pumping, the technique depicted in the right of Figure 4.5.1, depends upon the alteration of the properties of the isomeric storage level produced by the scattering of large intensities of long wavelength radiation from the nuclei. In ferromagnetic and ferroelectric hosts the active nuclei are immersed in extremely large fields capable of developing substantial interaction energies across a nuclear volume when switched by relatively modest applied fields. If transitions to the storage level exist in the nuclei at energies comparable to that of a photon of the driving fields, the properties of the other state of the transition will be mixed into those of the storage level. It is assumed that this other state is better able to radiate gamma radiation. While the driving field need not be precisely resonant with the transition energy, the detuning, ΔE from resonance must be comparable to the interaction energy if properties are to be fully mixed. In such cases, the metastability of the storage level against gamma-ray emission is switched off by the admixture of properties from the other state of the low energy transition being driven. It is this concept which comprises the foundation of the scheme for coherently pumping a gamma-ray laser.

While precise computations of the threshold for coherent pumping are not yet available, estimates from perturbation theory[3,10-12] suggest that the threshold requirements in idealized cases are comparable to those for incoherent pumping. The principal difficulty in this case is that, again, estimates are extremely sensitive to material specifics. For coherent upconversion to be viable, a real nucleus must be found with two accidentally degenerate levels, one being a long-lived isomeric state. Such a combination would be completely invisible to current techniques of nuclear spectroscopy.

REFERENCES

1. **Baldwin, G. C., Solem, J. C., and Goldanskii, V. I.,** *Rev. Mod. Phys.*, 53, 687, 1981.
2. **Collins, C. B.,** in *Laser Techniques for Extreme Ultraviolet Spectroscopy*, McIlrath, T. J. and Freeman, R. R., Eds., AIP Conference Proceedings No. 90, New York, 1982, 454.
3. **Collins, C. B., Lee, F. W., Shemwell, D. M., DePaola, B. D., Olariu, S., and Popescu, I. I.,** *J. Appl Phys.*, 53, 4645, 1982.
4. **Sinor, T. W., Reittinger, P. W., and Collins, C. B.,** *Phys. Rev. Lett.*, 62, 2547, 1989.
5. **Anderson, J. A. and Collins, C. B.,** *Rev. Sci. Instrum.*, 58, 2157, 1987.
6. **Anderson, J. A. and Collins, C. B.,** *Rev. Sci. Instrum.*, 59, 414, 1988.
7. *Evaluated Nuclear Structure Data File* (Brookhaven National Laboratory, Upton, New York, 1986)
8. **Collins, C. B., Anderson, J. A., Paiss, Y., Eberhard, C. D., Peterson, R. J., and Hodge, W. L.,** *Phys. Rev.* 38, 1852, 1988.
9. **Collins, C. B., Eberhard, C. D., Glesener, J. W., and Anderson, J. A.,** *Phys. Rev.* 37, 2267, 1988.
10. **Collins, C. B.,** in *Advances in Laser Science-I*, Stwalley, W. C. and Lapp, M., Eds., AIP Conference Proceedings No. 146, Dallas, 1985, 40.
11. **Olariu, S., Popescu, I., and Collins, C. B.,** *Phys. Rev.*, 23, 50, 1981.
12. **Olariu, S., Popescu, I., and Collins, C. B.,** *Phys. Rev.*, 23, 1007, 1981.
13. **Ikonen, E., Helisto, P., Hietaniemi, J., and Katila, T.,** *Phys. Rev. Lett.*, 60, 643, 1988.
14. **West, P. J. and Matthias, E.,** *Z. Phys.*, 228, 369, 1978.
15. **Collins, C. B. and DePaola, B. D.,** *Optics Lett.*, 10, 25, 1985.
16. **DePaola, B. D. and Collins, C. B.,** *J. Opt. Soc. Am.*, B1, 812, 1984.

BRIEF REPORTS

Brief Reports are short papers which report on completed research or are addenda to papers previously published in the **Physical Review**. *A Brief Report may be no longer than four printed pages and must be accompanied by an abstract.*

Excitation of $^{123}Te^m$ and $^{125}Te^m$ through (γ,γ') reactions

J. J. Carroll, T. W. Sinor, D. G. Richmond, K. N. Taylor, and C. B. Collins
Center for Quantum Electronics, The University of Texas at Dallas, P. O. Box 830688, Richardson, Texas 75083

M. Huber, N. Huxel, P. v. Neumann-Cosel, A. Richter, C. Spieler, and W. Ziegler
Institut für Kernphysik, Technische Hochschule Darmstadt, D-6100 Darmstadt, Germany
(Received 5 October 1990)

Photoexcitation of the long-lived isomers $^{123}Te^m$, $T_{1/2}=119.7$ d, and $^{125}Te^m$, $T_{1/2}=58$ d, was produced with bremsstrahlung from the superconducting Darmstadt linear accelerator. The excitation function for the reaction $^{123}Te(\gamma,\gamma')^{123}Te^m$ was measured between 2 and 6 MeV. It indicated that the isomer was populated by resonant absorption through isolated intermediate states having integrated cross sections in excess of 10^{-26} cm^2 keV, i.e., values about 100 times larger than most (γ,γ') activation reactions reported previously. An excitation function was also obtained for the reaction $^{125}Te(\gamma,\gamma')^{125}Te^m$ in this energy range.

INTRODUCTION

It has been recently discovered[1] that the reaction $^{180}Ta^m(\gamma,\gamma')^{180}Ta$ occurs with an integrated cross section that is orders of magnitude larger than what could have been reasonably expected. At energies below the threshold for neutron evaporation the photoexcitation of isomers is usually characterized by values of 10^{-28}–10^{-27} cm^2 keV. Although the inverse, deexcitation of an isomer had not been previously observed, there was no *a priori* reason to expect it to be more probable, particularly since the transition requires a spin change of $\Delta K=8$. Of considerable astrophysical significance,[2,3] the result reported for $^{180}Ta^m$ approached 10^{-24} cm^2 keV and raised some interesting questions of nuclear structure. It also provided unexpected encouragement of schemes for pumping a γ-ray laser that would depend upon the sudden deexcitation of isomeric populations.[4]

Whether the deexcitation of $^{180}Ta^m$ was an isolated example limited to odd-odd nuclei with a high density of states was considered in two subsequent studies. In the first the excitation function for $^{180}Ta^m(\gamma,\gamma')^{180}Ta$ was measured with a bremsstrahlung source by varying the end point of the spectrum. It was found[5] that the (γ,γ') reactions of $^{180}Ta^m$ occurred for two discrete excitation energies of 2.8 and 3.6 MeV with integrated cross sections of 1.2×10^{-25} and 3.5×10^{-25} cm^2 keV, respectively. The high density of excited nuclear states seemed to play no particular role.

In the second experiment[6] 19 isomers were excited with the bremsstrahlung spectra from four different accelerators. Despite the relatively coarse mesh of energies at which end points could be set between 0.5 and 11 MeV, several isomers were excited through integrated cross sections that were surprisingly large at 4 MeV. One curiosity was the first report of the photoexcitation of 119.7*d*, $^{123}Te^m$, the longest-lived isomer ever populated by (γ,γ') reactions and one of the candidate nuclides for a γ-ray laser. This is a fairly light nucleus having no particularly high density of states. Also, there is little experimental or theoretical information on electromagnetic transitions between excited levels in ^{123}Te above 1 MeV.

It was the purpose of the experiment described in this Brief Report to measure the excitation function for both $^{123}Te^m$ and $^{125}Te^m$. Exploiting the precision with which the end points of the spectra could be set between 2 and 6 MeV, the (γ,γ') reactions were found to occur through relatively few gateways with large integrated cross sections approaching 10^{-25} cm^2 keV.

EXPERIMENTAL ANALYSIS AND RESULTS

Elemental tellurium samples were used in this study, and all isotopes were present in their natural abundances. Nominal amounts of 17 g were contained in plastic (Delrin) cylinders with outer diameters of 3.8 cm and heights of 1.5 cm. Calibration targets were fashioned from identical containers holding about 2 g of 99.9% pure SrF_2. Its use in calibrating bremsstrahlung spectra has been recently emphasized.[5,6]

Isomeric populations were produced by exposing the targets to bremsstrahlung from a 3-mm tantalum converter foil irradiated by the electron beam from the injector of the new 130-MeV S-DALINAC at the Technische Hochschule Darmstadt.[7] Electron energies were varied between 2 and 6 MeV with a typical step size of 250 keV. These electron energies were measured with an accuracy of 50 keV before and after each exposure. The diameter

of the beam at the converter, typically 2 mm, was also monitored. At each end point a sample stack of tellurium and strontium was irradiated axially in close proximity to the converter. The proper alignment of the beam was achieved by maximizing the dose delivered to a remote ionization chamber shielded to sample only the central 12 mrad of the bremsstrahlung cone. Variations in all beam parameters were recorded during the experiments. In particular, the charge passed to the converter was determined by digitizing the current and integrating it. Exposures were typically 4 h in duration for a beam current of about 20 μA.

The numbers of isomers produced by these irradiations were determined from the counting rates measured in distinctive fluorescence lines. The transitions responsible for the γ-ray signatures used in these measurements are indicated by bold arrows in the energy-level diagrams of Figs. 1(a) and 1(b).

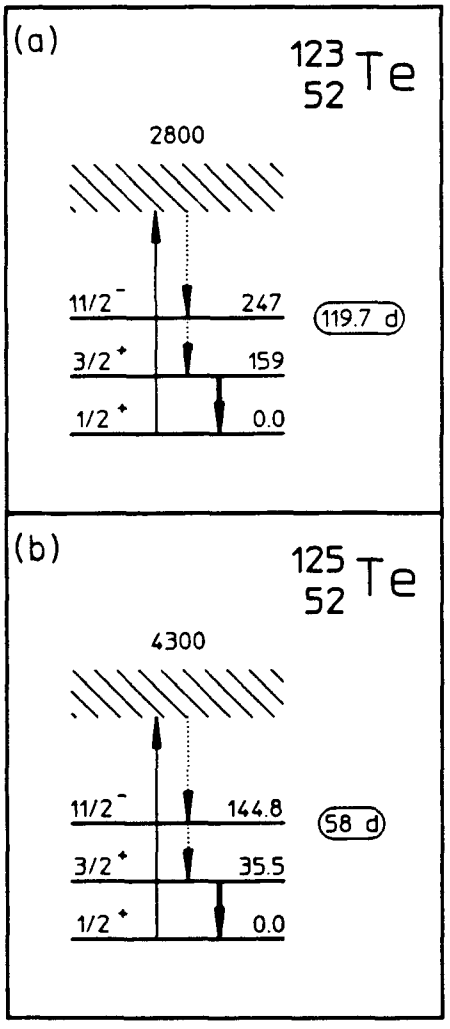

FIG. 1. Schematic energy-level diagrams for (a) ^{123}Te and (b) ^{125}Te. Half-lives of the isomers are shown in the ovals, and the energies of the levels shown are given in keV. The bold arrows show the transitions which give rise to distinctive γ-ray emissions measured in this work. The dashed arrows indicate transitions which are not directly observed.

After irradiation the tellurium samples were transported to the Center for Quantum Electronics, University of Texas at Dallas, where high-resolution spectra were collected with an HPGe detector. An example of the data obtained with a 6-MeV exposure is shown in Fig. 2. The fluorescence peak[8] at 159.0 keV from the decay of ^{123}Te^m is apparent, and even the γ rays from the strongly converted transition of ^{125}Te^m at 35.5 keV are clearly visible.

Because of the shorter isomeric lifetimes the SrF_2 calibration, samples[5,6] were counted on site with a Ge(Li) detector to measure the yield of ^{87}Sr^m. This isomer has a half-life of 2.8 h and a fluorescence signature at 388.4 keV. The raw number of counts in each peak was corrected for the finite durations of exposure and counting, the absolute counting efficiencies of the detectors, and the relative emission intensity. The opacity of the samples to the escape of the signature γ rays was compensated by a factor calculated with a Monte Carlo code for each detector geometry.

The experimentally measured yield of isomers, N_f resulting from the irradiation of N_T ground-state nuclei with bremsstrahlung is given analytically by

$$N_f = N_T \int_{E_C}^{E_0} \sigma(E) \frac{d\Phi(E)}{dE} dE \ , \tag{1}$$

where E_0 is the end-point energy, $d\Phi(E)/dE$ is the time-integrated spectral intensity in $cm^{-2}keV^{-1}$ of the photon field, and $\sigma(E)$ is the cross section in cm^2 for the reaction. The spectral intensity is conveniently expressed as the product of a flux of all photons above a cutoff energy E_C of 1 MeV, Φ_0 incident on the target, and a relative intensity function $F(E,E_0)$, which is normalized according to

$$\int_{E_C}^{E_0} F(E,E_0) dE = 1 \ . \tag{2}$$

Equation (2) allows the definition of a normalized yield, or activation per photon, $A_f(E_0)$ given by

$$A_f(E_0) \equiv \frac{N_f}{N_T \Phi_0} = \int_{E_C}^{E_0} \sigma(E) F(E,E_0) dE \ . \tag{3}$$

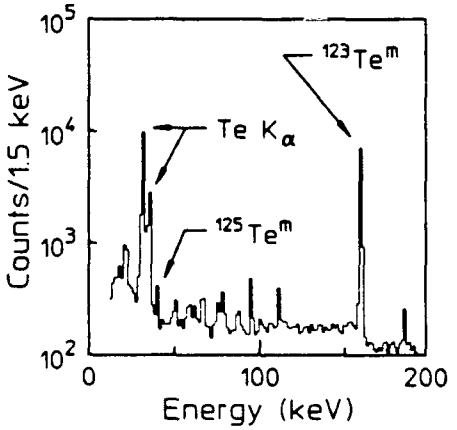

FIG. 2. Pulse-height spectrum obtained from a tellurium sample after a 6-MeV end-point irradiation. Peaks not explicitly marked are due to counting chamber background.

Plots of this quantity as a function of E_0 give the excitation functions for $^{123}Te^m$ and $^{125}Te^m$ shown in Figs. 3(a) and 3(b). This normalization makes these curves relatively insensitive to variations in isomeric population that occur simply because all the intensities increase when the end point is raised. Instead, their appearance is primarily determined by the density, location, and integrated cross sections of the states mediating the reactions.

Calculated spectra of both Φ_0 and $F(E,E_0)$ were obtained from the EGS4 electron-photon transport code developed at SLAC.[9] This Monte Carlo program is well established in the medical physics community, and its general validity has been demonstrated elsewhere.[10,11] In this work confidence in the calculated photon spectra was maintained by calibrating them with the reaction $^{87}Sr(\gamma,\gamma')^{87}Sr^m$ as discussed in Ref. 5.

At energies of interest in these experiments, gateways have widths that are small in comparison to their spacings, and Eq. (3) reduces to a summation, giving

$$A_f(E_0)=\sum_j (\sigma\Gamma)_{jj}F(E_j,E_0)\ , \tag{4}$$

where $(\sigma\Gamma)_{jj}$ is the integrated cross section and E_j is the excitation energy of the jth intermediate state feeding the isomer. It is then possible to define a quantity $R_M(E_0)$,

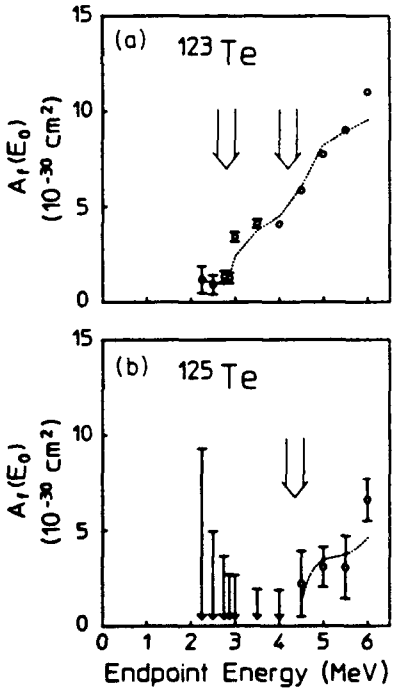

FIG. 3. Linear plots of yield normalized to the flux calculated for a low-energy cutoff of 1 MeV as functions of bremsstrahlung end-point energy for (a) ^{123}Te and (b) ^{125}Te. Where no error bars are shown, statistical errors are comparable to the symbol size. Error bars shown without symbols in (b) represent upper bounds on the activation where fluorescence was not observed above the level of background. Dotted curves plot the values calculated from the model of Eq. (4) using the results of Table I. The locations of the gateways determined in this work are indicated by the large arrows whose widths represent the available experimental resolution.

which represents the residue of activation after subtracting contributions from the M lowest-lying intermediate states:

$$R_M(E_0)=A_f(E_0)-\sum_{E_j=E_1}^{E_M}(\sigma\Gamma)'_{jj}F(E_j,E_0)\ , \tag{5}$$

where E_M is the resonance energy of the highest-lying intermediate state contributing. Fitted values of the integrated cross sections $(\sigma\Gamma)'_{jj}$ were found by minimizing $R_M(E_0)$ for the lowest-energy state giving a break in the excitation function, and then iterating after including any new gateways suggested by the data. In the case of ^{87}Sr, the calibration procedures described earlier[5,6] were confirmed in the present work as a test of confidence. This provided experimental validation of the calculated photon spectra as well as confirming the experimental practice.

An identical analysis for $^{123}Te^m$ was based upon the excitation function of Fig. 3(a). The pronounced increase in yield beginning near 3 MeV indicates the location of an intermediate state, while the low level of activation below this energy suggests the participation of smaller gateways having $E_j<2$ MeV. The number and location of these lower-energy states could not be determined in the current work; nor does the literature provide any information. It was found that a single state near 1 MeV with an integrated cross section of $(60\pm20)\times10^{-29}$ cm^2 keV could give the activation observed below 3 MeV, but this assignment is not unique. The possible variations are indicated in Table I and do not significantly contribute to the uncertainties reported for the other gateways. Using this hypothetical state to remove the base-line yield, the residue $R_1(E_0)$ indicated two strong gateways at 2.8 and 4.2 MeV. The fitted $(\sigma\Gamma)'_{jj}$ corresponding to these states are given in Table I and are much larger than the base-line state at 1 MeV. These values were determined to within the uncertainties explicitly shown in Table I.

The excitation function obtained for population of $^{125}Te^m$ provided less detail, but the data of Fig. 3(b) were still consistent with an intermediate state located between 4.2 and 4.5 MeV, as given in Table I.

Because of the low (γ,n) threshold of the naturally occurring component of the deuterium in the plastic sample containers, it was necessary to evaluate the effects of all neutrons produced in the irradiation environment.

TABLE I. Values of fitted integrated cross sections $(\sigma\Gamma)'_{jj}$ for gateway states determined from the excitation functions of Figs. 3(a) and 3(b) for the (γ,γ') reactions populating the isomers $^{123}Te^m$ and $^{125}Te^m$. The gateway excitation energies E_j for these levels are given at the centroid of the appropriate experimental bins.

Isotope	Gateway energy (MeV)	$(\sigma\Gamma)'$ (10^{-29} cm^2 keV)
^{123}Te	1.0 ± 0.5	$<60\pm20$
	2.8 ± 0.2	2000 ± 300
	4.2 ± 0.2	7000 ± 1000
^{125}Te	4.2–4.5	7000 ± 3000

The neutron flux was measured with standard activation techniques[12] by the inclusion of indium foils in the target stacks. Each disk was 0.0127 cm thick with a diameter of 3.8 cm and a mass of about 1 g. Epithermal neutrons were observed by detection of the 416.92-keV fluorescence from the 54.15-min isomer of ^{116}In, which is produced through neutron capture from the stable ^{115}In. At the highest photon end point of 6 MeV, there were found to be only 0.87 ± 0.05 neutrons $cm^{-2}s^{-1}$, and this flux decreased smoothly to zero as the end point was lowered to the deuterium (γ,n) threshold of 2.22 MeV. This low level of epithermal neutron flux produced negligible contributions to the yields of ^{123,125}Te^m and ^{87}Sr^m. The appearance of thermal neutrons was not expected because of the lack of sufficient moderators in the environment. The use of photon energies below the thresholds of all target and environmental materials excluded fast neutron production.

CONCLUSIONS

The excitation functions obtained in this work for the population of the isomers ^{125}Te^m and ^{125}Te^m indicate that their photoexcitation proceeds through absorption by isolated intermediate states. No consistent description could be obtained by assuming absorption through densely spaced levels which would have provided broadband absorption. The integrated cross sections determined for these states are about 100 times larger than most (γ,γ') activation reactions reported previously, being in excess of 10^{-26} cm^2 keV. Moreover, they are only an order of magnitude smaller than those determined in earlier measurements[1,5] for the depopulation of ^{180}Ta^m. Clearly, further investigations of the systematics of isomeric photoexcitation are needed in the range between 2 MeV and (γ,n) threshold energies in order to isolate the principal cause of the large photoexcitation rates being found. Experimental studies of a variety of different isomeric nuclei are currently underway to examine these questions. It would also be of great interest to have nuclear structure calculations illuminating the nature of the particular intermediate states through which the photoabsorption occurs.

ACKNOWLEDGMENTS

We thank K. Alrutz-Ziemssen, H.-D. Gräf, Th. Rietdorf, and H. Weise for their great support in operating the superconducting electron accelerator. In addition, we wish to thank our sponsors, the Department of Defense through the Naval Research Laboratory and the Bundesministerium für Forschung und Technologie, Contract No. 06DA184I.

[1] C. B. Collins, C. D. Eberhard, J. W. Glesener, and J. A. Anderson, Phys. Rev. C **37**, 2267 (1988).

[2] J. J. Carroll, J. A. Anderson, J. W. Glesener, C. D. Eberhard, and C. B. Collins, Astrophy. J. **344**, 454 (1989).

[3] Zs. Nemeth and F. Kaeppler, contribution to the Symposium on Nuclear Astrophysics, Baden, 1990 (unpublished).

[4] C. B. Collins, F. W. Lee, D. M. Shemwell, B. D. DePaola, S. Olariu, and I. I. Popescu, J. Appl. Phys. **53**, 4645 (1982).

[5] C. B. Collins, J. J. Carroll, T. W. Sinor, M. J. Byrd, D. G. Richmond, K. N. Taylor, M. Huber, N. Huxel, P. v. Neumann-Cosel, A. Richter, C. Spieler, and W. Ziegler, Phys. Rev. C **42**, 1813 (1990).

[6] J. J. Carroll, M. J. Byrd, D. G. Richmond, T. W. Sinor, K. N. Taylor, W. L. Hodge, Y. Paiss, C. D. Eberhard, J. A. Anderson, C. B. Collins, E. C. Scarbrough, P. P. Antich, F. J. Agee, D. Davis, G. A. Huttlin, K. G. Kerris, M. S. Litz, and D. A. Whittaker, submitted to Phys. Rev. C.

[7] H.-D. Gräf and A. Richter, in Proceedings of the 1988 Linear Accelerator Conference, Virginia, CEBAF Report No. 89-001, 1989, p. 231.

[8] E. Browne and R. B. Firestone, in *Table of Radioactive Isotopes*, edited by V. S. Shirley (Wiley, New York, 1986).

[9] Walter R. Nelson, Hideo Hirayama, and David W. O. Rogers, *The EGS 4 Code System* (SLAC Report No. 265, Stanford Linear Accelerator Center, Stanford, CA, 1985).

[10] R. Mohan, C. Chui, and L. Lidofsky, Med. Phys. **12**, 595 (1985).

[11] *Monte Carlo Transport of Electrons and Photons*, edited by T. M. Jenkins, Walter R. Nelson, and Alessandro Rindi (Plenum, New York, 1988).

[12] *ASTM Standard Method for Determining Thermal Neutron Reaction and Fluence Rates by Radioactivation Techniques*, Publication E 262-86 (American Society for Testing and Materials, Philadelphia, 1987), and references cited there.

Photoexcitation of nuclear isomers by (γ,γ') reactions

J. J. Carroll, M. J. Byrd, D. G. Richmond, T. W. Sinor, K. N. Taylor, W. L. Hodge,*
Y. Paiss,† C. D. Eberhard, J. A. Anderson,‡ and C. B. Collins
Center for Quantum Electronics, University of Texas at Dallas, Richardson, Texas 75083

E. C. Scarbrough and P. P. Antich
The University of Texas Southwestern Medical Center at Dallas, Dallas, Texas 75235

F. J. Agee, D. Davis, G. A. Huttlin, K. G. Kerris, M. S. Litz, and D. A. Whittaker
Aurora Simulator Facility, Harry Diamond Laboratories, Adelphi, Maryland 20783
(Received 21 April 1989)

Photoexcitation of the isomers of 19 nuclides was examined in this work. Four accelerators were used as sources of bremsstrahlung to expose the samples and end-point energies covered the range from 0.5 to 11 MeV. No evidence was found for nonresonant processes of excitation. However, more than half the cases showed enhanced channels for the resonant photoexcitation of isomers with integrated cross sections approaching 10^{-21} cm^2 keV. These results are three to four orders of magnitude larger than values usually characterizing (γ,γ') reactions.

INTRODUCTION

Because the photon carries relatively little momentum, (γ,γ') reactions must proceed through resonant channels for excitation with rather narrow widths. This aspect distinguishes photoexcitation from related processes such as (γ,n). The generation of an additional particle with which to conserve momentum provides a threshold of energy above which all incident photons can mediate the reaction. This facilitates the study of processes such as (γ,n) by increasing product yields and richly detailed results have been reported in the literature.[1] In contrast, the difficulties in exciting the narrow resonances for (γ,γ') reactions have inhibited investigations and relatively few results have been published in the past 50 years over which such processes have been known.[2,3]

In the region of energies from 0.1 to 10.0 MeV photon sources emit continuous spectra and the opportunity to probe (γ,γ') reactions with a tunable source of narrow width does not exist at practical levels of intensity. Even experiments designed to use γ sources are actually done with continua because of the degradation of the line spectra by Compton scattering in the real geometries employed.

The most tractable (γ,γ') reactions for study are those for the photoexcitation of isomeric states. The product lives long enough to be readily examined after termination of the input irradiation. The archetypical case has been the reaction ^{111}Cd$(\gamma,\gamma')^{111}$Cd^m exciting the 48.6 min isomer. Three of the most recent measurements of the integrated cross section $\sigma\Gamma$ were conducted in 1979, 1982, and 1987 with results of 35, 5.8, and 14 as reported in Refs. 4–6, respectively, in the usual units of 10^{-29} cm^2 keV. Probable errors were quoted as varying only from 7% to 14% and yet, no two of the measurements were even within a factor of 2 of each other. This discrepancy led to the curious suggestion[5] that some unknown mechanism for *nonresonant* nuclear absorption generally dominates the excitation step. Although fundamental considerations insist that for energies below the thresholds of neutron evaporation all (γ,γ') reactions must first excite bound nuclear states, the belief continued to spread that nonresonant processes were involved. The (γ,γ') reactions of ^{113}In, ^{87}Sr, and ^{180}Ta^m were all subsequently attributed to the unidentified nonresonant process.[7,8]

Recently, the technology has become available[9,10] to measure the spectrum of a source of pulsed bremsstrahlung, together with greatly improved computer codes[11,12] with which to calculate spectra for realistic geometries. These advances made it possible to resolve[13] the persisting controversies in the reaction ^{111}Cd$(\gamma,\gamma')^{111}$Cd^m, as well as those[14] in ^{115}In$(\gamma,\gamma')^{115}$In^m. As expected, it was found[13,14] that both ^{115}In^m and ^{111}Cd^m were excited by resonant absorption through intermediate gateway states near 1 MeV that were broadened by their short lifetimes. The sharp onset of the (γ,γ') reactions with increasing energy relegated to less than 3% any contributions from nonresonant processes and indicated that the gateway states were reasonably well connected by radiative transitions to both the ground states and the isomers. It appears that the principal cause for the large discrepancy between previous measurements was the difficulty in adequately characterizing the spectra of the irradiation. This was particularly true for radioactive sources since all spectral contributions away from the source lines were necessarily due to Compton continua generated by scattering in the irradiation environment.

The model for the photoexcitation of isomeric nuclei confirmed in recent work[13,14] is shown in Fig. 1. Only two gateway levels are drawn as examples and the number actually participating depends upon the sequence of energy levels and transition probabilities for the particu-

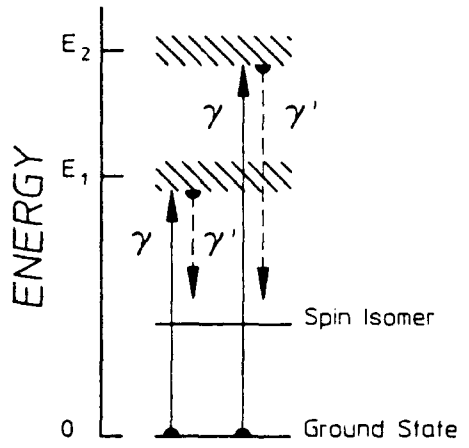

FIG. 1. Schematic representation of the (γ,γ') reactions used to populate isomeric states in these experiments. The resonant absorption of bremsstrahlung x rays, denoted as γ, excite populations of gateway states. Two are shown at excitation energies of E_1 and E_2 but the actual number will vary for each nuclide. Parts of the populations of the gateway states make transitions to the final state either directly or as part of a cascade of radiative transitions ending on the final state as indicated by the dashed arrows.

lar nucleus being considered. In the resolution of previous conflicts in ^{111}Cd and ^{115}In the values finally confirmed lay within the scatter of earlier measurements and generally agreed with nuclear parameters measured by other means.[15] However, when studies were extended to the deexcitation of an isomeric sample through the reverse of the sequence shown in Fig. 1, unexpectedly large results were obtained.[16] In contrast to values of a few $10's \times 10^{-29}$ cm^2 keV measured for the excitation of isomers, a value of $40\,000 \times 10^{-29}$ cm^2 keV was reported[16] for the deexcitation of ^{180}Ta^m with a 6 MeV linac. The reaction ^{176}Lu$(\gamma,\gamma')^{176}$Lu^m was reported to proceed with an integrated cross section of comparable magnitude.[17] The strength of the dumping reaction ^{180}Ta$^m(\gamma,\gamma')^{180}$Ta was confirmed[18] with bremsstrahlung from the injector to the Darmstadt superconducting electron accelerator operated at 12 different end-point energies. Two gateway levels for ^{180}Ta$^m(\gamma,\gamma')^{180}$Ta were reported with integrated cross sections that totaled to $47\,000 \times 10^{-29}$ cm^2 keV.

It was the purpose of the work reported here to examine the systematics of these giant resonances for the photoexcitation of isomeric states to determine whether such results were curiosities associated only with ^{176}Lu and ^{180}Ta^m or whether they were part of more generally prevalent phenomena. A secondary objective was to learn whether the large integrated cross sections were the results of a large number of reaction channels of more conventional size or rather, a few of unprecedented magnitude.

Unfortunately, the type of electron accelerators that provided bremsstrahlung spectra with end-point energies that were chosen at will in classical investigations[19] of (γ,γ') reactions is no longer available in North America. For the experiments reported here we could arrange access only to a combination of accelerators, some with limited variability of end-point energies such as DNA/PITHON at Physics International and DNA/Aurora at Harry Diamond Laboratories. Between the ranges of energies available from those machines we used two medical linacs having fixed end points of 4 and 6 MeV. This enabled us to examine the photoexcitation of 19 isomeric nuclei, most of them over the range from 0.5 to 11 MeV. The variety of accelerators and locations minimized the possibility of introducing any systematic bias which might have been associated with any particular machine or its environment.

METHODOLOGY

Analytic approach

The normalized activation $A_f(E_0)$ of a sample per unit photon flux Φ_0 produced with a bremsstrahlung source having an endpoint E_0 can be written as

$$A_f(E_0) \equiv \frac{N_f}{N_i \Phi_0} = \sum_j (\sigma\Gamma)_{fj} F(E_j, E_0) , \tag{1}$$

where N_i and N_f are the populations of initial and final nuclear states, respectively. In Eq. (1), $(\sigma\Gamma)_{fj}$ is the integrated cross section for the excitation of N_f through the jth gateway state as shown in Fig. 1. The function $F(E_j,E_0)$ is the spectral function describing the relative intensity at the photon energy, E_j, normalized so that

$$\int_0^{E_0} F(E,E_0)dE = 1 . \tag{2}$$

The normalized activation can be useful as a sensitive indication of the opening of (γ,γ') channels whenever photons of the requisite energies E_j become available. A change of the end-point energy E_0 of the bremsstrahlung spectrum modulates the spectral intensity function $F(E_j,E_0)$ in Eq. (1) at all of the important gateway energies, E_j. The largest effect in the excitation function occurs when E_0 is increased from a value just below some gateway at $E_j = E_k$ to one exceeding it so that $F(E_j,E_0)$ varies from zero to some finite value. In earlier work[19] plots of quantities equivalent to Eq. (1) as functions of the end-point energies of the irradiating spectra showed very pronounced activation edges which appeared as sharp increases at the energies, E_j, corresponding to excitation of new gateways.

In the work reported here the ratios of activation N_f/N_i to the irradiation dose were examined as functions of E_0. The relationships between dose, which was measured directly, and Φ_0, which had to be derived from it, depended upon $F(E,E_0)$. The normalization to dose rather than Φ_0 was chosen to avoid any dependence of the features of the excitation function upon simulation models.

Experimental details

Sample materials were exposed to photons having energies up to 1.5 MeV with the DNA/PITHON nuclear simulator at Physics International. This device was a flash x-ray source using a single transmission line pulsed by a Marx generator. Since the end-point energy could be varied to some degree by changing the charging voltage of the Marx, photoexcitation from 0.5 to 1.5 MeV could be investigated with a resolution limited by the available end-point energies. The samples were placed in front of a converter foil which terminated the transmission line, and were aligned to face the photon flash. These were exposed in complex packages to activate several materials in each shot from DNA/PITHON, an important detail since the pulse repetition frequency was less than 1 h^{-1}. All the sample packages were backed with thermoluminescent dosimeters (TLD's) to measure the dosage which each target received.

The 1.5 to 6 MeV range was studied with two fixed end-point medical linacs at the Department of Radiology of the University of Texas Southwestern Medical Center at Dallas. Irradiations with nominal 4 MeV bremsstrahlung were obtained with a Varian Clinac 4/100 linac which provided a dose rate of 200 rad(H_2O) min^{-1} at 101.2 cm from the converter target. Bremsstrahlung having a nominal end point of 6 MeV was obtained with a Varian Clinac 1800 linac operating in the 6 MeV mode. This device produced 400 rad(H_2O) min^{-1} at 101.5 cm from the converter target. For both machines, the dose rate was determined by in-line ion chambers whose calibrations were directly traceable to NIST. Samples were exposed in packages confined to the region of most uniform dose distribution.

Irradiations in the 6 to 11 MeV range were provided with the DNA/Aurora nuclear simulator,[20] located at the Harry Diamond Laboratories. Powered by a Marx bank, photons were generated by converter foils which terminated four separate transmission lines. These converged on a target volume of roughly 0.1 m^3 in which the photon field was most intense. Again, the Marx charging voltage was varied to provide irradiations with different end-point bremsstrahlung. Samples were positioned in the high intensity spot and were backed by TLD's. These packages were oriented to face the centerline of the machine rather than any particular transmission line.

The spectra of these four machines have been well characterized, particularly the linacs which are committed to patient treatment. Photon spectra of the DNA/PITHON and DNA/Aurora accelerators were obtained through use of the Integrated TIGER Series (ITS) computational program.[12] They were calibrated by matching the end-point energy and the total dosage to the shape of the calculated spectrum. The DNA-PITHON device could also be cross calibrated by the activation technique described in Refs. 9 and 10. Typical spectra are given in Fig. 2 which shows the relative intensity function $F(E,E_0)$, on the meshes of energies for which data were available. For the DNA/PITHON shot shown, $\Phi_0 = 4\times10^{14}$ photons cm^{-2} and for the DNA/Aurora shot, $\Phi_0 = 5\times10^{13}$ photons cm^{-2}.

The output spectra of the medical linacs employed in this work were calculated with the EGS4 code developed at SLAC.[11] Unfortunately, the relative spectral intensity functions of these devices that were found in the literature[21] contained a computational artifact. To minimize that feature the spectra had to be modeled as part of this work. Results are shown in Fig. 3, together with the

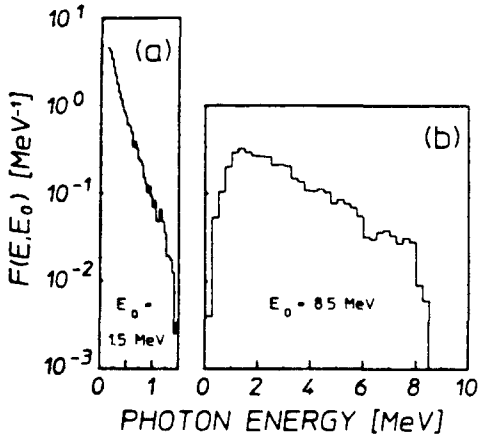

FIG. 2. Relative spectral intensities $F(E,E_0)$ of the bremsstrahlung typically produced by nuclear simulators used to irradiate samples in these experiments. The curves are normalized so that their areas are unity. The devices employed were (a) DNA/PITHON, with an end point of $E_0 = 1.5$ MeV; (b) DNA/Aurora, with an end point of $E_0 = 8.5$ MeV.

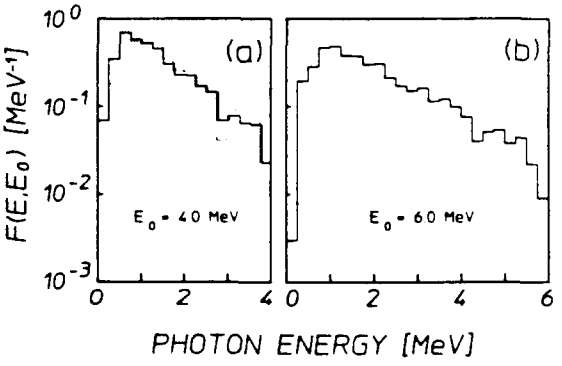

FIG. 3. Relative spectral intensities $F(E,E_0)$ of the bremsstrahlung produced by the medical linacs used to irradiate samples in these experiments. The curves are normalized so that their areas are unity. The solid lines indicate empirical fits to the calculated spectra as discussed in the text. The devices employed were as follows: (a) Varian Clinac 4/100, with a nominal end point of 4 MeV. The dotted curve shows the spectrum obtained from Ref. 21 that contains a computational artifact at about 3 MeV. (b) Varian Clinac 1800, operated in the nominal 6 MeV end-point mode.

literature values for a typical case.[21] The total fluxes at 100 cm were 3.23×10^{11} photons cm^{-2} min^{-1} for the nominally 4 MeV device, and 5.35×10^{11} photons cm^{-2} min^{-1} for the Clinac 1800 in the 6 MeV mode.

The isotopes studied in these experiments are listed in Table I along with the relevant physical parameters. The techniques employed to obtain measurements of activation depended upon the lifetimes of the isomeric states and whether or not these were long enough to transport the irradiated samples by simple means.

Isomers of the first nine nuclides listed in Table I have half-lives of less than 3 min and therefore required special treatment. These samples consisted of either powders or metallic foils enclosed in cylindrical polyethylene vials which were pneumatically transported to a well-type NaI(Tl) detector after exposure. The low energy resolution of this detector necessitated some care in the identification of the prominent features in the pulse height spectra. In all cases, confirmations that these were the fluorescence signatures of the isomers were made by determining the half-lives of the product populations. This was made possible by simultaneously acquiring data

TABLE I. Summary of isomeric nuclei studied. Nuclei marked * were present in isotopically enriched samples. In the sample column, *R* refers to samples contained in vials transferred pneumatically, *P* to flat planchettes, *F* to metallic foils, and *B* to scintillation bottles. The ^{180}Ta sample consisted of a dusting of oxide on a thin aluminum plate, referred to by *D*. In the case of the ^{176}Lu sample, β^- particles were observed instead of fluorescence photons; the NA in the transparency column indicates that this factor was not applicable for ^{176}Lu.

Nuclide	Abundance (%)	Sample form	$T_{1/2}$	Principal fluorescence (keV)	Transparency (%)
^{166}Er	91.54*	Er_2O_3	2.28	207.79	57.90
		(*R*)	sec	(41.70%)	
^{79}Br	50.69	LiBr	4.86	207.20	84.90
		(*R*)	sec	(75.80%)	
^{191}Ir	37.30	Ir	4.94	129.43	10.50
		(*R*)	sec	(25.70%)	
^{197}Au	100.00	Au	7.80	279.11	92.70
		(*R*)	sec	(73.00%)	
^{89}Y	100.00	YF_3	16.06	909.15	94.70
		(*R*)	sec	(99.14%)	
^{77}Se	94.38	Se	17.45	161.92	72.28
		(*R*)	sec	(52.40%)	
^{179}Hf	13.63	HfO_2	18.68	214.31	52.40
		(*R*)	sec	(94.20%)	
^{199}Hg	16.90	Hg_2Cl_2	43.20	158.40	43.96
		(*R*)	sec	(53.00%)	
^{135}Ba	11.74	BaF_2	153.12	661.66	95.50
		(*R*)	sec	(90.10)	
^{111}Cd	12.80	Cd	48.6	245.49	76.35
		(*F*)	min	(94.00%)	
^{115}In	4.30	In	1.66	391.69	98.30
		(*F*)	h	(64.20%)	
^{87}Sr	7.00	SrF_2	2.81	388.40	95.78
		(*P*)	h	(82.30%)	
^{176}Lu	2.59	$LuCl_3$	3.63	beta	NA
		(*B*)	h		
^{115}In	95.70	In	4.49	336.26	98.00
		(*F*)	h	(45.80%)	
^{180}Ta	4.00*	TaO_2	8.15	55.79	100.00
		(*D*)	h	(36.00%)	
^{135}Ba	6.60	BaF_2	1.20	268.27	94.33
		(*P*)	d	(15.60%)	
^{195}Pt	33.80	Pt	4.02	98.88	4.76
		(coin)	d	(11.40%)	
^{117}Sn	7.70	Sn	13.6	158.56	92.89
		(*F*)	d	(86.40%)	
^{123}Te	0.908	Te	119.7	158.99	62.68
		(*P*)	d	(84.00%)	

through two Ortec 918A ADCAM multichannel buffers controlled by a personal computer. While one ADCAM served to produce a pulse height spectrum, the other collected a record of the total counts received in the preset dwell interval as a function of time. A typical example of the data obtained in this way is given in Figs. 4(a) and 4(b), showing measurements for the isomer $^{167}Er^{m}$.

The remaining nuclides in Table I had half-lives longer than 48.6 min, and could be transported by hand to a nearby solid-type NaI(Tl) detector for counting. Samples containing particularly long-lived isomers like 119.7 d $^{123}Te^{m}$ and 13.61 d $^{117}Sn^{m}$ were transported to the Center for Quantum Electronics where they were counted using a high-purity, *n*-type germanium (HPGe) detector. The physical form of the materials in this slower class consisted either of thin metallic disks or flat polyethylene planchettes containing metallic chips or chemical compounds.

Since the HPGe detector provided greater resolution it was not necessary to monitor the time decay in detail. For some samples, however, energy spectra were acquired after several different elapsed times to provide additional confirmation of the product signature. For example, a pulse height spectrum of $^{123}Te^{m}$ after a 6 MeV exposure is shown in Fig. 5(a). The fluorescence line at 159 keV is well defined and gives 5% counting statistics. Since this was the longest-lived isomer ever reported to be excited by a (γ,γ') reaction, the time decay was experimentally determined from a sequence of energy spectra taken after a 6 MeV exposure. The decay of the count rate is shown in Fig. 5(b). A fit to these data gives a half-life which is in excellent agreement with the literature value.

The nuclide, ^{176}Lu, was examined with a different

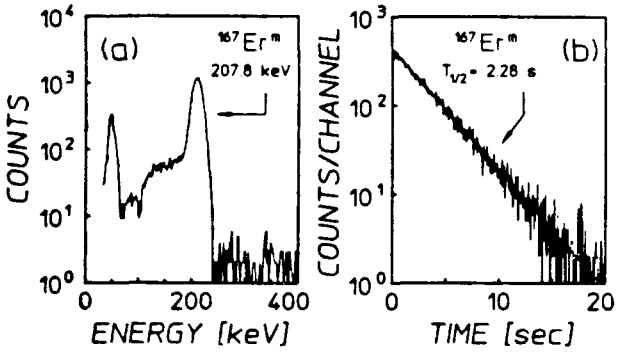

FIG. 4. Fluorescence data for the 207.8 keV line from the decay of $^{167}Er^{m}$ following a 6 MeV exposure. These were obtained with a 7.6 cm×7.6 cm diameter NaI(Tl) detector having a 5.1 cm×2.5 cm diameter well. The sample was irradiated for 25 sec. (a) Pulse height spectrum obtained with a counting period 5 sec in duration after a transport time of 2.06 sec from the end of irradiation to the start of counting. (b) Total counting rates observed in successive dwell intervals of 0.05 sec as a function of the time elapsed from the start of the counting interval following a 6 MeV exposure. The solid line indicates the literature value of the half-life, 2.28 sec.

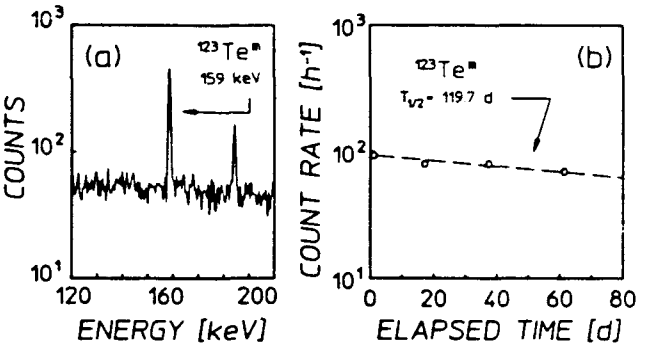

FIG. 5. Fluorescence data for the 159 keV line from the decay of $^{123}Te^{m}$ following a 6 MeV exposure. These were obtained with an *n*-type high-purity germanium detector. The sample was irradiated for 2 h. (a) Pulse height spectrum obtained with a counting period of 10 h duration after a delay from the finish of the irradiation of 22.98 h. (b) Points represent the counting rates in pulse height spectra at different elapsed times. The sizes of the symbols are comparable to one standard deviation and the counting periods were all 10 h. The dashed line shows the literature value for half-life of 119.7 d.

detection scheme. Since the isomer does not return to the ground state by a radiative transition, the number of excited nuclei must be measured by the detection of either β^- particles or the photons from the daughter nucleus. The ground state β^- decays with an end-point energy of 565 keV and the isomer β^- decays with end-point energies of 1313 keV (39.6%) and 1225 keV (60.4%). This difference allowed the use of a Cerenkov detector. Samples consisting of $LuCl_3$, dissolved in distilled water, were contained in polyethylene scintillation bottles. The Cerenkov threshold in water is about 250 keV and β^- particles emitted in the decay of the isomeric states were nearly 10 times more efficient in producing Cerenkov events than those emitted from ground state nuclei. Photons from these events were measured in coincidence, thereby recognizing only signals from the Cerenkov photons produced by single β^- particles. The detector was calibrated with ^{40}K decays from a KCl solution of known activity, since the resulting β^- particles had roughly the same end-point energy as those from $^{176}Lu^{m}$. In these measurements, the individual count rates were monitored to avoid contributions from accidental coincidences triggered by separate β^- events or by thermoluminescence from the material of the bottle. A fit to the experimental data shown in the typical spectrum of Fig. 6 produced a value for the half-life for $^{176}Lu^{m}$ of 3.58±0.05 h, which is in good agreement with the literature value of 3.63 h.

The yields of each of the final state populations were determined from the numbers of counts collected in the corresponding peaks in pulse height spectra. These raw data were then corrected in a standard manner for the photopeak detector efficiency, the fraction of fluorescence photons per decay, and the finite times of sample transport and counting. The latter factor used literature values of the half-lives.[15] It was also necessary to account

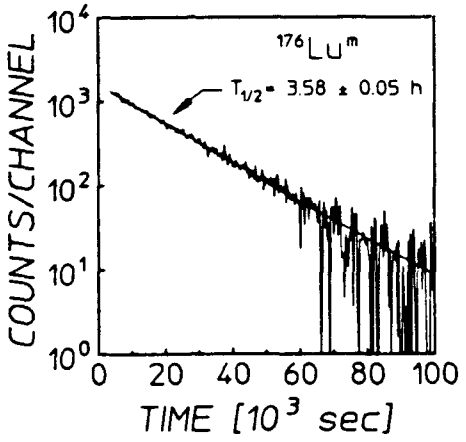

FIG. 6. Data typical of the counting rates observed in successive dwell time intervals of 320 sec for $^{176}Lu^m$ as a function of the time following a 6 MeV exposure. The sample was irradiated for 40 min and the delay time to the beginning of the counting was 53 min. A fit to the data is shown by the solid line for a half-life of 3.58±0.05 h, in good agreement with the literature value of 3.63 h.

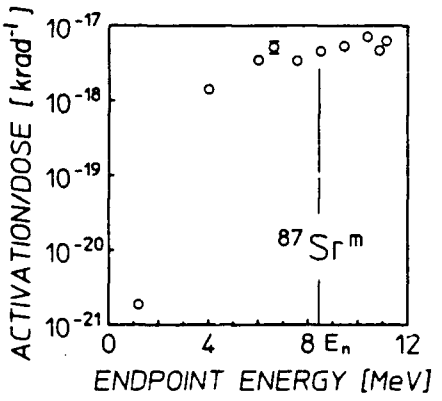

FIG. 7. Normalized activation obtained from irradiations with all four accelerators for $^{87}Sr^m$. The size of the symbols is comparable to one standard deviation except where error bars are explicitly shown. The point at 1.2 MeV determined from a DNA/PITHON exposure is an upper bound on the excitation since no fluorescence photons were observed above the level of background. The vertical line indicates the neutron evaporation threshold at $E_n = 8.4$ MeV.

for some attenuation of the fluorescence photons within the samples themselves because of absorption and scattering events. This effect was accommodated by Monte Carlo calculations of a transparency factor for each sample. These corrections were confirmed by comparing the activations obtained from targets containing identical materials, but in different geometries.

RESULTS

Strontium as a benchmark

Normalized activation measurements obtained from all four accelerators for $^{87}Sr^m$ are shown in Fig. 7, which also indicates the threshold energy for (γ,n) reactions, E_n at 8.428 MeV. The datum at 1.2 MeV represents an upper limit since no fluorescence photons were observed above the background level. Although lacking in resolution in the critical range from 1.2 to 6 MeV, the data allow several conclusions to be drawn about the photoexcitation process. First is that there is no evidence to support the participation of any nonresonant processes. This type of mechanism, if present, would be heavily dependent upon the density of nuclear states, which rises sharply at energies approaching E_n. The slow increase in the excitation function above 6 MeV relative to the change seen below 4 MeV precludes this as the dominant means of photoexcitation.

The large increase in normalized activation from 1.2 to 4 MeV indicates that at least one resonant gateway of significant magnitude lies in that range. The experimental resolution, however, does not allow a clear observation of the activation edges so the details of these states cannot be directly determined.

Fortunately, the isomer $^{87}Sr^m$ is distinguished by the degree to which its photoexcitation has been characterized in the literature. An early work[19] examined the production of this isomer by bremsstrahlung with end points which could be varied up to 3 MeV. The tunability of that device allowed three distinct gateways to be identified at 1.22, 1.88, and 2.66 MeV, and their integrated cross sections to be measured. In the usual units of 10^{-29} cm^2 keV, these were found to be 8.5^{+4}_{-3}, 16^{+8}_{-5}, and 380^{+200}_{-100}, respectively.

Figure 8(a) shows the ^{87}Sr data together with the nor-

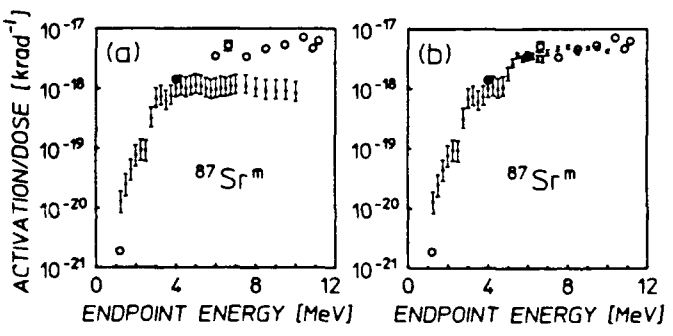

FIG. 8. Open circles plot normalized activations obtained from irradiations with all four accelerators for $^{87}Sr^m$ as previously shown in Fig. 7. Also displayed as solid bars are excitation functions calculated from Eq. (1) for the following: (a) Expected photoexcitation through the three known gateways of Ref. 19. The error bars indicate the uncertainties in the measurements of $(\sigma\Gamma)$ in that work. (b) Expected photoexcitation through the three known gateways plus that of a hypothetical state near 5 MeV with an integrated cross section on the order of 4000×10^{-29} cm^2 keV. The error bars indicate only the uncertainties in the measured $(\sigma\Gamma)$ of Ref. 19.

malized activations that should have been excited through the known gateways by photons with energies below 4 MeV. These values were calculated from Eq. (1) for different end-point energies by using typical bremsstrahlung spectra scaled from those shown in Fig. 3. The composite graph produced in this way exhibits the required activation edges at 1.22 and 2.66 MeV in agreement with the actual measurements. No edge is apparent at 1.88 MeV, but this is due to the comparable magnitude and proximity of this level to the one at 1.22 MeV. The correlation of the expected values near 4 MeV with the datum there indicates that no new states are required to explain all of the normalized activation obtained with the 4 MeV linac.

The data above 6 MeV in Fig. 8(a) significantly exceed the photoexcitation which could have been produced through the three known gateways. This extra activation must have therefore represented (γ,γ') reactions which proceeded through one or more unidentified levels. The simplest picture which matches the data is that of a single gateway near 5 MeV with an integrated cross section of the order of 4000×10^{-29} cm^2 keV. The normalized activation expected from this state, as well as those previously identified, is shown in relation to the experimental data in Fig. 8(b).

The nuclide ^{87}Sr provides a benchmark for other (γ,γ') studies since this is the only instance in which the current work can be compared with earlier experiments over a significant range of energies. It is apparent that the present measurements of the photoexcitation of ^{87}Sr^m below 4 MeV are completely explained by resonant absorption of photons through gateways already reported in the literature.[19]

Nuclide survey

All of the nuclei of Table I were irradiated with at least three of the four accelerators available. In all cases the general phenomenology seen in Fig. 7 was reproduced, but with considerable variance in the heights of the plateaus of activation reached at the higher energies. A typical example is shown in Fig. 9, which displays data obtained for the isomer ^{167}Er^m along with those for ^{87}Sr^m. Several interesting aspects are apparent. Although the normalized activations achieved with ^{167}Er nuclei are nearly two orders of magnitude larger than those of the ^{87}Sr benchmark, both isomers display similarly slow increases in activation above 6 MeV. This is surprising since nonresonant processes might be expected to be more significant for the photoexcitation of a nucleus as massive as ^{167}Er. Nevertheless, resonant absorption appears to be the dominant means of isomeric production for this nucleus as it was for the benchmark nuclide. The increase in normalized activation between the 4 and 6 MeV data strongly implies that a large gateway lies in this range. The magnitude of the data near 1.2 MeV suggests that a smaller activation edge lies at lower energy.

The measurements obtained from several nuclides, ^{77}Sr, ^{79}Br, ^{111}Cd, and ^{115}In allowed the identification of resonances below 1.5 MeV. The integrated cross sections of those were found to be on the order of 1 to 10×10^{-29} cm^2 keV, and results were reported previously.[9,10,13,14] The isotope, ^{179}Hf, while not providing such detailed information, did indicate an activation edge at about 1.1 MeV for its 18.7 sec isomer ^{179}Hf^m. Its excitation function is displayed in Fig. 10 and again the relatively slow

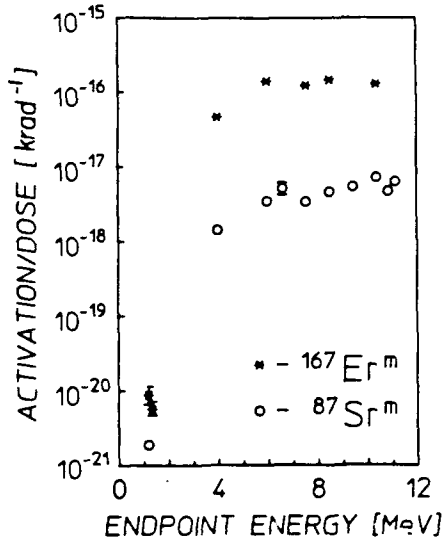

FIG. 9. Normalized activation obtained from irradiations with all four accelerators for ^{167}Er^m. Also included for the purpose of comparison are those values for ^{87}Sr^m. The size of the symbols is comparable to one standard deviation except where error bars are explicitly shown. The point at 1.2 MeV for ^{87}Sr^m determined from a DNA/PITHON exposure is an upper bound on the excitation since no fluorescence photons were observed above the level of background. The neutron evaporation thresholds for ^{167}Er and ^{87}Sr are 6.4 and 8.4 MeV, respectively.

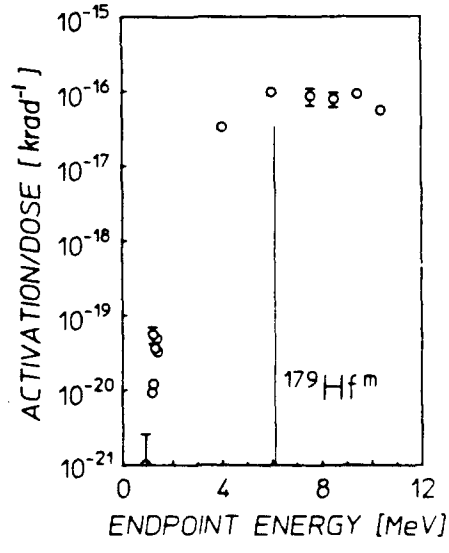

FIG. 10. Normalized activation obtained from irradiations with all four accelerators for 18.7 sec ^{179}Hf^m. The size of the symbols is comparable to one standard deviation except where error bars are explicitly shown. The vertical line indicates the neutron evaporation threshold at $E_n = 6.1$ MeV.

rise at high energies suggests resonant photoexcitation even for this large nucleus.

The absence of any evidence for nonresonant excitation made it useful to tabulate the results of this work in terms of an effective integrated cross section $(\sigma\Gamma)$, which was a weighted average of the actual values appearing in Eq. (1),

$$(\sigma\Gamma)\equiv\sum_j(\sigma\Gamma)_{fj}\frac{F(E_j,E_0)}{F(2.125,E_0)}\ . \tag{3}$$

The choice of normalizing the relative intensities to 2.125 MeV was arbitrary. However, since the excitation enegies of all of the dominant gateways exceeded 2.125 MeV and since $F(2.125,E_0)>F(E_j,E_0)$ for those gateways, the ratio used to weight individual $(\sigma\Gamma)_{fj}$ in Eq. (3) was always less than unity. This insured that the effective $(\sigma\Gamma)$ was not greater than the sum of all integrated cross sections for a particular nuclide. Substitution of Eq. (3) into Eq. (1) gives

$$(\sigma\Gamma)=\frac{N_f}{N_i\Phi_0F(2.125,E_0)}\ , \tag{4}$$

which in turn shows the effective $(\sigma\Gamma)$ to be the value that would have been necessary for a gateway at 2.125 MeV to produce the observed activation. The results are shown in Table II for the two different values of E_0 of the bremsstrahlung from the two linacs.

Neutron excitations

All of the accelerators used, other than DNA/PITHON, were capable of evaporating neutrons from their environments. Since neutrons can also excite nuclei into their isomeric states it was important to determine the amount of normalized activation which was attributable to these particles. In principle, two types of neutron reactions could have occurred: inelastic (n,n') reactions which would have required hot neutrons and neutron capture (n,γ) processes driven by fluxes of thermal or epithermal neutrons.

Contributions to the observed activations from (n,γ) reactions could be directly determined. The thermal neutron fluxes were measured by irradiating two thin indium foils, one of which was shielded from thermal neutrons by a cadmium cover. In accordance with standard techniques,[22] energy spectra obtained from these foils were examined after exposure for photons from the isomer $^{116}In^m$, which is produced by a branch of the reaction $^{115}In(n,\gamma)^{116}In^{m,g}$. In all cases such activations were negligible. For example, the magnitudes of the fluorescence lines observed in both the bare and the shielded

TABLE II. Summary of experimental results. The quantity ΔJ is the change in spin between ground state and isomer. For both 4 and 6 MeV irradiations, the integrated cross sections of a single gateway state at the reference energy of 2.125 MeV are given as $(\sigma\Gamma)$ and have been corrected for thermal and epithermal neutron contaminations. The ratio of 6 MeV values to those at 4 MeV are given as κ_1. The ratio of integrated cross sections obtained from 10.4 MeV to 6 MeV measurements is κ_2. Also given is the fraction of thermal and epithermal neutron contamination in the total activation, A_n/A_{tot}. The comment NA is used in the column for A_n/A_{tot} when no naturally abundant parent is available for (n,γ) reactions. An entry NA in the κ_2 column indicates that this information is not currently available.

		4 MeV		6 MeV			
Nuclide	ΔJ	$(\sigma\Gamma)$ (10^{-29} cm^2 keV)	A_n/A_{tot} (%)	$(\sigma\Gamma)$ (10^{-29} cm^2 keV)	A_n/A_{tot} (%)	κ_1	κ_2
^{167}Er	3	4600±110	0.01	34000±360	0.32	7.4	1.0
^{79}Br	3	660±17	NA	1900±23	NA	2.9	1.5
^{191}Ir	4	7600±610	NA	36000±960	NA	4.7	NA
^{197}Au	4	2600±40	NA	13000±64	NA	5.0	NA
^{89}Y	4	9±5	NA	260±8	NA	29	2.9
^{77}Se	3	330±4	0.03	6500±32	0.76	20	NA
^{179}Hf	4	9400±120	0.04	25000±110	6.41	2.7	1.1
^{137}Ba	4	330±23	<0.01	1900±23	0.07	5.8	1.4
^{199}Hg	6	260±10	0.05	1400±42	5.40	5.4	NA
^{111}Cd	5	920±12	<0.01	2500±44	0.07	2.7	NA
^{113}In	4	1300±59	NA	4700±180	NA	3.6	0.71
^{87}Sr	4	390±13	<0.01	870±18	0.89	2.2	2.3
^{176}Lu	6	14000±95	0.01	35000±2300	1.51	2.5	NA
^{115}In	4	1800±16	NA	6700±14	NA	3.7	1.5
^{180}Ta	8	18000±6600	NA	35000±650	NA	1.9	NA
^{135}Ba	4	1300±62	<0.01	6000±110	0.39	4.6	4.0
^{195}Pt	4	3000±160	<0.01	14000±220	0.03	4.7	NA
^{117}Sn	5	320±47	<0.01	880±26	0.07	2.8	0.84
^{123}Te	5	4200±730	<0.01	6800±320	1.45	1.6	NA

samples allowed the determination of the thermal neutron flux of 12 neutrons cm^{-2} sec^{-1} in the 6 MeV linac environment. The contributions to the activations from thermal neutrons are summarized in Table II for each of the 19 nuclides studied.

Because of a beryllium window used in the construction of the 6 MeV linac, that environment had the largest neutron flux. Nevertheless, the results of Table II show that under no conditions did the thermal neutrons contribute more than a few percent of the activation. In most cases neutron contamination represented a few $\times 10^{-4}$ fraction of the observed activations from the 6 MeV linac. The fast neutron flux was expected to be even less important and attempts to record any flux with the (n,p) reactions of ^{46}Ti, ^{47}Ti, and ^{58}Ni were completely negative. Calculations indicated a flux of fast neutrons from the photodisintegration of environmental sources consistent with this negative and limited contamination from (n,n') reactions to tenths of a percent.

CONCLUSIONS

The principal conclusion of this work is that some of the integrated cross sections for exciting isomers can be extraordinarily large, approaching 10^{-21} cm^2 eV. This is about three to four orders of magnitude larger than what has been usually reported in the past.

Typified by the reaction $^{167}Er(\gamma,\gamma')^{167}Er^m$, these enhanced processes seem to occur through discrete gateways or through narrow bands of gateway states. The data of Fig. 9 for ^{167}Er have a compelling resemblance to those for the excitation of ^{87}Sr which is known to occur through a few discrete levels. The same sharp jump in activation with increasing x-ray end point is followed by relatively level yield up to 11 MeV. It is possible to fit the data for ^{167}Er with a single gateway near 4 MeV but this is not a unique choice. The excitation function for the reaction $^{179}Hf(\gamma,\gamma')^{179}Hf^m$ shown in Fig. 10 also seems compelling in suggesting a single jump in activation at energies below 4 MeV. Table II shows that more than half of the 19 reactions studied had (γ,γ') reaction channels producing isomers with integrated cross sections greater than 1000×10^{-29} cm^2 keV.

The possibility that these unexpectedly large channels for the photoexcitation of isomers were the results of poor calibrations of fluxes was minimized by the use of four different accelerators in diverse environments and by the fact that the yields of the reaction $^{87}Sr(\gamma,\gamma')^{87}Sr^m$ up to 4 MeV were completely explained by the accepted values of integrated cross sections. Contamination of the products by activations from photoneutrons was shown to be generally less than 1%. It would seem that these enhanced channels for (γ,γ') reactions are the results of surprisingly favorable transitions to intermediate states that can be excited at energies less than 4 MeV. Earlier works reported in the literature were generally limited to 3 MeV and did not find activations of this magnitude, so it would be reasonable to speculate that these highly favored channels might lie between 3 and 4 MeV above the ground state.

While the ratios of activations found with 4 MeV bremsstrahlung to that produced around 1 MeV were of the order of thousands, the further increases from 4 to 6 MeV were much smaller. In Table II, the quantity κ_1 summarizes the increases in activation produced by raising the end point from 4 to 6 MeV and the quantity κ_2 records the further change resulting from an increase from 6 to 10 MeV. With a few obvious exceptions, the general trend supports the hypothesis that the principal nuclear structure responsible for the order-of-magnitude enhancement of (γ,γ') reactions lies below 4 MeV. Much smaller increases occur between 4 and 6 MeV and perhaps none between 6 and 10 MeV. Despite the care taken in reconciling the different environments, values of $0.7 \le \kappa_2 \le 1.5$ are probably not significantly different from unity. There is no persuasive evidence that additional channels opened between 6 and 10 MeV. In turn, this seems to imply that the giant dipole resonances have nothing to do with the enhancement of these (γ,γ') reactions.

The difficulties in explaining the sizes of the integrated cross sections reported in this work accrue from the large changes in angular momentum, J separating ground states from isomers. Most of the larger values belong to nuclei which are spheroidal and the projections of angular momentum, K, upon the axes of elongation differ greatly in ground and isomeric states. With an absorption transition of reasonable probability, changes in J and K are limited to $\Delta J \le 2$ and $\Delta K \le 2$. While the first might be satisfied by making a transition from the ground state to a high member of a rotational band built upon the final state, the second would be violated because K is conserved within a rotational band. What is needed is a mechanism to mix K values of nuclear levels belonging to rotational bands built upon initial and final states of the (γ,γ') reaction.

It is interesting to speculate that this might occur as a result of couplings to states built upon cores of nonfissioning shape isomers.[23] Such states show double minima in energy as functions of elongation, even at low values of spin. At some values of excitation energy the shape of such a nucleus would be unstable and projections upon its principal axes would no longer be conserved. In this way the transition from a K value characteristic of the ground state to one consistent with the isomer might occur by mixing with such a state. In any case the frequency with which giant values of integrated cross sections for photoexcitation were found in this work argues for some type of core property varying slowly with increasing nuclear size. Further work is needed to resolve the precise cause of this phenomenon.

This work was supported by the Strategic Defense Initiative Organization/Innovative Science and Technology Directorate and directed by the Naval Research Laboratory.

*Present address: High Energy Laser Associates, Oakland, CA 94611.
†Present address: Plasma Physics Department, Soreq Nuclear Research Center, Israel.
‡Present address: The University of Texas Southwestern Medical Center, Dallas, TX 75235.

[1]See, for example, the review, S. S. Dietrich and B. L. Berman, At. Data Nucl. Data Tables **38**, 199 (1988).
[2]B. Pontecorvo and A. Lazard, C. R. Acad. Sci. **208**, 99 (1939).
[3]G. B. Collins, B. Waldman, E. M. Stubblefield, and M. Goldhaber, Phys. Rev. **55**, 507 (1939).
[4]Y. Watanabe and T. Mukoyama, Bull. Inst. Chem. Res., Kyoto Univ. **57**, 72 (1979).
[5]M. Krcmar, A. Ljubicic, K. Pisk, B. Logan, and M. Vrtar, Phys. Rev. C **25**, 2097 (1982).
[6]I. Bikit, J. Slivka, I. V. Anicin, L. Marinkov, A. Ruydic, and W. D. Hamilton, Phys. Rev. C **35**, 1943 (1987).
[7]M. Krcmar, A. Ljubicic, B. A. Logan, and M. Bistrovic, Phys. Rev. C **33**, 293 (1986).
[8]E. B. Norman, S. E. Kellogg, T. Bertram, S. Gil, and P. Wong, Astrophys. J. **281**, 360 (1984).
[9]J. A. Anderson and C. B. Collins, Rev. Sci. Instrum. **58**, 2157 (1987).
[10]J. A. Anderson and C. B. Collins, Rev. Sci. Instrum. **59**, 414 (1988).
[11]Walter R. Nelson, Hideo Hirayama, and David W. O. Roger, SLAC Report 265, 1985.
[12]J. A. Halbleib and T. A. Mehlhorn, Sandia National Laboratories Report SAND84-0573, 1984.
[13]J. A. Anderson, M. J. Byrd, and C. B. Collins, Phys. Rev. C **38**, 2833 (1988).
[14]C. B. Collins, J. A. Anderson, Y. Paiss, C. D. Eberhard, R. J. Peterson, and W. L. Hodge, Phys. Rev. C **38**, 1852 (1988).
[15]*Evaluated Nuclear Structure Data File,* Information Analysis Center Report BNL-NC5-51655 (Brookhaven National Laboratory, Upton, New York, 1983).
[16]C. B. Collins, C. D. Eberhard, J. W. Glesener, and J. A. Anderson, Phys. Rev. C **37**, 2267 (1988).
[17]J. J. Carroll, J. A. Anderson, J. W. Glesener, C. D. Eberhard, and C. B. Collins, Astrophys. J. **344**, 454 (1989).
[18]C. B. Collins, J. J. Carroll, T. W. Sinor, M. J. Byrd, D. G. Richmond, K. N. Taylor, M. Huber, N. Huxel, P. v. Neumann-Cosel, A. Richter, C. Spieler, and W. Ziegler, Phys. Rev. C **42**, 1813 (1990).
[19]E. C. Booth and J. Brownson, Nucl. Phys. **A98**, 529 (1967).
[20]B. Bernstein and I. B. Smith, IEEE Trans. Nucl. Sci. **NS-20**, 294 (1973).
[21]R. Mohan, C. Chui, and L. Lidofsky, Med. Phys. **12**, 595 (1985).
[22]*ASTM Standard Method for Determining Thermal Neutron Reaction and Fluence Rates by Radioactivation Techniques,* Publication E 262-86 (American Society for Testing and Materials, Philadelphia, 1987), and references cited there.
[23]M. Girod, J. P. Delaroche, D. Gogny, and J. F. Berger, Phys. Rev. **62**, 2452 (1989).

Comment on "Resonant and nonresonant contributions to the photoactivation of ^{111}Cd"

P. von Neumann-Cosel and A. Richter
Institut für Kernphysik, Technische Hochschule Darmstadt, D-6100 Darmstadt, Germany

J. J. Carroll and C. B. Collins
Center for Quantum Electronics, The University of Texas at Dallas, P. O. Box 830688, Richardson, Texas 75083
(Received 2 January 1991)

The most recent investigation of the photoactivation of isomeric nuclei reported by Krčmar *et al.* continues to contain a strong contribution from nonresonant channels. In this Comment we report that integrated cross sections for resonant photoactivation of isomeric levels in ^{87}Sr, ^{111}Cd, and ^{113,115}In have been calculated from recent nuclear structure data and compared to those experimental results which assert that nonresonant contributions are important. The latter have shown systematically smaller values and the amount of missing resonant strength can be correlated to the magnitude of nonresonant cross section found in these investigations. Monte Carlo simulations of realistic experimental geometries display important components in the photon fields, resulting from environmental Compton scattering, which have been omitted in previous analyses of experimental data. The strength and shape of this contribution as a function of the experimentally important parameters suggest that the data can be explained entirely on the basis of a resonant excitation mechanism without any need to introduce a nonresonant contribution.

Photoactivation cross sections for the reaction ^{111}Cd$(\gamma,\gamma')^{111}$Cd^m have been inferred by Krčmar *et al.* [1] to proceed through *nonresonant* channels of excitation. The study of the photoactivation of isomeric states has a strong tradition in nuclear structure studies, and it has been generally accepted that the isomer population occurs via *resonant* excitation of higher-lying intermediate states which show finite branching ratios for a γ decay (or a cascade) to the isomer. Nonresonant cross sections from higher-order photonuclear interactions are typically many orders of magnitude smaller and have never been considered important for these reactions. However, in the last few years a series of experiments has been performed [2–4] on the photoactivation of ^{115,113}In^m, ^{111}Cd^m, and ^{87}Sr^m in order to search for possible nonresonant contributions. The paper [1] upon which we comment is the most recent example in this series.

The experiments designed to show nonresonant excitation typically involved strong ^{60}Co sources. The methodology depended upon the distortion of the source spectrum by interposing lead scatterers of varying thickness. In this way the ratio of photon fluxes at energies of resonant intermediate states and at source-line energies were changed in a definite way. The intensities at the energies of the source lines were believed to dominate the nonresonant interaction. The excitation probability per unit time of the isomeric level, P, was then fitted to a sum of resonant and nonresonant contributions:

$$P=\Phi_R(E_R)\sigma\Gamma_R+\Phi_{\mathrm{NR}}\sigma_{\mathrm{NR}}\ \mathrm{s}^{-1}\ . \tag{1}$$

In this expression Φ_R was the photon flux at resonance energy E_R, $\sigma\Gamma_R$ represented the integrated isomeric cross section from resonance fluorescence, Φ_{NR} was the nonresonant photon flux integrated over energy, and σ_{NR} was a total nonresonant cross section.

The authors of Refs. [1–4] (called the Zagreb group hereafter) claim that the nonresonant contribution to the population of isomers is significant and even dominates in experiments using radioactive sources. Because of its potential importance, these findings stimulated a series of experimental and theoretical work over the last years. Hot atom chemical studies [5] and investigations using bremsstrahlungs sources [6,7] found no evidence for nonresonant cross sections in ^{115}In and ^{111}Cd. Bikit *et al.* [8] repeated the ^{111}Cd experiment of Ref. [3], but used iron instead of lead scatterers. They, too, report a null result within experimental limits. All attempts to explain theoretically such a strong nonresonant excitation mechanism have failed so far [2,9,10].

Most recently, the Zagreb group has repeated the ^{111}Cd experiment including iron scatterers also [1]. They report large nonresonant cross sections independent of the absorber type or excitation energy of the dominant resonant intermediate state, which is not well established in ^{111}Cd. A comprehensive discussion of their views of the validity of the experiments described in Refs. [5–8] is additionally presented.

We would like to discuss several aspects which raise serious doubts about the results presented in Refs. [1–4]. In particular, we will compare their results to resonant cross sections calculated from recent nuclear structure data and show that their results deviate significantly in those cases where the largest nonresonant contribution is obtained with their method. We will further show that an accurate knowledge of the impinging photon field is crucial for the data analysis. The incident spectrum depends strongly upon the experimental environment, and the approximation used for the unknown photon field in

those experiments [1–4] turns out to be poor. The neglect of forward Compton scattering in collimators and other environmental material could have led to severe errors.

Discussion of nuclear structure data.—The excitation probability of isomeric levels through resonant photon absorption to intermediate states can be calculated easily when the relevant quantum numbers of the intermediate states are known. The integrated cross section is given by

$$\sigma\Gamma_R = \frac{\lambda^2}{4}\,\frac{2J_f+1}{2J_i+1} b_0 b_{\rm iso}\Gamma\ , \qquad (2)$$

with $b_0=\Gamma_0/\Gamma$, $b_{\rm iso}=\Gamma_{\rm iso}/\Gamma$, and $\lambda=2\pi\hbar c/E_R$. The quantity E_R denotes the energy of the intermediate state, $J_{i,f}$ are the spins of the initial and final states, Γ and Γ_0 represent the total and partial widths for direct decay to the ground state, and $\Gamma_{\rm iso}$ is the effective partial decay width to the isomer (including possible cascades). The branching ratios b_0, $b_{\rm iso}$, and Γ (or the lifetime $\tau=\hbar/\Gamma$) or Γ_0 have been measured with a variety of experimental methods for the nuclei studied by the Zagreb group. Table I presents adopted values from the most recent Nuclear Data Sheets plus additional results from new experiments. It has been argued in Ref. [2] that such a comparison shows variations of the different experimental data much too wide to allow for any conclusion. Thus this question will be discussed in detail for the nuclides studied.

^{115}In. Two resonant states are known in the energy region accessible by ^{60}Co sources. The lower level at 0.941 MeV contributes roughly an order of magnitude less to the isomer cross section than the state at 1.078 MeV. The branching ratios have been measured by various methods including Coulomb excitation, β decay, and $(n,n'\gamma)$ reactions [11]. There is, however, a discrepancy of the $(n,n'\gamma)$ results adopted in Ref. [11] with two $(n,n'\gamma)$ studies [12, 13] quoting significantly larger $b_{\rm iso}$ values (35–40 %) for the 1.078-MeV state. At first sight this is surprising, since $(n,n'\gamma)$ results were generally found to agree well with each other, as well as with other experiments. A closer inspection of the original γ spectra resolves the problem. The corresponding γ transition is placed on the tail of a much stronger line with a separation in energy close to the resolution of the detectors used. Accordingly, results are very sensitive to small variations of the line shape, and a systematic error must be assumed for the integration, which might easily reach a factor 2 or more.

The lifetime has been measured by Coulomb excitation [14] and nuclear resonance fluorescence [15] (NRF) with reasonable agreement of both results. Some older NRF experiments quote a larger total width [16,17], but Ref. [16] gives a very large error. The most recent NRF experiment is considered superior to Ref. [17] because the critical evaluation of the bremsstrahlung flux and spectral distribution was achieved from a consistent set of self-absorption measurements. In any case the integrated cross section calculated is at least 2 times bigger than the result of Ref. [2]. The agreement with recent experimental work [5,6] and with the older survey of Booth and Brownson [18] is acceptable. Allowing for the Γ values of Refs. [16,17] would only enlarge the discrepancy with Ref. [2].

^{113}In. The result of Ref. [4] is roughly 40% smaller than the calculation, if one includes the weaker 1.021-MeV level. Again, the branching ratios are well defined by different experiments [19], but the lifetimes are given only by one measurement [14]. While this allows the possibility for some systematic error, the agreement might still be regarded as acceptable. The only other experimental result [18] on $^{113}In^m$ shows an error compatible with both the calculation and Ref. [4].

^{111}Cd. No calculations can be performed for ^{111}Cd, since the branching ratios are not known and since there are conflicting results about the excitation energy of the main resonant state [1,7,18,20]. Recent studies have re-

TABLE I. Energies, spins, half-lives, and branching ratios of resonant intermediate states populating $^{87}Sr^m$, $^{111}Cd^m$, and $^{113,115}In^m$ that could be excited in ^{60}Co source experiments. The calculated integrated cross sections are compared to values for the resonant and nonresonant contributions derived by the Zagreb group [1–4].

Nucl.	E_x (MeV)	J^π	$T_{1/2}$ (ps)	b_0 (%)	$b_{\rm iso}$ (%)	Calc. $\sigma\Gamma_R$ (μb keV)	Zagreb group[a] $\sigma\Gamma_R$ (μb keV)	$\sigma_{\rm NR}$ (nb)
^{115}In	0.941	$\frac{5}{2}^+$	15.1(1.4)	88(2)	12(2)	8(1)		
	1.078	$\frac{5}{2}^+$	0.99(10)	83(2)	16(2)	120(15)	54(7)	380(40)
^{113}In	1.021	$\frac{5}{2}^+$	3.6(3)	89(2)	11(2)	23(2)		
	1.131	$\frac{5}{2}^+$	0.97(7)	85(2)	14(2)	101(9)	81(1)	20(3)
^{111}Cd	1.190[b]						78(8)[c]	10(3)[c]
							97(6)[d]	7(3)[d]
	1.330[b]						62(5)[c]	12(2)[c]
							83(5)[d]	10(2)[d]
^{87}Sr	1.229	$\frac{5}{2}^+$	0.97(35)	86(3)	14(3)	86(33)	47(7)	32(4)

[a]For other experimental $\sigma\Gamma_R$ results see Table I in Ref. [6] (^{115}In), Ref. [18] (^{113}In), Table I in Ref. [7] (^{111}Cd), and Table I in Ref. [4] (^{87}Sr). [b]Assumed energy of the main intermediate state. [c]Results obtained with lead scatterer/absorber. [d]Results obtained with iron scatterer/absorber.

vealed a low-lying state which is probably the last step of cascades towards the isomer [21], but the intermediate states for photoabsorption were not discovered. Németh and Veres [22] have constructed a possible scheme of levels assuming a similarity to the nuclear structure of the lowest intermediate states in ^{87}Sr and ^{113,115}In. It should be noted, however, that the ground state and isomeric spins completely differ ($\frac{1}{2}^+ \rightarrow \frac{11}{2}^-$ for ^{111}Cd and $\frac{9}{2}^+ \rightarrow \frac{1}{2}^-$ for the others). A similar structure of the last three is suggested by the single neutron (Sr) or proton (In) hole relative to the shell closure $N=50$. A microscopic analysis within the unified model [23,24] shows indeed that the wave functions of all three main intermediate states are dominated by amplitudes of $[(A+1,2_1^+)\otimes g_{9/2}^{-1}]_{5/2+}$ character, while the structure of a corresponding state in ^{111}Cd depends on a completely different region of valence single-particle and hole states.

Certainly, further experimental clarification of the ^{111}Cd low-energy spectrum is needed. The resonant cross sections for the population of the isomer in Ref. [1] are within the bandwidth of other experimental results, and no further conclusions are possible. However, it seems remarkable that the $\sigma\Gamma_R$ values presented in Ref. [1] disagree with each other, depending on the scatterer type (iron or lead).

^{87}Sr. The branching ratios are averages of three different experimental methods [25–27], which agree with each other within 3%. A half-life measurement obtained from the Doppler shift attenuation method is given by Ref. [26]. The calculated value agrees with Ref. [18], but the result of Ref. [4] is significantly smaller, even regarding the error quoted for the half-life value.

The discussion shows that the integrated cross sections for resonant isomer excitation given by the Zagreb group are generally smaller than values calculated from nuclear structure data characterized and established by a variety of independent experimental methods. A clear correlation can be found between the missing resonant cross section and the magnitude of the nonresonant cross section derived in Refs. [1–4]. This points toward problems related to the data analysis of their experimental method, which we address next.

Monte Carlo simulations.—A crucial point of all photoactivation experiments is the characterization of the incident photon field. The spectra resulting from strong radioactive sources (of the order of kCi) cannot be measured easily. Thus the following approximation has been used [1–4,8] for the unknown variation with the thickness of the scatterer of Φ at the energies of the resonant states and of full-energy γ rays (defining Φ_{NR}): The function $f(E_R,d)$, describing the flux ratio, was taken from data measured with a weak ^{60}Co source which emits full-energy photons only. Because of the finite volume and additional shielding, typical for a strong source of the type used in the reported experiments, a certain fraction k is scattered out of the full-energy lines to form a low-energy tail even at $d=0$. Assuming that the distribution of k is constant in the vicinity of the resonance energies, k can be treated as a free parameter which is fixed by the data.

Neglecting small differences in the attenuation coefficients $\mu \simeq \mu(E_R) \simeq \mu(E_0)$, the reaction rate $P(d)$ is then given by [1–4,8]

$$P(d)=\frac{A}{4\pi r^2(1+k)} \times e^{-\mu d}\left\{\sigma_{NR}+\left[\frac{k}{\Delta E}+f(E_R,d)\right]\sigma\Gamma_R\right\}. \quad (3)$$

Here ΔE is the interval of energies over which k is distributed, and A and r represent the activity of the source and distance to the target, respectively. In Refs. [1–4,8] values for $\sigma\Gamma_R$, σ_{NR}, and k resulted from simultaneous least-squares fits to the experimental $P(d)$ values.

For the preparation of these comments, the validity of this approach was investigated in three aspects: (i) the approximations included in the term in square brackets of Eq. (3), (ii) the importance of the experimental environment as a source of additional Compton-scattered photons, and (iii) the influence of a collimator as used in Ref. [2]. The discussion is based on Monte Carlo simulations performed with the code GEANT [28]. The characteristic quantity

$$F(E_R,d)=\frac{N(E_R)}{\Delta E' N(E_0)} \quad (4)$$

is calculated for a variety of geometries and may be compared to $f(E_R,d)$ described above. The number $N(E_0)$ is determined by the sum of the contents of the intervals containing the 1.173- and 1.332-MeV lines, and $N(E_R)$ is averaged over $\Delta E'=50$ keV in order to improve statistics. In the case of ^{87}Sr, where the main intermediate state lies above the 1.173-MeV level, only the 1.332-MeV line is counted for $N(E_0)$.

(i) As an example, results for the 1.229-MeV state in ^{87}Sr are discussed. The characteristic ratio $F(E_R,d)$ is compared in Fig. 1 for a pointlike source, an extended cylindrical source of 1 cm^3 volume, and an extended source surrounded by 1 and 2 cm of lead shielding, respectively. The function obtained for the pointlike source, simulating $f(E_R,d)$ in Eq. (3), is shifted such that $k/\Delta E = F(E_R,0)$ for the extended source geometries. The agreement is acceptable, although a slightly slower increase with d is systematically indicated for the pointlike case. Such an effect would significantly alter the results of the Zagreb group, if source shielding material equivalent to 2 cm Pb or more was present in the experiments.

(ii) An important contribution not considered in Eq. (3) is the presence of *additional* photons at the resonance energies from scattering in the experimental environment. At energies around 1 MeV, the Compton cross sections are large and the Klein-Nishina formula is only moderately peaked in the forward direction. The schematic view of the experimental setup of the ^{87}Sr and ^{113}In measurements [4], presented in Fig. 4 of Ref. [29], indicates the presence of enough scattering material to provide a substantial contribution of this type. The geometry is simplified in the present calculations by replacing these scatterers with a lead cone having an open-

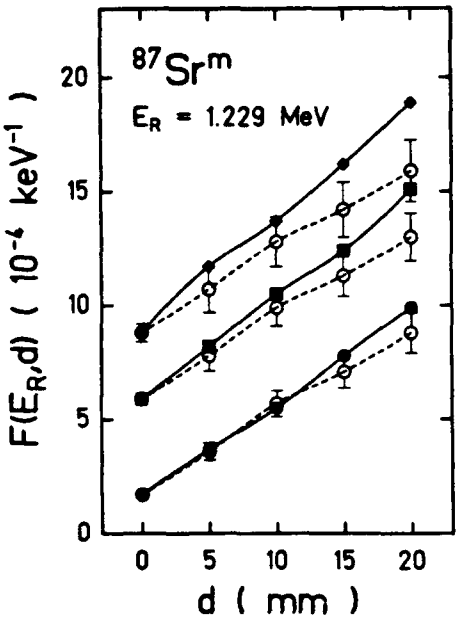

FIG. 1. Comparison of the photon flux at resonance energy E_R to the 1.332-MeV line flux for different geometries of a ^{60}Co source. The characteristic ratio $F(E_R,d)$ is shown as a function of the Pb scatterer thickness for a pointlike source (open circles), an extended source (solid circles), an extended source plus 1-cm Pb shielding (squares), plus 2-cm Pb shielding (diamonds). For details of the extended source geometry, see text. Statistical errors of the extended source calculations (not shown) are of the order of the symbol size. The straight and dashed lines are drawn to guide the eye.

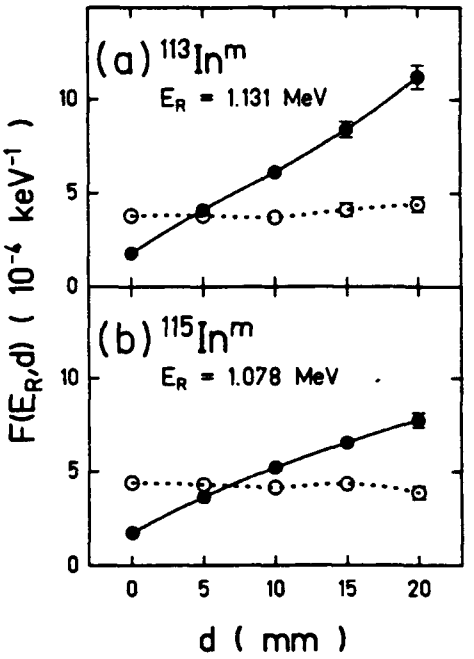

FIG. 2. Direct (solid circles) and scattered (open circles) contributions to $F(E_R,d)$ from the simulation of the experiments described (a) in Ref. [4] and (b) in Ref. [2]. For details, see text. The straight and dashed lines are drawn to guide the eye.

ing of 4 cm at the source, widening to 11 cm at a target distance of 22 cm. The source itself is assumed to be extended as described above and without additional lead shielding. Using ^{113}In as example, the contributions of the direct and indirect (i.e., scattered) parts are shown in Fig. 2(a) as a function of d by solid and open symbols, respectively. *The flux at resonance produced by scattered photons reveals a completely different functional behavior and even dominates at* $d=0$.

From Eq. (3) it is obvious that a roughly constant additional contribution directly competes with the σ_{NR} term. Because of the strength indicated by the calculations, any need for a nonresonant cross section to describe the $P(d)$ data in Ref. [4] is completely destroyed. This statement would still hold even if the geometry used were to overestimate the indirect contribution in the experiment up to a factor of about 4. Note that the additional photon flux cannot be accounted for by an increase of the parameter k in Eq. (3) because of the presence of the $(1+k)^{-1}$ factor.

(iii) An even more striking example of the role of Compton-scattered photons in the experimental analysis is found in the anomalously large nonresonant cross section reported [2] in ^{115}In (see Table I). In contrast to the other experiments, a collimator was used. While no further details of the collimator were given, we tried to follow the experiment description given in Ref. [2] as close as possible. A distance source target of 28 cm was chosen, and the target diameter and collimator width were set to 2.54 cm. The source description corresponds to case (ii). Figure 2(b) shows again that the shape of $F(E_R,d)$ differs completely for the direct and indirect contributions, and that the indirect flux even dominates in the absence of the lead/iron scatterers. The strength of scattered photons in such a geometrical arrangement is absolutely sufficient to explain the experimental $P(d)$ values in Ref. [2] without a nonresonant cross section. We also ascertained that this result is valid independent of a variation of the collimator radius within reasonable limits.

In conclusion, a comparison of experimental integrated cross sections for resonant photoexcitation obtained by the Zagreb group with results calculated from independent nuclear structure data shows systematic deviations. The amount of resonant cross section missing from the Zagreb measurements is closely correlated to the magnitude of the nonresonant cross sections they report.

We have shown with Monte Carlo simulations of typical experimental geometries that important parts of the photon spectra are missed in the approximation used by the Zagreb group for their data analysis. The computational results demonstrate the importance of additional photon flux resulting from Compton scattering in the experimental environment. In particular, the results derived for ^{115}In are severely affected by the use of a collimator, and the data analysis reported in those experiments must be reconsidered. This neglected contribution seems to be sufficient to explain all published experimental data without any need to introduce a nonresonant

cross section.

Finally, we remark that the calculations presented do not attempt to provide a detailed characterization of the experiments in Refs. [1–4], since not enough details were given there. A measurable nonresonant contribution to the photoexcitation of isomers cannot be definitely excluded by our arguments, but any claim for its existence from the experimental methods reported to date will have to be based on an accurate description of the photon field in the respective experimental geometry.

We are indebted to N. Huxel for his assistance with the Monte Carlo calculations. This work has been supported by the Bundesministerium für Forschung und Technologie of the Federal Republic of Germany under Contract No. 06DA184I.

[1] M. Krčmar, S. Kaučić, T. Tustonić, A. Ljubičić, B. A. Logan, and M. Bistrović, Phys. Rev. C **41**, 771 (1990).
[2] A. Ljubičić, K. Pisk, and B. A. Logan, Phys. Rev. C **23**, 2238 (1981).
[3] M. Krčmar, A. Ljubičić, K. Pisk, B. A. Logan, and M. Vrtar, Phys. Rev. C **25**, 2097 (1982).
[4] M. Krčmar, A. Ljubičić, B. A. Logan, and M. Bistrović, Phys. Rev. C **33**, 293 (1986).
[5] K. Yoshihara, Zs. Németh, L. Lakosi, I. Pavlicsek, and Á Veres, Phys. Rev. C **33**, 728 (1986).
[6] C. B. Collins, J. A. Anderson, Y. Paiss, C. D. Eberhard, R. J. Peterson, and W. L. Hodge, Phys. Rev. C **38**, 1852 (1988).
[7] J. A. Anderson, M. J. Byrd, and C. B. Collins, Phys. Rev. C **38**, 2838 (1988).
[8] I. Bikit, J. Slivka, I. V. Aničin, L. Marinkow, A. Rudić, and W. D. Hamilton, Phys. Rev. C **35**, 1943 (1987).
[9] K. Pisk, M. Krčmar, A. Ljubičić, and B. A. Logan, Phys. Rev. C **25**, 2226 (1982).
[10] R. Horvat, K. Pisk, and B. A. Logan, Phys. Rev. C **29**, 1614 (1984).
[11] J. Blachot and G. Marguier, Nucl. Data Sheets **52**, 565 (1987).
[12] A. Marcinkowski, A. Bäcklin, and I. Bergquist, Nucl. Phys. **A179**, 781 (1972).
[13] A. B. Smith, P. T. Guenther, F. J. Whalen, I. J. van Heerden, and W. C. McMurray, J. Phys. G **11**, 125 (1985).
[14] W. K. Tuttle III, P. H. Stelson, R. L. Robinson, W. T. Milner, F. K. McGowan, S. Raman, and W. K. Dengenhart, Phys. Rev. C **13**, 1036 (1976).
[15] Y. Cauchois, H. Ben Abdelaziz, B. Khérouf, and C. Schlesing-Möller, J. Phys. G **7**, 1539 (1981).
[16] M. Boivin, Y. Cauchois, and Y. Heno, Nucl. Phys. **A176**, 626 (1971).
[17] W. J. Alston III, Phys. Rev. **188**, 1837 (1969).
[18] E. C. Booth and J. Brownson, Nucl. Phys. **A98**, 529 (1967).
[19] J. Lyttkens, K. Nilson, and L. P. Ekström, Nucl. Data Sheets **33**, 1 (1981); J. Blachot, *ibid.* **59**, 729 (1990).
[20] M. Boivin, Y. Cauchois, and Y. Heno, Nucl. Phys. **A137**, 520 (1969).
[21] M. Vesković, I. Bikit, I. Aničin, W. D. Hamilton, J. Copnell, M. Krmar, and J. Slivka, Phys. Rev. C **42**, 588 (1990).
[22] Zs. Németh and Á. Veres, Phys. Rev. C **38**, 533 (1988).
[23] K. Heyde, P. van Isacker, M. Waroquier, J. L. Wood, and R. A. Mayer, Phys. Rep. **102**, 291 (1983).
[24] J. E. Kitching, Z. Phys. **258**, 22 (1973).
[25] S. K. Basu and A. P. Patro, J. Phys. G **3**, 701 (1977).
[26] L. P. Ekström, G. D. Jones, F. Kearns, T. P. Morrison, A. Nilsson, V. Paar, P. J. Twin, R. Wadsworth, F. Wallander, and N. J. Ward, J. Phys. G **7**, 85 (1981).
[27] C. Winter, B. Krusche, K. P. Lieb, H. H. Schmidt, T. von Egidy, P. Hungerford, F. Hoyler, and H. G. Börner, Nucl. Phys. **A460**, 501 (1986).
[28] R. Brun, F. Bruyant, M. Maire, A. C. McPherson, and P. Zanarini, CERN Report No. DD/EE/84-1, 1987.
[29] M. Krčmar, A. Ljubičić, B. A. Logan, and M. Bistrović, Nucl. Instrum. Methods A **255**, 99 (1987).

Physics Letters B 266 (1991) 9–13
North-Holland

PHYSICS LETTERS B

Resonant photoexcitation of isomers. $^{115}In^{m}$ as a test case ☆

P. von Neumann-Cosel, A. Richter, C. Spieler, W. Ziegler
Institut für Kernphysik, Technische Hochschule Darmstadt, W-6100 Darmstadt, FRG

J.J. Carroll, T.W. Sinor, D.G. Richmond, K.N. Taylor, C.B. Collins
Center for Quantum Electronics, University of Texas at Dallas, Richardson, TX 75083-0688, USA

and

K. Heyde
Institute for Theoretical Physics, Proeftuinstraat 86, B-9000 Ghent, Belgium

Received 17 April 1991

Large integrated cross sections for the photoexcitation of $^{115}In^{m}$ have been detected around $E_x = 3$ MeV. Complementary nuclear resonance fluorescence studies prove that the g.s. transition strength is largely confined to the same energy region and the intermediate excited states are identified. Unified-model calculations indicate magnetic dipole $1g_{9/2} \rightarrow 1g_{7/2}$ spin-flip transitions as the major excitation mechanism.

1. Introduction

The photoactivation of isomers has a long tradition in nuclear structure studies [1]. Most investigations have concentrated on two areas, viz. the region around particle threshold and the region of low excitation energies, typically $E_x < 2$ MeV. The former reveals information like the average ratio of isomeric to total photoabsorption cross sections [2] or serves as a test of statistical aspects of γ-decay at high excitation energies [3]. In the low energy regime, the isomer population occurs via resonant photoabsorption of selectively excited intermediate states which show a finite branching for a γ-decay (or a cascade) to the isomeric level. These intermediate levels provide unique nuclear structure information, often hardly accessible by other means [4].

☆ Work supported by the German Federal Minister for Research and Technology (BMFT) under contract number 06DA1841 and the Department of Defense through the Naval Research Laboratory.

Recent studies of the little explored energy region between these two extremes have shown surprising results. Very large cross sections for the population of isomeric states at energies $E_x \simeq 2$–4 MeV have been observed in a variety of nuclei [5,6]. By investigating the excitation function it has been demonstrated [7] for the special case of the deexcitation of $^{180}Ta^{m}$ that the resonant photoabsorption proceeds through two intermediate states only (or closely spaced groups within the experimental resolution of ≈ 200 keV). The corresponding cross sections are three orders of magnitude larger than typical values in other isomers below 2 MeV. Similar data have been reported [8] for the 120 d isomer in ^{123}Te. Besides the obvious question of a nuclear structure interpretation, these findings provide unexpected encouragement of schemes for pumping a γ-ray laser that depend upon the sudden deexcitation of isomeric populations [9].

The experiments presented in this letter are a first effort to gain some deeper understanding of the nuclear structure phenomena responsible for the results

described above. The choice of ^{115}In was based on several considerations: (i) The photoactivation of the $E_x = 0.335$ MeV, $J^\pi = \frac{1}{2}^-$ isomer in this isotope (g.s. $J^\pi = \frac{9}{2}^+$) is probably the most extensively studied case (see refs. [4,10,11] for references) and nuclear structure data are available [12] to completely determine the contribution of all intermediate states in the region below 2 MeV which is not covered in the present experiments. (ii) The large natural abundance (95.6%) easily permits a complementary nuclear resonance fluorescence (NRF) study which characterizes the levels important in photoabsorption in more detail. (iii) The low-energy part of the ^{115}In spectrum has been successfully described [13] within the unified-model approach [14] and an extension to somewhat higher energies seems promising. Thus, a microscopic interpretation of the mixing, which distinguishes the intermediate states, can be given. (iv) The vibrational odd–even nucleus ^{115}In can be regarded as a prototype for many isotopes in this mass region containing an isomer.

2. Photoactivation experiments

Experiments were performed at the superconducting linear electron accelerator (S-DALINAC) in Darmstadt [15]. Bremsstrahlungs spectra with endpoint energies $E_0 = 2$–5 MeV were generated by irradiating a Ta converter. Disks of nominally 1 g of natural Indium (diameter 3.8 cm) were placed in the photon beam. Typical irradiation times were 4 h with an average electron current of 20 μA. The endpoint energies were varied in steps of 125 or 250 keV. The characteristic 336 keV isomeric transition of ^{115}In, measured with a Ge(Li) detector, served as a signature of the activation and the yields were determined as described in ref. [7]. The isomeric yield N_f can be expressed as

$$N_f = N_t \int_{E_c}^{E_0} \sigma(E) \frac{\mathrm{d}\phi(E, E_0)}{\mathrm{d}E} \mathrm{d}E , \qquad (1)$$

where N_t denotes the number of target atoms, $\mathrm{d}\phi/\mathrm{d}E$ describes the spectral intensity per cm^2 of the photon field for an endpoint energy E_0, and $\sigma(E)$ is the resonant absorption cross section. A description of the incident photon spectra was obtained from calculations with the electron–photon transport code EGS4 whose general validity has been demonstrated [16]. The lower integral limit in eq. (1) is defined by a cut-off energy E_c in the calculations.

The typical widths of resonant intermediate states are small enough to assume that $\mathrm{d}\phi/\mathrm{d}E$ is constant over the resonance region. Then, eq. (1) can be simplified,

$$N_f = N_t \sum_j (\sigma\Gamma)^2_{iso} \phi(E_j, E_0) , \qquad (2)$$

with $(\sigma\Gamma)^2_{iso}$ giving the integrated cross section of the jth level. We note that nonresonant cross sections, which would inhibit the use of eq. (2), are not considered. Claims of important nonresonant contributions [17] to the photoexcitation of isomers have recently been disproved [18].

Information on new intermediate states is extracted from the experimental excitation function shown in fig. 1 by including calculated $(\sigma\Gamma)_{iso}$ values for all intermediate states below 2 MeV and then introduce a new state whenever a break in the excitation function requires additional strength. For the former, branching ratios and radiative widths are known [12] from independent experimental results. The integrated cross sections can be calculated from

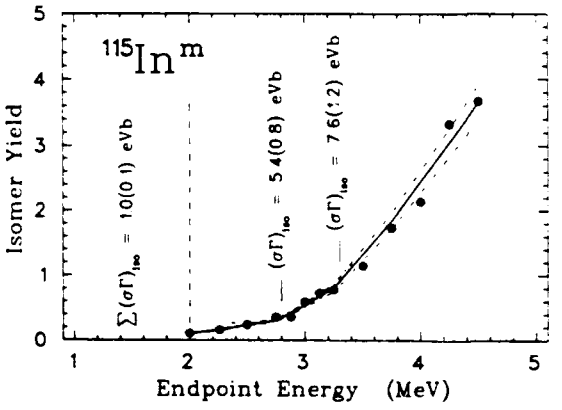

Fig. 1. Isomer yield as a function of endpoint energy. The straight line is calculated using intermediate states at 2.8 and 3.3 MeV with the strengths indicated. The contributions of states below 2 MeV are taken from the literature [12]. Statistical errors are smaller than the data point size. The error region spanned by the dashed lines additionally includes statistical errors of the photon spectra and an assumed 15% error for each individual $(\sigma\Gamma)^2_{iso}$ value.

$$(\sigma\Gamma)_{iso} = \pi^2\left(\frac{\hbar c}{E_\gamma}\right)^2 g \frac{\Gamma_0 \Gamma_{iso}}{\Gamma}, \quad (3)$$

with $g=(2J_f+1)/(2J_i+1)$. Here, $J_{i,f}$ are the spins of the g.s. and intermediate state, Γ_0 and Γ_{iso} are the partial g.s. width and the effective width to the isomer (including cascades), and Γ is the total width. A yield curve calculated in this way is presented as a solid line in fig. 1. No further states had to be included to describe the measured yields up to $E_x=2.8$ MeV. The breaks in the theoretical excitation function, where new states were introduced, are indicated in fig. 1 and the corresponding cross sections given.

3. Nuclear resonance fluorescence experiments

The experimental setup especially designed for NRF experiments is described in ref. [19]. An absolute calibration of the photon spectra was attained by the use of In/Al and In/B sandwich targets which provide well-determined reference transitions. In order to cover an energy range $E_x \simeq 1.5$–4.5 MeV, measurements were performed at endpoint energies $E_0=3.1$, 4.6 and 5.2 MeV. The variation of E_0 also enables us to distinguish g.s. transitions from decays to excited states. For details of the data analysis see ref. [19].

Integrated cross sections for g.s. transitions $(\sigma\Gamma)_0$ comparable to the isomer activation results, eq. (3), can be obtained from

$$(\sigma\Gamma)_0 = \pi^2\left(\frac{\hbar c}{E_\gamma}\right)^2 g \frac{\Gamma_0^2}{\Gamma} W(\Theta). \quad (4)$$

The additional factor $W(\Theta)$ accounts for the nonisotropic decay characteristic which depends on the multipolarity (dipole/quadrupole) and the mixing ration δ of E2 and M1 transitions. It can be shown that due to the large g.s. spin ($J^\pi=\frac{9}{2}^+$) results obtained in the present experimental geometry are insensitive within $\pm 10\%$ to the unknown final state spin as well as an arbitrary choice of the mixing parameter and the $W(\Theta)$ dependence can be neglected.

A full account of the NRF results will be given elsewhere [20]. Here, we present only results important for the isomer population and restrict the discussion of the lower energy region to a few comments in relation to other (γ, γ') studies. The agreement with the results of Cauchois et al. [21] is good, in particular for the 1.132 and 1.463 MeV state which they obtained with the self absorption technique. The correspondence to the results of Alston [22] is reasonable for stronger transitions and mediocre for the others. Below $E_x=2.5$ MeV, branching ratios have been measured [23] for all levels observed in the present study and assure that no significant partial width to the isomer is missed in the analysis of the excitation function.

The excitation energy region corresponding to the large $(\sigma\Gamma)_{iso}$ values is shown in the upper part of fig. 2. The brackets represent the experimental uncertainty of the energies of the intermediate states identified in the photoactivation. The striking results is that, except for a few moderate levels around 3.0 and 3.7 MeV, all (γ, γ') transitions are found within these energy regions. Thus, these states (or a part of them) must be responsible for the isomer population. It is further demonstrated in the lower part of fig. 2 that

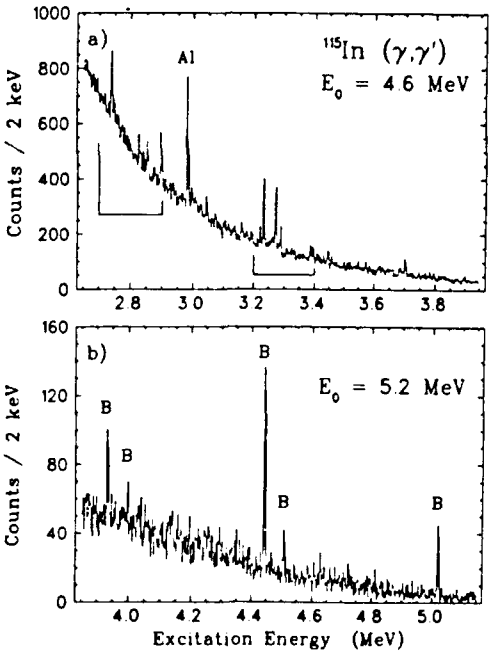

Fig. 2. Spectra of the ^{115}In(γ, γ') reaction obtained for endpoint energies $E_0=4.6$ and 5.2 MeV. The brackets indicate regions where significant strength for the population of the isomer is found in the excitation function (see fig. 1). The strongest lines marked B and Al are calibration lines.

no other resolved (γ, γ') state is detected up to $E_x = 5$ MeV (an upper limit of ≈ 5 eV b is estimated for possible $(\sigma\Gamma)_0$ strength above 4 MeV). These results confirm that all important intermediate states have been identified up to 4.5 meV.

4. Nuclear model calculations and discussion

In order to compare the intermediate states at low and higher energies, the isomeric ratio $R = \Gamma_{iso}/(\Gamma_0 + \Gamma_{iso})$ is introduced. The important states at low energies show typical values $R \simeq 0.1$–0.2 For the observed groups around $E_1 = 2.8$ MeV and $E_1 = 3.3$ MeV, values $R_1 = 0.32$ and $R_2 = 0.27$ are obtained by averaging over all the states within the brackets. These numbers represent lower limits of R only, since not all the states necessarily show a branching to the isomer. In principle, states with $R \simeq 1$ could lead to appreciable $(\sigma\Gamma)_{iso}$ values also and would eventually be missed in the (γ, γ') data because of a too small Γ_0. Such contributions, however, seem to play no important role in ^{115}In.

Further insight is attained from an analysis within the unified-model [14]. In the case of ^{115}In, the configuration space is built by proton 1h-states (relative to the semimagic ^{116}Sn nucleus) and 1p–2h states across the major shell (relative to ^{114}Cd) coupled to collective phonons (up to three quadrupole and two octupole) in the underlying cores. The two subspaces are mixed by a residual interaction which connects the pairing mode describing the 2h-core (^{114}Cd) coupled configurations with the surface model [14].

The parameters used for the calculation of energies and wavefunctions closely follow ref. [13]. For the study of M1 transitions, g-factors $g_s = 0.7 g_s^{free}$ for the quenched proton spin value and $g_R = Z/A$ for the gyromagnetic ratio were used. Alternatively, we tested the other extreme: $g_R = 0$. This variation shows some influence in detail, but the general conclusions described below are not affected. The comparison to experiment proceeds by first computing all possible E1/M1/E2 upward transitions. Then, for states with a large partial g.s. width the full decay cascade is taken into account. In this way, model values for $(\sigma\Gamma)_0$ and $(\sigma\Gamma)_{iso}$ as well as branching ratios are determined.

Some general properties of the results, which are surprisingly insensitive to details of the calculations, are summarized first. In accordance with the experimental results, intermediate states are found in a limited energy region above $E_x = 2.5$ MeV only. Also, typical $(\sigma\Gamma)_{iso}$ values at lower energies are suppressed by a factor of about 10–100. The number of important states is small, similar to the experimental NRF results.

Fig. 3 presents a comparison of both experiments and the model results. The calculations show a rough division into two groups which might be related to the experimental $(\sigma\Gamma)_{iso}$ data. A one-to-one correspondence, however, is certainly beyond the limits of the approach. Summing the model $(\sigma\Gamma)_{iso}$ strength, the isomeric ratios $R_1 = 0.25$ and $R_2 = 0.46$ compare favourably to the experimental numbers. However, an overall factor of 4 is needed to reach absolute values of integrated cross sections similar to the measured ones.

We have investigated whether this shortcoming might result from a model-inherent deviation of the average strength for the different transition types compared to experiment. Model distributions of reduced transition probabilities $B(\pi L)$ for E1/M1/E2 were produced from a complete decay study of all states up to 4 MeV and compared to the experimental systematics of Endt [24] for this mass region. The resulting patterns look very similar and experiment/model ratios $F(E1) = 0.2$, $F(M1) = 2$ and $F(E2) = 10$ are deduced from the position of the maxima. A repetition of the decay cascade calculation with each transition modified by the correction factors leads to an agreement of absolute $(\sigma\Gamma)_0$ and $(\sigma\Gamma)_{iso}$ values within a factor of two, but slightly detoriating isomeric ration results $R_1 = 0.13$ and $R_2 = 0.60$.

The overall agreement seems quite encouraging and indicates that no major part of the relevant configuration space is missed. A detailed analysis of the main decay branches reveals a clear picture of the important amplitudes in the intermediate state wavefunctions. All theoretical states shown in fig. 3 have $J^\pi = \frac{7}{2}^+$ and the g.s. coupling is dominated in *all* cases by single-particle $1g_{9/2} \rightarrow 1g_{7/2}$ spin-flip transitions. The first step of the decay to the isomer in the model calculations proceeds mainly via E1 or E2 transitions, depending on the application of the correction factors which strongly suppress E1 versus E2. In the former case, the E1 operator leads to configurations including negative parity 1h-states which effectively

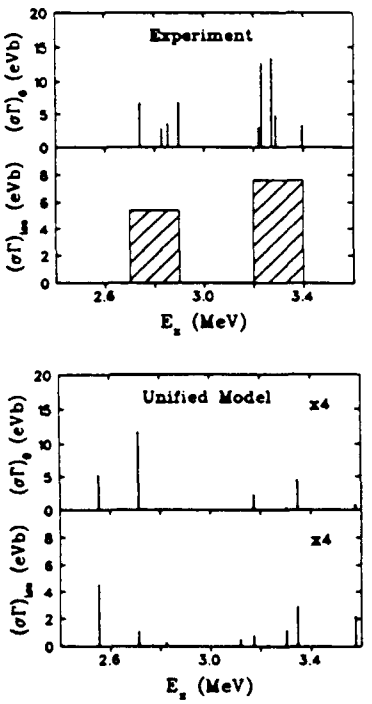

Fig. 3. Comparison of the experimental $(\sigma\Gamma)_0$ and $(\sigma\Gamma)_{iso}$ results with unified-model calculations. The dashed histograms for the experimental $(\sigma\Gamma)_{iso}$ strength indicate that they might be the sum of unresolved states within the experimental resolution.

populate the $J^\pi = \frac{1}{2}^-$ isomer. In the latter scenario, higher phonon Cd-core configurations which are admixed to a few important levels in the cascade open an efficient path for collective E2 depopulation of the intermediate states.

To summarize, large cross sections feeding the isomer in ^{115}In have been found around $E_x = 3$ MeV. A complementary (γ, γ') study clearly demonstrates that the strength is induced by a small number of discrete intermediate states. A microscopic analysis within the unified-model indicates that M1 spin-flip transitions ($1g_{9/2} \rightarrow 1g_{7/2}$) are most important for the resonant absorption into excitations with a significant 1p–2h component while admixtures to the wave functions permitting E1 single-hole transitions or collective E2 strength from higher phonon Cd-core configurations are responsible for the branching to the isomer. The importance of $1g_{7/2}$ strength for the γ-decay has also been demonstrated [25] in the even–even neighbour ^{116}Sn. The combined study of isomer excitation function and nuclear resonance fluorescence turns out to be an efficient tool for further investigations in the revived field of photoexcitation of isomers.

Acknowledgement

We are indebted to Dr. H.-D. Gräf and the S-DALINAC crew for their great support in operating the accelerator. We thank M. Huber and N. Huxel for their assistance in the experiment.

References

[1] G.B. Collins et al., Phys. Rev. 55 (1939) 507.
[2] Z.M. Bigan et al., Sov. J. Nucl. Phys. 49 (1989) 567.
[3] L.Z. Dzhilavyan et al., Sov. J. Nucl. Phys. 51 (1990) 215.
[4] E.C. Booth and J. Brownson, Nucl. Phys. A 98 (1967) 529.
[5] C.B. Collins et al., Phys. Rev. C 37 (1988) 2267.
[6] J.J. Carroll et al., Phys. Rev. C 43 (1991) 1238.
[7] C.B. Collins et al., Phys. Rev. C 42 (1990) R1813.
[8] J.J. Carroll et al., Phys. Rev. C 43 (1991) 897.
[9] C.B. Collins et al., J. Appl. Phys. 53 (1982) 4645.
[10] W.J. Varhue and T.G. Williamson, Int. J. Appl. Radiat. Isot. 37 (1986) 155.
[11] C.B. Collins et al., Phys. Rev. C 38 (1988) 1852.
[12] J. Blachot and G. Marguier, Nucl. Data Sheets 52 (1987) 565.
[13] K. Heyde, M. Waroquier and R.A. Meyer, Phys. Rev. C 17 (1978) 1219.
[14] K. Heyde et al., Phys. Rep. 102 (1983) 291.
[15] K. Alrutz-Ziemssen et al., Part. Acc. 29 (1990) 53.
[16] T.M. Jenkins, W.R. Nelson and A. Rindi, eds., Monte Carlo transport of photons and electrons (Plenum, New York, 1988).
[17] A. Ljubičić et al., Phys. Rev. C 23 (1981) 2238; M. Krčmar et al., Phys. Rev. C 33 (1986) 293; C 41 (1990) 771.
[18] P. von Neumann-Cosel et al., Phys. Rev. C, in press.
[19] W. Ziegler et al., Phys. Rev. Lett. 65 (1990) 2515.
[20] C. Spieler et al., to be published.
[21] Y. Cauchois et al., J. Phys. G 7 (1981) 1539.
[22] W.J. Alston III, Phys. Rev. 188 (1969) 1837.
[23] A.B. Smith et al., J. Phys. G 11 (1985) 125.
[24] P.M. Endt, At. Data Nucl. Data Tables 26 (1981) 47.
[25] J.M. Schippers et al., KVI annual report (1988) p. 7; J.M. Schippers, Ph.D. thesis, Rijksuniversiteit Groningen (1988).

Common thresholds and the role of deformations in the photoexcitation of isomers

by

C. B. Collins, J. J. Carroll, K. N. Taylor,
D. G. Pichmond, and T. W. Sinor
Center for Quantum Electronics
University of Texas at Dallas
P.O. Box 830688
Richardson, TX 75083-0688

and

M. Huber, P. von Neumann-Cosel, A. Richter,
and W. Ziegler
Institut für Kernphysik
Technische Hochschule Darmstadt
D-6100 Darmstadt, Germany

ABSTRACT

Photoexcitations of the short-lived isomers $^{167}Er^{m}$, $T_{1/2}$ = 2.28 s, $^{179}Hf^{m}$, $T_{1/2}$ = 18.68 s, $^{191}Ir^{m}$, $T_{1/2}$ = 4.94 s, and $^{197}Au^{m}$, $T_{1/2}$ = 7.8 s were produced with bremsstrahlung from the superconducting Darmstadt linear accelerator. Excitation functions were measured for the population of these isomers by (γ,γ') reactions between 2 and 7 MeV. They indicated that the isomers were excited by resonant absorption through isolated intermediate states having integrated cross sections in excess of 10^{-26} cm^2 keV, i.e., values about 1000 times larger than most (γ,γ') activation reactions reported previously although they were comparable to those reported earlier for the dumping reaction $^{180}Ta^{m}(\gamma,\gamma')^{180}Ta$. In all four nuclei a common onset was observed near 2.5 MeV for intermediate states with strengths much larger than those occurring at lower energies. The summed cross sections exhibit a clear correlation with the ground state deformations.

INTRODUCTION

The photoexcitation of nuclear isomers by (γ,γ') reactions has been known for more than 50 years.[1,2] For most of this time studies of this phenomenon have been concentrated either upon higher photon energies around particle thresholds, or upon relatively low energies of excitation, $E \leq 2$ MeV. Results in the former case have been dominated by the photoabsorption through the giant dipole resonance and have emphasized concerns for the gross properties of the photoexcitation process[3] or for tests of statistical models of γ-decay at high excitation energies.[4] At the lower energies efforts have been characterized by the excitation of discrete intermediate states that have branched or cascaded back to an isomer with a significant probability.[5] Under those conditions the integrated cross sections for the photoexcitation of isomers have been typically 10^{-29} to 10^{-27} cm^2 keV.

Only recently have studies been extended systematically into the intermediate range of energies, and then with surprising results. Initiated with the observation[6] of the deexcitation of the isomer $^{180}Ta^m(\gamma,\gamma')^{180}Ta$ with an unprecedented integrated cross section exceeding 10^{-25} cm^2 keV, such extraordinary values were subsequently reported[7] for $^{176}Lu(\gamma,\gamma')^{176}Lu^m$, also. A large survey of 19 nuclides was reported[8] that covered the broad range of endpoint energies 0.5 - 11 MeV from four different accelerators and established that comparable integrated cross sections can be found in the majority of cases studied. However, the relatively coarse mesh over which those measurements were conducted prevented the extraction of the excitation energies and strengths of individual intermediate states (IS).

As a next step, a series of experiments was performed in the 2 - 7 MeV range in order to identify and characterize the important intermediate levels. These studies were motivated by two principal aspects. First, the very efficient coupling of ground state (g.s.) and isomer demonstrated in Refs. [6 - 8] provided unexpected encouragement of schemes[9] to use the resonant photoexcitation of isomers (or the reverse process, the sudden depopulation of an isomer) as a mechanism to pump a γ-ray laser. Amongst other conditions, the feasibility

depends sensitively on the locations and coupling strengths of the resonant states. Second, the reaction mechanism selects a unique set of states with two features: a large partial g.s. width and strong admixtures in the wave function which induce the decay into states efficiently cascading to the isomer. In the excitation energy region investigated, the underlying nuclear structure is almost unexplored and theoretical interpretations are badly needed. To our knowledge, the only attempt to interpret similar data on a microscopic base is found in Ref. [10]. On the other hand, such data provide stringent constraints for any model calculation.

A study of the deexcitation of $^{180}Ta^{m}$ confirmed the striking results of Ref. [6]. It was found to occur through two intermediate states at 2.8 and 3.6 MeV with integrated cross sections of 1.2×10^{-25} and 3.5×10^{-25} cm^2 keV, respectively.[11] The excitation of isomers with large probabilities through discrete intermediate states in the reactions[12,13] of $^{123,125}Te(\gamma,\gamma')^{123,125}Te^{m}$, and $^{115}In(\gamma,\gamma')^{115}In^{m}$ was also established. However, in these latter cases integrated cross sections were of the order of 10^{-26} to 10^{-25} cm^2 keV.

Utilizing the large natural abundance of ^{115}In, complementary nuclear resonance fluorescence experiments were performed and the important intermediate states were identified.[13] Unified model[14] calculations provided a qualitative explanation of the IS as being due to fragmented $g_{9/2} \longrightarrow g_{7/2}$ spin-flip strength.

The next step in understanding would require an extension of the information available on IS in a variety of nuclei which might build a base for more systematic nuclear structure interpretations. The recent survey[8] indicates two empirical trends, viz. an average increase of yields with mass number and a correlation with the g.s. deformation. These findings are illustrated in Figs. 1a) and 1b) in which the integrated cross sections obtained at an electron energy of 6 MeV are plotted versus A and N_pN_n, respectively. The latter is the product of open-shell proton and neutron occupation numbers and is a well-established measure of the deformation driving proton-neutron interactions.[15] Its application is restricted to nuclei with $A > 90$. While the above-mentioned trends are clearly visible, before attempting a detailed comparison one should

keep in mind that these integrated cross sections have been normalized by arbitrarily assuming a single IS at 2 MeV.

One purpose of the present experiments was to investigate the empirical correlation with the g.s deformation more closely. Therefore, the nuclides ^{167}Er, ^{179}Hf, ^{191}Ir, and ^{197}Au were chosen because they cover a large span of deformations (δ = 0.09 - 0.32) but lie within the same group in Fig. 1a) and have comparable mass numbers. Furthermore, the well-deformed ^{167}Er and ^{179}Hf are prime candidates to verify that the extraordinarily large cross sections of the IS derived[11] for $^{180}Ta^{m}$ are indeed not uncommon. Additional results obtained in the A = 70 - 90 mass region will be presented elsewhere.

EXPERIMENTS

Methods

Elemental samples of Ir, Au, In (as a calibration standard) and the compounds HfO_2, Er_2O_3 of typically 5 - 15 g served as targets. The materials were contained in hollow aluminum cylinders with 3.5 cm length and 1.4 cm outer diameter.

Isomeric populations were produced by exposing the targets to bremsstrahlung from a 3 mm tantalum converter foil irradiated by the electron beam from the injector of the new superconducting S-DALINAC accelerator at the Technische Hochschule Darmstadt.[16] Electron energies were varied from 2 to 7 MeV with a minimum step size of 125 keV. The electron energies were measured with an accuracy of 50 keV before and after each exposure. At each endpoint, individual samples were irradiated axially in close proximity to the converter. Each target cylinder was held in position by an aluminum stop which terminated a plastic transfer tube. The proper alignment of the beam was achieved by maximizing the dose delivered to a remote ionization chamber shielded to observe only the central 12 mrad of the bremsstrahlung cone.

Variations in all beam parameters were recorded during the experiments. In particular the charge passed to the converter was determined for each exposure

by integrating the current with an analog circuit whose time constant for charging was arranged to match the lifetime of the isomer being investigated. Nominal beam currents were 5 μA. The lengths of the exposures were typically chosen to be twice the halflife of the isomer in question, while the calibration sample, $T_{1/2}$ = 4.486 h was exposed for 5 min.

The termination of each irradiation provided a trigger signal which initiated the pneumatic transport of each sample through the plastic tube to a well-type NaI(Tl) detector for counting. This detector and all necessary electronics for the experiments were located in a room separate from the accelerator hall. A phototransistor signalled the arrival of the sample within the detector and started the simultaneous acquisition of both pulse-height and multichannel-scalar spectra. Examples of spectra obtained in this way are shown in Figs. 2 and 3. A quad counter/timer was gated by TTL signals at the start and end of irradiation, and at the arrival of the sample in the detector to measure the precise durations of exposure and transport.

The numbers of isomers produced by these irradiations were determined from the counting rates measured in distinctive fluorescence lines. The particular γ-ray signatures used in these measurements and other relevant parameters are given in Table I. The raw number of counts in each peak was corrected for the finite durations of exposure, transport and counting, the absolute counting efficiencies of the detector and the relative emission intensities. The opacity of the samples to the escape of the signature γ rays was compensated by a factor calculated with a Monte-Carlo code specifically adapted for the well-type detector geometry.

Data Analyses

The experimentally measured yield of isomers, N_f resulting from the irradiation of N_T ground state nuclei with bremsstrahlung is given analytically by

$$N_f = N_T \int_{E_C}^{E_0} \sigma(E) \frac{d\Phi(E)}{dE} dE \ , \qquad (1)$$

where E_0 is the endpoint energy and $d\Phi(E)/dE$ is the time-integrated spectral intensity in cm^{-2} keV^{-1} of the photon field, and $\sigma(E)$ is the cross section in cm^2 for the reaction. The spectral intensity is conveniently expressed as the product of a flux, Φ_0 of all photons above a cutoff energy E_C of 0.5 MeV incident on the target and a relative intensity function, $F(E,E_0)$ which is normalized according to

$$\int_{E_C}^{E_0} F(E,E_0)\ dE = 1 \ . \qquad (2)$$

Equation (2) allows the definition of a normalized yield, or activation per photon, $A_f(E_0)$ given by

$$A_f(E_0) \equiv \frac{N_f}{N_T \Phi_0} = \int_{E_C}^{E_0} \sigma(E)\ F(E,E_0)\ dE \ . \qquad (3)$$

At energies of interest in these experiments, IS have widths that are small in comparison to their spacings and it can be assumed that $d\Phi/dE$ is constant over each resonance region. Then Eq. (3) reduces to the summation,

$$A_f(E_0) = \sum_j (\sigma\Gamma)_{fj}\ F(E_j,E_0) \ , \qquad (4)$$

with $(\sigma\Gamma)_{fj}$ giving the integrated cross section of the j^{th} IS having excitation energy E_j. We note that nonresonant cross sections which would inhibit the use of Eq. (4) are not considered. The previous claims for the significance of nonresonant contributions[17] have recently been disproven[18] and shown to have resulted merely from the omission of the importance of intense contributions to

the photon fields arising in such experiments from environmental Compton scattering.

The normalized activation, A_f can be useful as a sensitive indication of the opening of (γ,γ') channels whenever photons of the requisite energies, E_j become available. A change of the endpoint energy, E_0 of the bremsstrahlung spectrum modulates the spectral intensity function $F(E_j,E_0)$ in Eq. (3) at all of the important IS energies. The largest effect in the excitation function occurs when E_0 is increased from a value just below some state at E_j to one exceeding it so that $F(E_j,E_0)$ varies from zero to some finite value. In earlier work[5] plots of quantities equivalent to Eq. (3) as functions of the endpoint energies of the irradiating spectra showed very pronounced activation edges which appeared as sharp increases at the energies, E_j corresponding to excitations of new intermediate states.

Calculated spectra of both Φ_0 and $F(E,E_0)$ were obtained from the EGS4 electron-photon transport code. This Monte Carlo program is well-established in the medical physics community and its general validity has been demonstrated elsewhere.[19] In this work confidence in the calculated photon spectra was maintained by calibrating them with the reaction $^{115}In(\gamma,\gamma')^{115}In^m$. This reaction is now sufficiently well characterized in the literature[13] to support its use in this way and in this effort was preferred over the calibration reaction $^{87}Sr(\gamma,\gamma')^{87}Sr^m$ used in other work[11,12] because of the completeness of the experimental information for it in the low energy region not covered in the present experiments.

RESULTS

Figure 2 shows a typical pulse height spectrum of the fluorescence from an isomeric population pumped by bremsstrahlung through some intermediate state(s). In this particular case the data from $^{167}Er^m$ are shown for an electron energy of E_0 = 6 MeV. Even with the limited resolution of the NaI(Tl) well detector, the distinctive signature line of $^{167}Er^m$ is clear in the data obtained from one 10 s exposure of an erbium sample. Nevertheless, to confirm the identity of the peak

a measurement of the time decay of the fluorescent state population was taken in parallel. Such a decay curve is shown for $^{167}Er^{m}$ in Fig. 3 together with a fit which agrees well with the literature value[20] of the halflife, $T_{1/2}$ = 2.28 s.

To improve statistics, at least nine successive repetitions of the cycle for irradiation and counting were made for each nuclide at each endpoint energy of the bremsstrahlung. Each was corrected for slight variations of the photon flux on that particular exposure, as well as for any variations in the transit time from the site of exposure to the counting enclosure. The resulting curves of A_f obtained from Eq. (3) as functions of bremsstrahlung endpoint, E_0 are shown in Figs. 4-7. The results at 6 MeV given by Carroll et al.[8] are included for comparison. The agreement of these values obtained in completely different experimental environments is excellent.

Values for the integrated cross sections, $(\sigma\Gamma)_{fj}$ were found by fitting Eq. (4) to the data of Figs. 4-7. A useful measure of the degree of fit was provided by the residue of activation, $R_M(E_0)$ remaining after subtracting contributions from the M lowest lying intermediate states,

$$R_M(E_0) = A_f(E_0) - \sum_{E_j = E_1}^{E_M} (\sigma\Gamma)_{fj} F(E_j, E_0) \quad , \qquad (5)$$

where E_M is the resonance energy of the highest lying intermediate state already included. Fitted values of the integrated cross sections, $(\sigma\Gamma)_{fj}$ were found by minimizing $R_M(E_0)$ for the lowest energy state giving a break in the excitation function, and then iterating after including any new gateways suggested by the data. The contribution of IS below E_0 = 2 MeV that could not be distinguished by the present experiments was estimated by assuming a single state for which properties were adjusted to give the best description of A_f values for energies below 2.5 MeV. Because of the sudden jump of intermediate state strength of typically more than a factor of 10 around 2.5 MeV, variations of the IS cross sections at lower energies have little effect on the results.

The results of fitting the model of Eq. (4) to the data of Figs. 4-7 are summarized in Table II. Uncertainties are shown explicitly. It should be noted

that within the energy errors given for the IS locations the present approach cannot distinguish between single states and contributions from fragmented strength.

DISCUSSION

Examination of the results presented in Table II reveals some interesting phenomena. All four nuclei show a sudden jump of very significant magnitude in the values of integrated cross sections accessed around 2.5 MeV. This same phenomenology had been reported earlier[11,12,13] in $^{180}Ta^{m}$, ^{123}Te and ^{115}In. Confirmed for ^{115}In both by studies of resonant scattering and by unified model calculations, the IS strength there accrued from $g_{9/2}$ --> $g_{7/2}$ spin flip transitions. However, in the present work the chosen nuclei, together with the $^{180}Ta^{m}$, represent cases of both unpaired protons and unpaired neutrons in different major shells. A common mechanism independent of the details of nuclear structure would be indicated for this group of IS.

Before attempting to find the means to explain such extraordinary strengths for these IS, a first concern is the extent to which these measurements may be supported by prior work. Unfortunately there are few compelling results in the literature. The only precedents are the recent measurements made over a very coarse mesh of energies[8] and the 1970 work of Johnson, Chertok, and Dick[21], (JCD). The agreement is excellent between values of A_f obtained in the present work and those obtained with three of the four different accelerators employed previously.[8] No arbitrary factors were used to scale any of those earlier data and the agreement seen in the Figs. 4-7 is a measure of the accuracy with which absolute measurements can be made for (γ,γ') reactions. Reference back to the original data of Ref. [8] shows that comparisons with activations produced by the fourth accelerator, a 4 MeV medical linac were less satisfactory. With that device it was not possible either to monitor or control the endpoint energy of the electrons, nominally fixed at 4.0 MeV. Because of the amount of structure now reported for activation curves near 4 MeV the effects of small variations of endpoint energy would be expected to be magnified in the resulting

yields. Not surprisingly, disagreements as great as a factor of two were obtained with that accelerator.

Comparisons with the JCD results are more difficult. Published in a Letter, both results and procedures were too briefly described to permit any repetition of the work. Details were promised for publication in a subsequent article which never appeared. Both the strengths and excitation energies of the IS reported by JCD disagree completely with those summarized in Table II. However, the uniqueness of such values depends upon the degree to which inflections in curves of A_f as functions of endpoint energy can be precisely located. The fragments of data shown by JCD in the letter are insufficient to support the uniqueness of the values they reported.

The degree to which the results of this work reported in Table II agree with prior measurements is best summarized in Fig. 8. There are plotted the values of A_f that were recently obtained in this work for the reaction $^{167}Er(\gamma,\gamma')^{167}Er^m$ together with those from Ref. [8], including the one made with the 4 MeV linac of lessened reliability. No scale factors were used and absolute measurements have been plotted. From the JCD Letter it is possible only to calculate values of A_f which would have resulted from excitation through the IS they report by bremsstrahlung with reasonable spectra. Since they did not report IS below 2.5 MeV, a single hypothetical intermediate state had to be included in all computations of A_f to represent contributions from those lower energies. That state was chosen to give the closest agreement with the rest of the values plotted. The results are shown in Fig. 8 which now permits a comparison of all known measurements of the activation of $^{167}Er(\gamma,\gamma')^{167}Er^m$ in the energy range from 2 - 7 MeV.

Agreement of the results of JCD from 20 years ago with the present work is at least as good as has been obtained with the 4 MeV medical linac, about a factor of 2. However, it is doubtful whether the procedures of Eq. (5) would deliver the same number and magnitudes of the IS reported by JCD if now applied to the corresponding data of Fig. 8. Values they reported were sufficient for the description of their measured A_f, but were not unique. Despite the generally favorable agreement of all of the measurements summarized in Fig. 8, we believe

it reasonable to ascribe a greater weight to those from the current experiment. A primary consideration is that each exposure in the present work also included the activation of $^{115}In(\gamma,\gamma')^{115}In^{m}$, believed now to be well-understood from a unique level of agreement of photoexcitation, resonant scattering and model interpretation. Through this constant recalibration the effects of experimental uncertainties were minimized.

The resulting IS cross sections of Table II show a general tendency to increase with increasing excitation energy. We have investigated whether photoabsorption through the tail of the isovector electric giant dipole resonance (GDR) provides a quantitative explanation of the excitation functions. It is well-known that the extrapolation of the GDR to lower energies describes γ-strength functions[22] and the statistical distribution of low energy E1 transitions[23] reasonably well. This extrapolation might be extended down to about 4 - 5 MeV in nuclei far from closed shells, but nuclei near the ^{208}Pb shell closure show strong irregularities and experimental results tend to be significantly overestimated.[22] In this analysis we therefore show a comparison for both ^{167}Er and ^{197}Au as representative examples of the two groups.

The following simplifications are assumed for the calculations. The photoabsorption cross section is taken from the usual Lorentzian parametrization

$$\sigma_{abs}(E) = \sum_{i} \sigma_{max} \frac{E^2\Gamma^2}{(E^2 - E^2_{max})^2 + E^2\Gamma^2} \qquad (6)$$

with E_{max} and σ_{max} being the energy and cross section at maximum, respectively, and Γ is the width. For spherical nuclei i = 1 and for deformed nuclei i = 1 or 2, corresponding to oscillations with respect to the different axes. Equation (6) is substituted into Eq. (3) to obtain A_t values comparable to the experiment. In order to simplify the integral the σ_{abs} is described as a histogram with a mesh interval Δ equal to the stepsize of the photon intensity function $F(E,E_o)$. Then, the integral can again be reduced to a simple summation

$$A_f(E_0) = \sum_{i=1}^{N} F(E_i, E_0) \quad \sigma(E_i - \Delta/2,\ E_i + \Delta/2) \ , \qquad (7)$$

with $E_i = E_{i-1} + \Delta$. The Lorentzian parameters were taken from Ref. 24 and the experimental results of ^{nat}Er were used for ^{167}Er.

The results are shown in Fig. 9 as hatched areas above 3.5 MeV (model A). The upper and lower borders correspond to the limits of reasonable branching ratio values of $b_0 b_{iso} = 0.05$ and 0.25. Below 3.5 MeV, results based on the single-particle model multiplied with an average experimentally deduced[25] hindrance factor of 3×10^{-5} (model C) are displayed. This approach has been tested by Zurmühl et al.[26] for various well deformed heavy nuclei. Alternatively, an extrapolation of the GDR using an energy dependent damping width of the form $\Gamma(E) = \Gamma_{max}(E/E_{max})^{\gamma}$ has been proposed[27,28] with typical values $\gamma = 1.5 - 2$. As an example, we adopt the approach of Kopecky and Uhl[28] (with $T = 0$ since we measure the upward strength function), which is displayed as model B.

A comparison of the ^{167}Er and ^{197}Au results reveals considerable differences. In ^{167}Er, model A provides a reasonable description slightly below particle threshold, while results of model B are much too small. On the contrary, as shown in Fig. 10, model A predicts too large photoabsorption cross sections in ^{197}Au in line with other investigation of the γ-strength function[22], while model B accounts well for the data down to about 4 MeV. It is also clear that an average E1 transition strength (model C) could explain the low energy data in this case.

The extraordinary photoabsorption strength around 2.5 MeV in ^{167}Er is reflected by the failure of model C which predicts values which are much too small. The empirical relation to the deformation parameter and the IS parameters in Table II indicate that collective degrees of freedom should play a decisive role. However, recent studies of low energy collective dipole strength in rare earth nuclei[29-32] provide no fully satisfactory explanation. For the IS at 2.5 MeV, reduced transition probabilities $B(M1)\uparrow = 3.6\ \mu^2_N$, and $B(E1)\uparrow = 40 \times 10^{-3}\ e^2\ fm^2$ can be extracted assuming a favorable $b_0 b_{iso} = 0.2$.

These numbers roughly correspond to the total experimental M1 and E1 transition strengths[31,33] typically observed below 4 MeV in the experiments. However, all the above data have been taken in even-even nuclei. Recently, a first attempt to investigate low-lying dipole transitions in an odd-even case, ^{165}Ho was reported.[34] Only intrinsic single-particle transitions were excited with reasonable magnitude and significant collective M1 or E1 strengths were not observed below 3 MeV.

The importance of the quadrupole deformation already suggested in Fig. 1b) is clearly confirmed in the present results, if one compares the cross sections of different nuclei at about equal energies. The integrated isomer cross sections can be related to photon scattering results via

$$(\sigma\Gamma)_{iso} = \pi^2 \left(\frac{\hbar c}{E_\gamma}\right)^2 \left(\frac{2J_f+1}{2J_i+1}\right) b_0 b_{iso} \Gamma \quad , \tag{8}$$

with b_0 and b_{iso} being the g.s. and summed isomer branching ratios, respectively, E_γ being the photon energy and Γ being the total decay width of the IS. From recent nuclear resonance fluorescence work[29-34] in the rare earth region it can be concluded that for energies below 4 MeV the absorption step is most likely mediated by dipole rather than quadrupole strength. A comparison of $(\sigma\Gamma)_{iso} \sim \Gamma E_\gamma^{-2}$ and the reduced dipole transition probability $B(E1,M1) \sim \Gamma E_\gamma^{-3}$ suggests the utility of the quantity

$$S = \sum_{i=1}^{N} (\sigma\Gamma)_i^{red} \quad , \tag{9}$$

where $(\sigma\Gamma)^{red} = (\sigma\Gamma)_{iso}/E_\gamma$. Defined in this way, S should be proportional to the energy independent transition matrix elements. However, one should take note that this definition neglects variations in the product of the branching ratios, $b_0 b_{iso}$ which can be expected to vary within a factor of 2 to 3 for the IS considered here.

In Fig. 11 the summed strength S is plotted versus the quadrupole deformation δ of the ground states that have been derived from measured moments.[35] The correlation is obvious and can be well-fitted with the direct proportionality shown by the solid line. This result is surprising and such a linear dependence is not easily understood. The relationship between S and δ could be simply fortuitous and should be viewed with caution because it depends on the excitation energy interval considered and because the number of data points is too small for a final conclusion. However, it is clear that a correlation exists. We also note that the same conclusion is reached if it is assumed that quadrupole transitions are responsible for the excitation although a linear relationship is no longer suggested.

CONCLUSIONS

In the present work, the main IS between 2 and 7 MeV have been identified for ^{167}Er, ^{179}Hf, ^{191}Ir and ^{197}Au. A sudden jump of IS cross sections of typically more than an order of magnitude is observed in all cases around 2.5 MeV. This coincides with previous results[13,12,11] in ^{115}In, ^{123}Te and ^{180}Ta, where similar phenomena were observed below 3 MeV, and indicates the presence of a common excitation mechanism.

The magnitudes of IS cross sections reveal a clear correlation to the g.s. deformation. Assuming that solely dipole transitions are responsible for the excitation (which can be justified from recent photon-scattering experiments[29-34] in this mass region), the reduced transition probability of the IS summed over the 2 - 7 MeV region displays a linear behavior as a function of the deformation parameter δ. The variation of branching ratios is neglected and the number of data points is small, so the claim of a linear relation needs further experimental confirmation. However, the present results clearly indicate that a correlation exists.

While the measurements seem clear, the extremely large integrated cross sections for the photoexcitation of well-deformed isomers are difficult to interpret in a single particle model and a puzzle of comparable complexity is

found in the efficiency with which ΔK is transferred. Many of these isomers have values of K that differ considerably from the ground state values. It is an interesting speculation that at certain energies of excitation, collective oscillations of the core nucleons could break some of the symmetries upon which rest the identifications of the pure single-particle states. If single particle states of differing K were mixed in this way, the possibility for transferring larger amounts of ΔK with greater partial widths might be enhanced. Some support for such a speculation was found in the unexpected enhancements measured very recently for the deexcitation of the $^{174}Hf^{m}$ isomer.[36] There also the decay of the isomer was found to occur primarily by transition through an intermediate state lying at 2685 keV in which K mixing occurred so that $\Delta K = 14$ was lost between isomer and the ground state band. This is remarkably close to the energies of the IS shown in Table II. The similarity of results for nuclei with such dissimilar single-particle structures does seem to support the identification of this K-mixing process with some type of core property varying only slowly among neighboring nuclei, despite the fact these are not even-even nuclei.

At present, it remains an open question what might be the nuclear structure underlying the particularly strong IS below 3 MeV observed in ^{167}Er, ^{176}Lu, ^{179}Hf and ^{180}Ta and whether a common excitation mechanism dominates or whether the detailed interplay of collective and single-particle aspects in each particular nucleus is responsible. Microscopic calculations are clearly needed.

ACKNOWLEDGMENTS

We thank H.-D. Gräf, Th. Rietdorf, P. Schardt, and H. Weise for their great support in operating the superconducting electron accelerator, and M. L. Williams for his assistance in analyzing the data. In addition, we wish to thank our sponsors, the Department of Defense through the Naval Research Laboratory and the Bundesministerium für Forschung und Technologie, Contract No. 06DA184I.

TABLE I

Summary of the abundances, halflives, principal fluorescence signature lines and sample transparencies of nuclides studied.

Nuclide	Abundance (%)	$T_{1/2}$ (s)	Principal fluorescence (keV)	Transparency (%)
^{167}Er	22.95	2.28	207.79	48
^{179}Hf	13.63	18.68	214.31	43
^{191}Ir	37.30	4.94	129.43	13
^{197}Au	100.00	7.80	279.11	11

TABLE II

Values of integrated cross sections, $(\sigma\Gamma)_{fj}$ and excitation energies, E_j of the intermediate states most important in the production of these isomers by (γ,γ') reactions. Values needed to fit the data were determined in this work by minimizing the residues of Eq. (5).

Isomer	E_j (MeV)	$(\sigma\Gamma)_{fj}$ (10^{-29} cm^2 keV)
$^{167}Er^m$	1.9 ± .1	1500 ± 200
	2.5 ± .1	8000 ± 2000
	3.1 ± .15	28000 ± 4000
	3.8 ± .2	50000 ± 15000
$^{179}Hf^m$	1.5 ± .2	40 ± 10
	2.5 ± .1	1200 ± 200
	3.0 ± .15	6000 ± 1000
	4.3 ± .2	75000 ± 15000
$^{191}Ir^m$	1.2 ± .3	180 ± 50
	2.5 ± .1	2500 ± 300
	3.2 ± .15	5000 ± 500
	4.3 ± .2	30000 ± 4000
$^{197}Au^m$	1.7 ± .3	70 ± 30
	2.5 ± .1	500 ± 50
	3.2 ± .15	4500 ± 500
	4.2 ± .2	20000 ± 4000

REFERENCES

1. B. Pontecorvo and A. Lazard, C. R. Acad. Sci. 208, 99 (1939).
2. G. B. Collins, B. Waldman, E. M. Stubblefield, and M. Goldhaber, Phys. Rev. 55, 507 (1939).
3. Z. M. Bigan, E. L. Lazarev, V. M. Mazur, and V. Sokolnyk, Sov. J. Nucl. Phys. 49, 567 (1989).
4. L. Z. Dzhilavyan, V. L. Kauts, V. I. Furman, and A. Y. Chaprikov, Sov. J. Nucl. Phys. 51, 215 (1990).
5. E. C. Booth and J. Brownson, Nucl. Phys. A98, 529 (1967).
6. C. B. Collins, C. D. Eberhard, J. W. Glesener, and J. A. Anderson. Phys. Rev. C 37, 2267 (1988).
7. J. J. Carroll, J. A. Anderson, J. W. Glesener, C. D. Eberhard, and C. B. Collins, Astrophys. J. 344, 454 (1989).
8. J. J. Carroll, M. J. Byrd, D. G. Richmond, T. W. Sinor, K. N. Taylor, W. L. Hodge, Y. Paiss, C. D. Eberhard, J. A. Anderson, C. B. Collins, E. C. Scarbrough, P. P. Antich, F. J. Agee, D. Davis, G. A. Huttlin, K. G. Kerris, M. S. Litz, and D. A. Whittaker, Phys. Rev. C 43, 1238 (1991).
9. C. B. Collins, F. W. Lee, D. M. Shemwell, B. D. DePaola, S. Olariu, and I. I. Popescu, J. Appl. Phys. 53, 4645 (1982).
10. V. Ponomarev, A. P. Dubenskij, V. P. Dubenskij, and E. A. Boykova, J. Phys. G 16, 1727 (1990).
11. C. B. Collins, J. J. Carroll, T. W. Sinor, M. J. Byrd, D. G. Richmond, K. N. Taylor, M. Huber, N. Huxel, P. von Neumann-Cosel, A. Richter, C. Spieler, and W. Ziegler, Phys. Rev. C. 42, 1813 (1990).
12. J. J. Carroll, T. W. Sinor, D. G. Richmond, K. N. Taylor, C. B. Collins, M. Huber, N. Huxel, P. von Neumann-Cosel, A. Richter, C. Spieler, and W. Ziegler, Phys. Rev. C 43, 897 (1991).
13. P. von Neumann-Cosel, A. Richter, C. Spieler, W. Ziegler, J. J. Carroll, T. W. Sinor, D. G. Richmond, K. N. Taylor, C. B. Collins, and K. Heyde, Phys. Lett. B266, 9 (1991).

14. K. Heyde, P. van Isaker, M. Waroquier, J. L. Wood, and R. A. Mayer, Phys. Reports 102, 291 (1983).

15. R. F. Casten, Nucl. Phys. A443, 1 (1985).

16. K. Alrutz-Ziemssen, D. Flasche, H-D. Gräf, V. Huck, M. Knirsch, W. Lotz, A. Richter, T. Rietdorf, P. Schardt, E. Spamer, A. Staschek, W. Voigt, H. Weise, and W. Ziegler, Part. Acc. 29 (1990) 53.

17. A. Ljubičić, M. Pisk, and B. A. Logan, Phys. Rev. C 23, 2238 (1981); M. Krčmar, A. Ljubičić, B. A. Logan, and M. Bistrović, Phys. Rev. C 33, 293 (1986); M. Krčmar, S. Kaučić, T. Tustonić, A. Ljubičić, B. A. Logan, and M. Bistrović, Phys. Rev. C 41, 771 (1990).

18. P. von Neumann-Cosel, A. Richter, J. J. Carroll, and C. B. Collins, Phys. Rev. C 44, 554 (1991).

19. *Monte Carlo Transport of Photons and Electrons*, eds. T. M. Jenkins, W. R. Nelson, and A. Rindi, (Plenum Press, New York, 1988).

20. *Table of Radioactive Isotopes*, E. Browne and R. B. Firestone, ed. by V. S. Shirley (John Wiley & Sons, New York, 1986).

21. W. T. K. Johnson, B. T. Chertok, and C. E. Dick, Phys. Rev. Lett. 25, 599 (1970).

22. G. A. Barthelomew, E. D. Earle, A. J. Ferguson, J. W. Knowles, and M. A. Lone, Adv. Nucl. Phys. 7, 229 (1972).

23. M. Schumacher, U. Zurmühl, F. Smend, and R. Nolte, Nucl. Phys. A438, 493 (1985).

24. S. S. Dietrich and B. L. Berman, At. Data Nucl. Data Tables 38, 199 (1988).

25. P. M. Endt, At. Data Nucl. Data Tables 26, 47 (1981).

26. U. Zurmühl, P. Rullhusen, F. Smend, M. Schumacher, and H. G. Börner, Phys. Lett. B114, 99 (1982).

27. G. Maino, A. Ventura, L. Zuffi, and F. Iachello, Phys. Rev. C 30, 2101 (1984).

28. J. Kopecky and M. Uhl, Phys. Rev. C 41, 1941 (1990).

29. C. Wesselborg, P. von Brentano, K. O. Zell, R. D. Heil, H. H. Pitz, U. E. P. Berg, U. Kneissl, S. Lindenstruth. U. Seemann, and R. Stock, Phys. Lett. B207, 22 (1988).

30. H. H. Pitz, U. E. P. Berg, R. D. Heil, U. Kneissl, R. Stock, C. Wesselborg, and P. von Brentano, Nucl. Phys. A492, 411 (1989).

31. A. Zilges, P. von Brentano, C. Wesselborg, R. D. Heil, U. Kneissl, S. Lindenstruth, H. H. Pitz, U. Seemann, and R. Stock, Nucl. Phys. A507, 399 (1990)

32. W. Ziegler, C. Rangacharyulu, A. Richter, and C. Spieler, Phys. Rev. Lett. 65, 2515 (1990).

33. A. Zilges, P. von Brentano, H. Friedrichs, R. D. Heil, U. Kneissl, S. Lindenstruth, H. H. Pitz, and C. Wesselborg, Z. Phys. A340, 155 (1991).

34. N. Huxel, W. Ahner, H. Diesener, P. von Neumann-Cosel, C. Rangacharyulu, A. Richter, C. Spieler, W. Ziegler, C. De Coster, and K. Heyde (submitted to Nucl. Phys. A).

35. P. Raghavan, At. Data Nucl. Data Tables 42, 189 (1989).

36. P. M. Walker, F. Sletten, N. L. Glørup, M. A. Bentley, J. Borggreen, D. Fabricius, A. Holm, D. Howe, J. Pedersen, J. W. Roberts, and J. F. Sharpey-Schafer, Phys. Rev. Lett. 65, 416 (1990).

CAPTIONS

Figure 1: Integrated cross sections of Ref. [8] for an electron energy of 6 MeV determined according to the assumption of a single hypothetical intermediate state at 2 MeV plotted versus a) mass number A and b) the product of open-shell proton and neutron occupation numbers, N_pN_n calculated according to Ref. [15].

Figure 2: Pulse-height spectrum of the γ decay of the isomer $^{167}Er^m$ pumped by bremsstrahlung from a 6 MeV electron beam.

Figure 3: Time decay spectrum of the isomer $^{167}Er^m$. The straight line represents a best fit with $T_{1/2} = 2.26 \pm 0.04$ s.

Figure 4: Normalized yield, A_f of the activation of $^{167}Er^m$ as a function of electron energy. The star represents the experimental result of Ref. [8] obtained at 6 MeV. The energies at which intermediate states were indicated according to Eq. (5) are marked by the arrows (see Table II).

Figure 5: Normalized yield, A_f of the activation of $^{179}Hf^m$ as a function of electron energy. The star represents the experimental result of Ref. [8] obtained at 6 MeV. The energies at which intermediate states were indicated according to Eq. (5) are marked by the arrows (see Table II).

Figure 6: Normalized yield, A_f of the activation of $^{191}Ir^m$ as a function of electron energy. The star represents the experimental result of Ref. [8] obtained at 6 MeV. The energies at which intermediate states were indicated according to Eq. (5) are marked by the arrows (see Table II).

Figure 7: Normalized yield, A_f of the activation of $^{197}Au^m$ as a function of electron energy. The star represents the experimental result of Ref. [8] obtained at 6 MeV. The energies at which intermediate states were indicated according to Eq. (5) are marked by the arrows (see Table II).

Figure 8: Comparison of the present experiments with previous work for $^{167}Er^m$. The stars denote the A_f results of Ref. [8] attained at 4 and 6 MeV. The dashed curve was calculated with the intermediate states given in Ref. [21] plus an

arbitrary state below 7.5 MeV to account for the unknown lower-energy contributions not covered in that early work. The energy, E = 1.9 MeV and integrated cross section, $\sigma\Gamma$ = 2250 x 10^{-29} cm^2 keV of this state were adjusted to achieve an optimum agreement with the present data in the 2.5 - 3.6 MeV region accessed in both experiments.

Figure 9: Comparison of the $^{167}Er^m$ excitation function with extrapolations of the photoabsorption through the tail of the GDR assuming a Lorentzian shape (model A) or a Lorentzian with an energy-dependent damping width (model B), and with a single-particle model (model C). The Lorentzian parameters were taken from Ref. [24]. The borders of the hatched regions showing the model predictions correspond to reasonable limits assumed for the unknown branching-ratio values $b_0 b_{iso}$ = 0.25 and 0.05.

Figure 10: Comparison of the $^{197}Au^m$ excitation function with extrapolations of the photoabsorption through the tail of the GDR assuming a Lorentzian shape (model A) or a Lorentzian with an energy-dependent damping width (model B), and with a single particle model (model C). The Lorentzian parameters were taken from Ref. [24]. The borders of the hatched regions showing the model predictions correspond to reasonable limits assumed for the unknown branching-ratio values $b_0 b_{iso}$ = 0.25 and 0.05.

Figure 11: Reduced integrated cross sections, S calculated with Eq. (9) and summed over the energy region from 2 - 7 MeV versus the ground-state deformation parameter δ. The straight line is a best fit assuming a zero intercept.

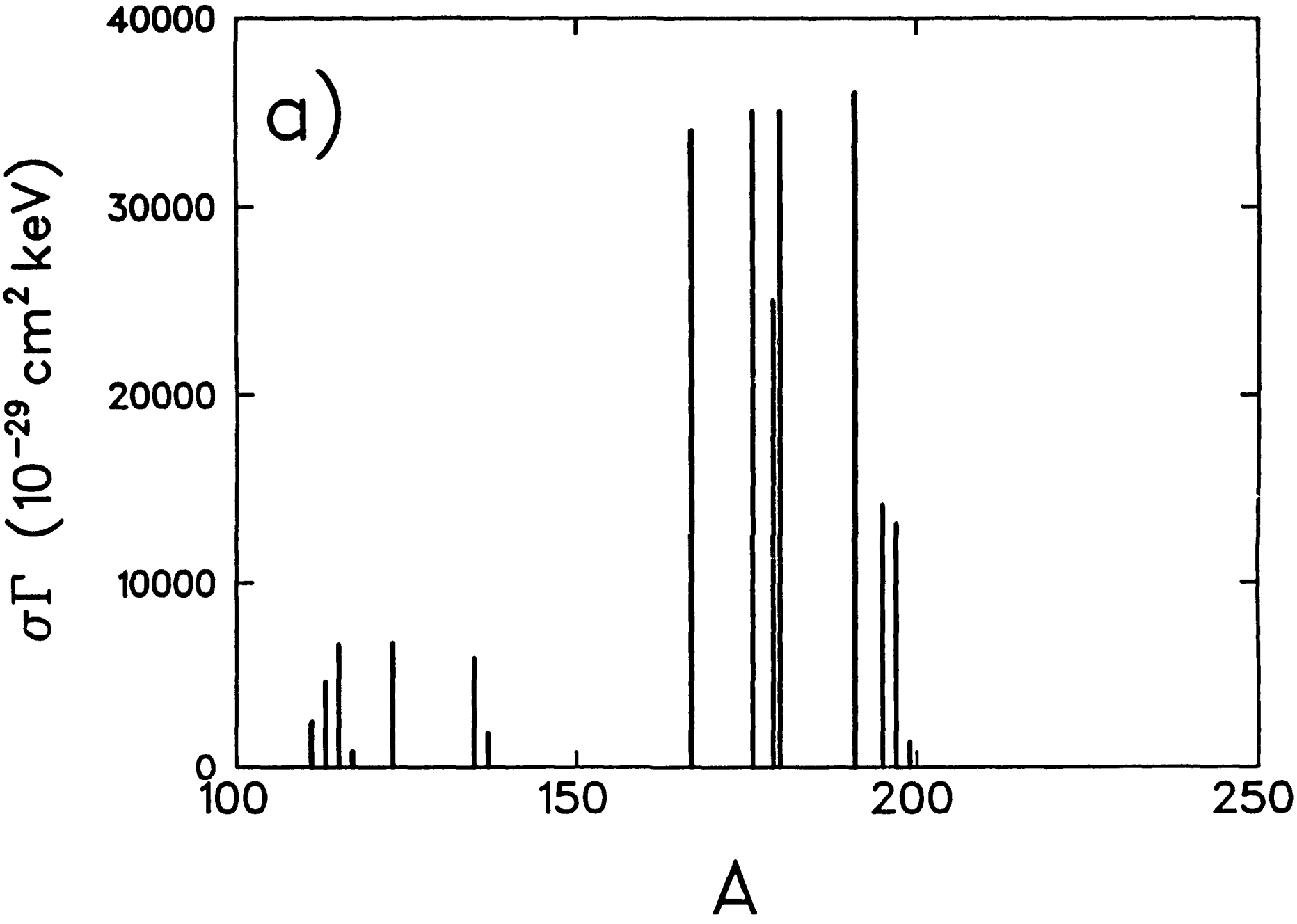
a)
40000
30000
20000
10000
0
100
150
200
250
σΓ (10^-29 cm^2 keV)
A

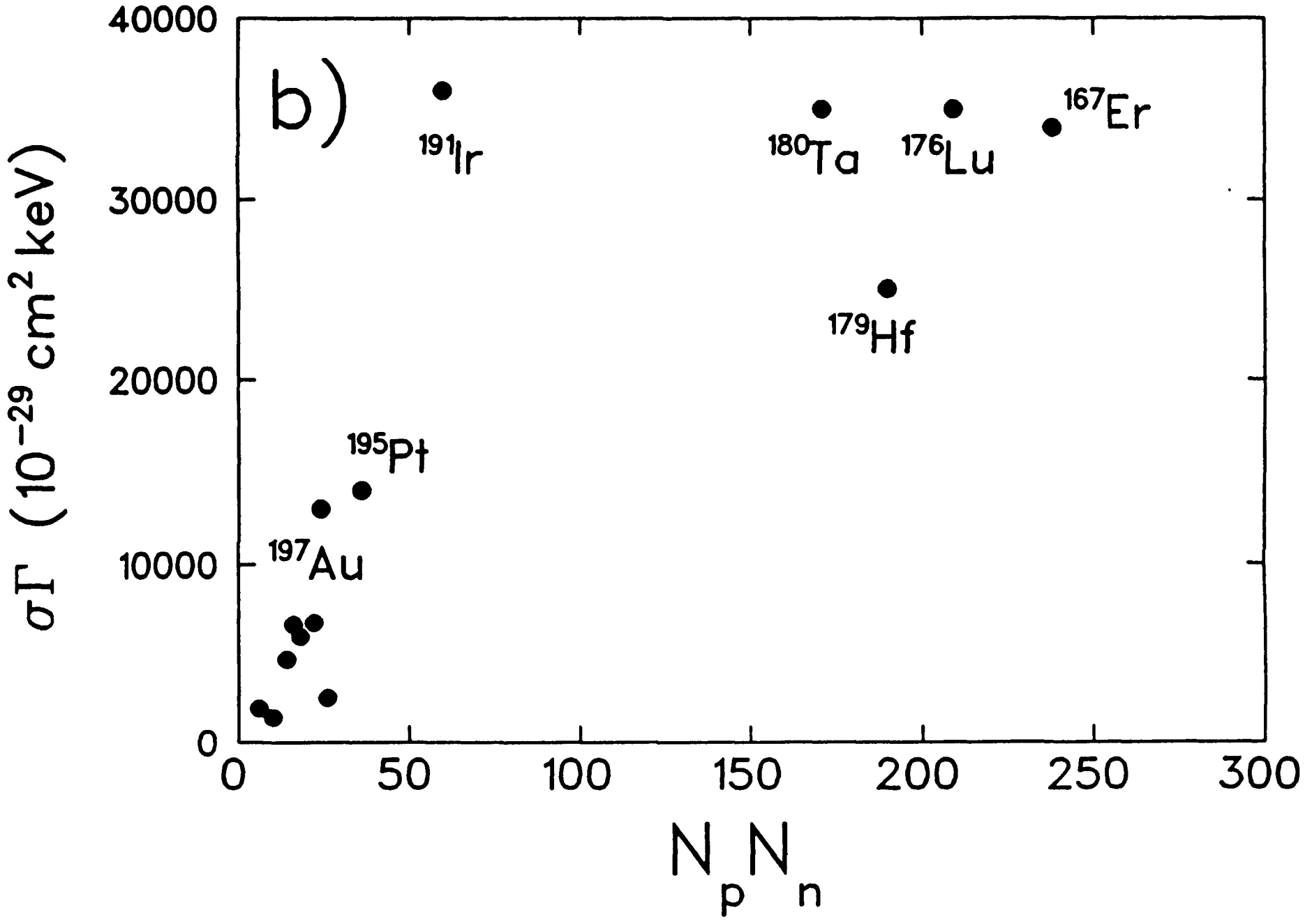
b)
40000
30000
20000
10000
0
0
50
100
150
200
250
300
σΓ (10^-29 cm^2 keV)
N_p N_n
191Ir
180Ta
176Lu
167Er
179Hf
195Pt
197Au

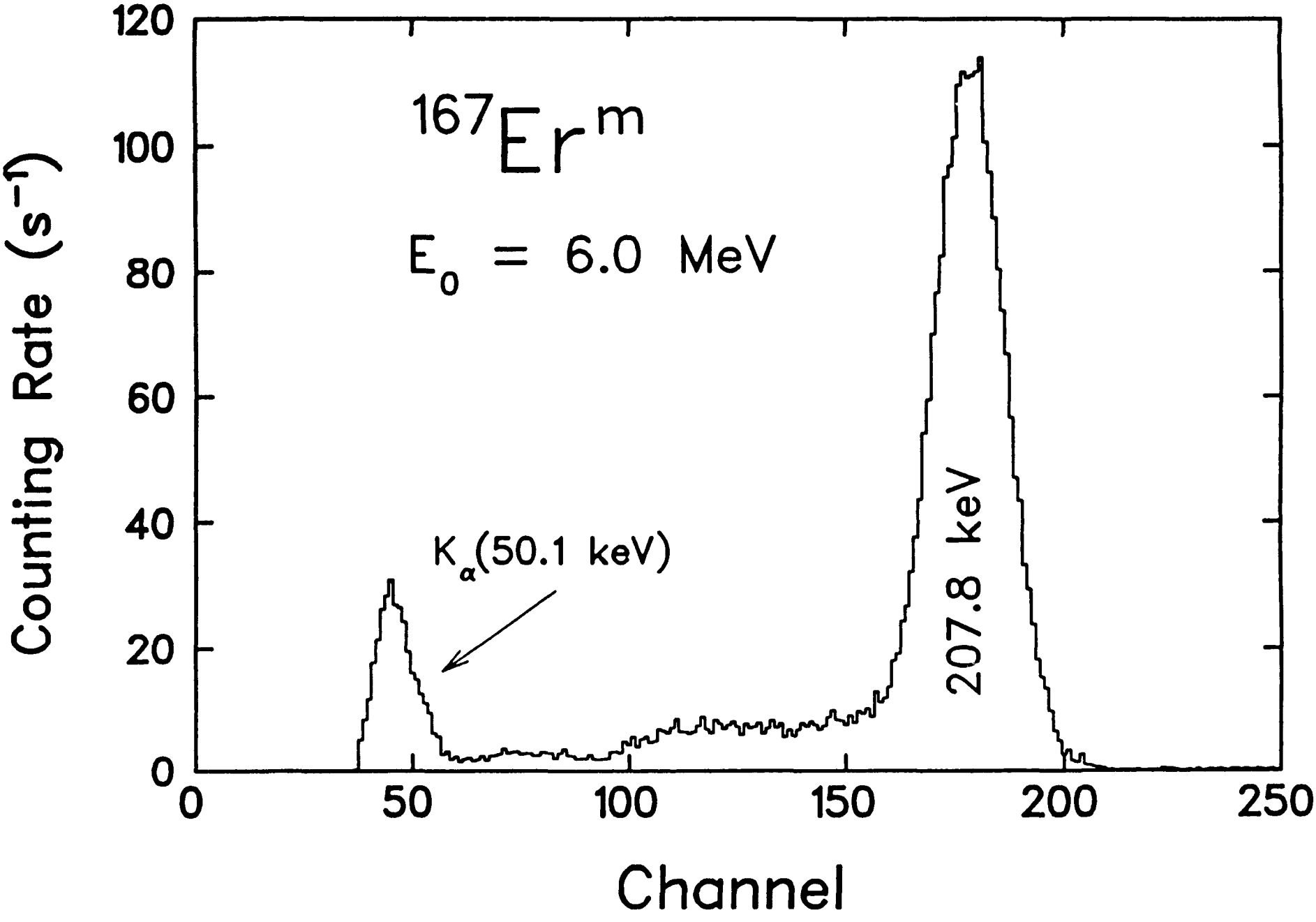
$^{167}Er^{m}$
E_0 = 6.0 MeV
K_α(50.1 keV)
207.8 keV
Counting Rate (s^{-1})
Channel
0
20
40
60
80
100
120
0
50
100
150
200
250

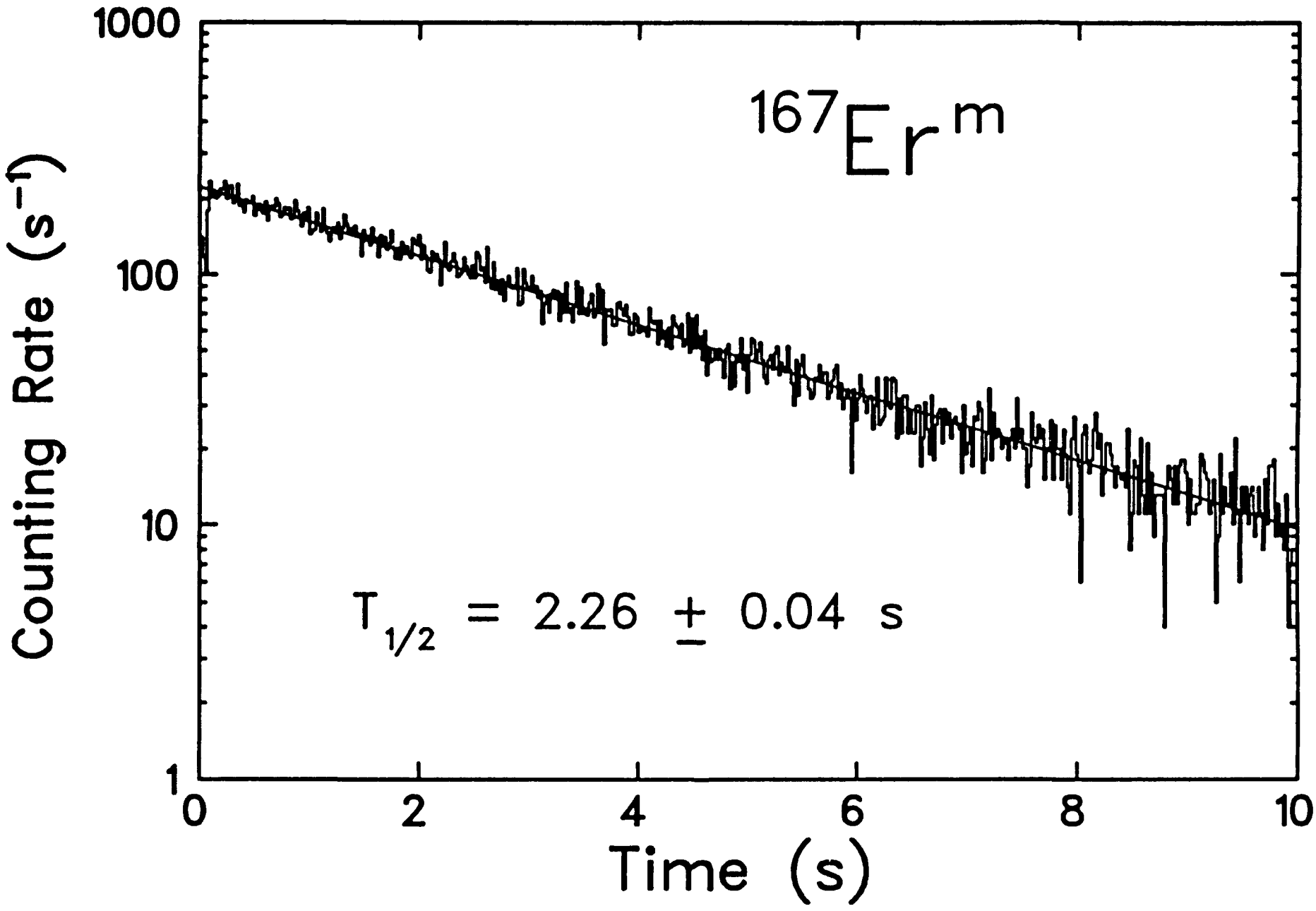
1000
100
10
1
Counting Rate (s⁻¹)
167Erm
T1/2 = 2.26 ± 0.04 s
0
2
4
6
8
10
Time (s)

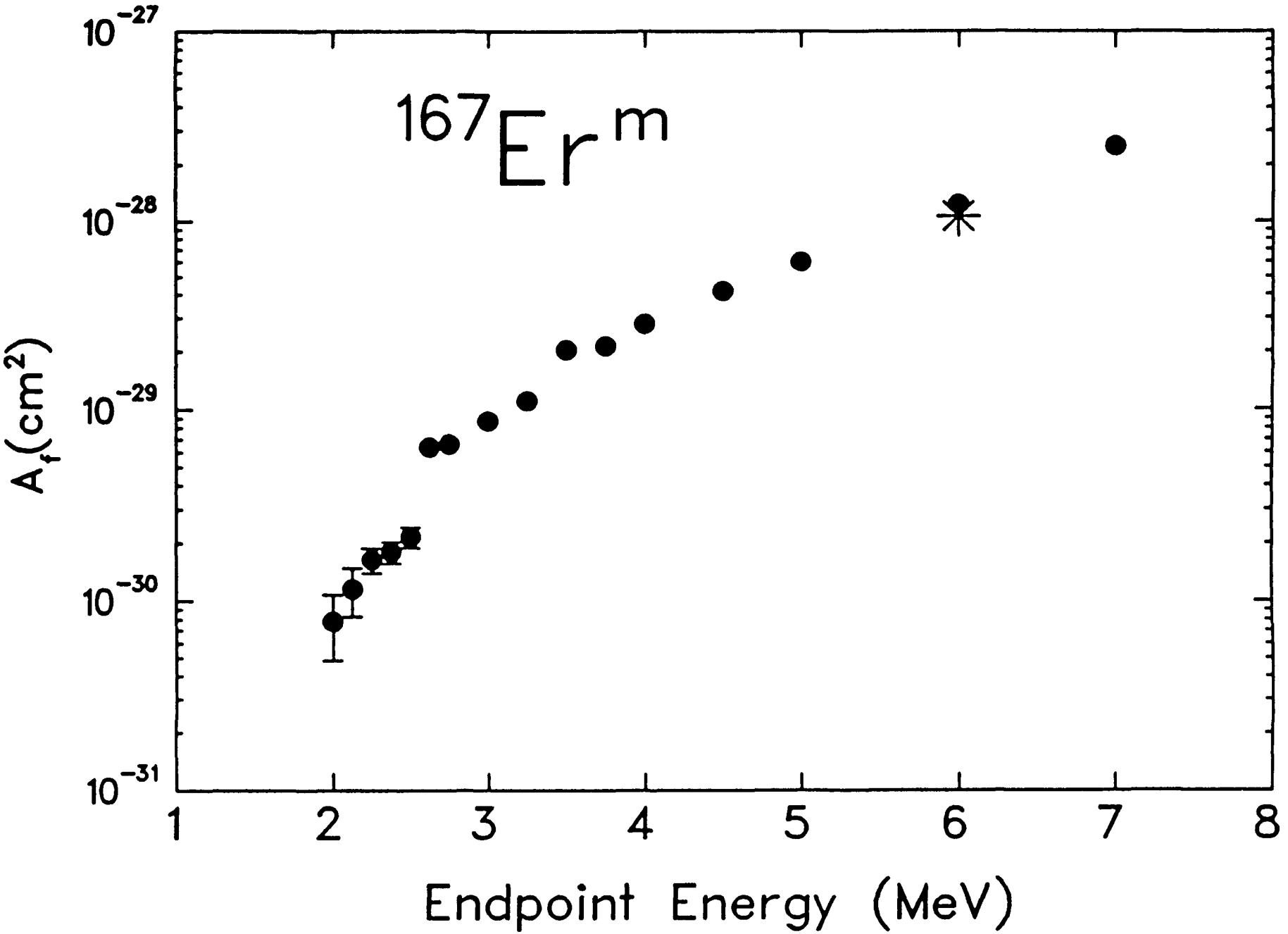
$^{167}Er^{m}$
10^{-27}
10^{-28}
10^{-29}
10^{-30}
10^{-31}
$A_f(cm^2)$
1
2
3
4
5
6
7
8
Endpoint Energy (MeV)

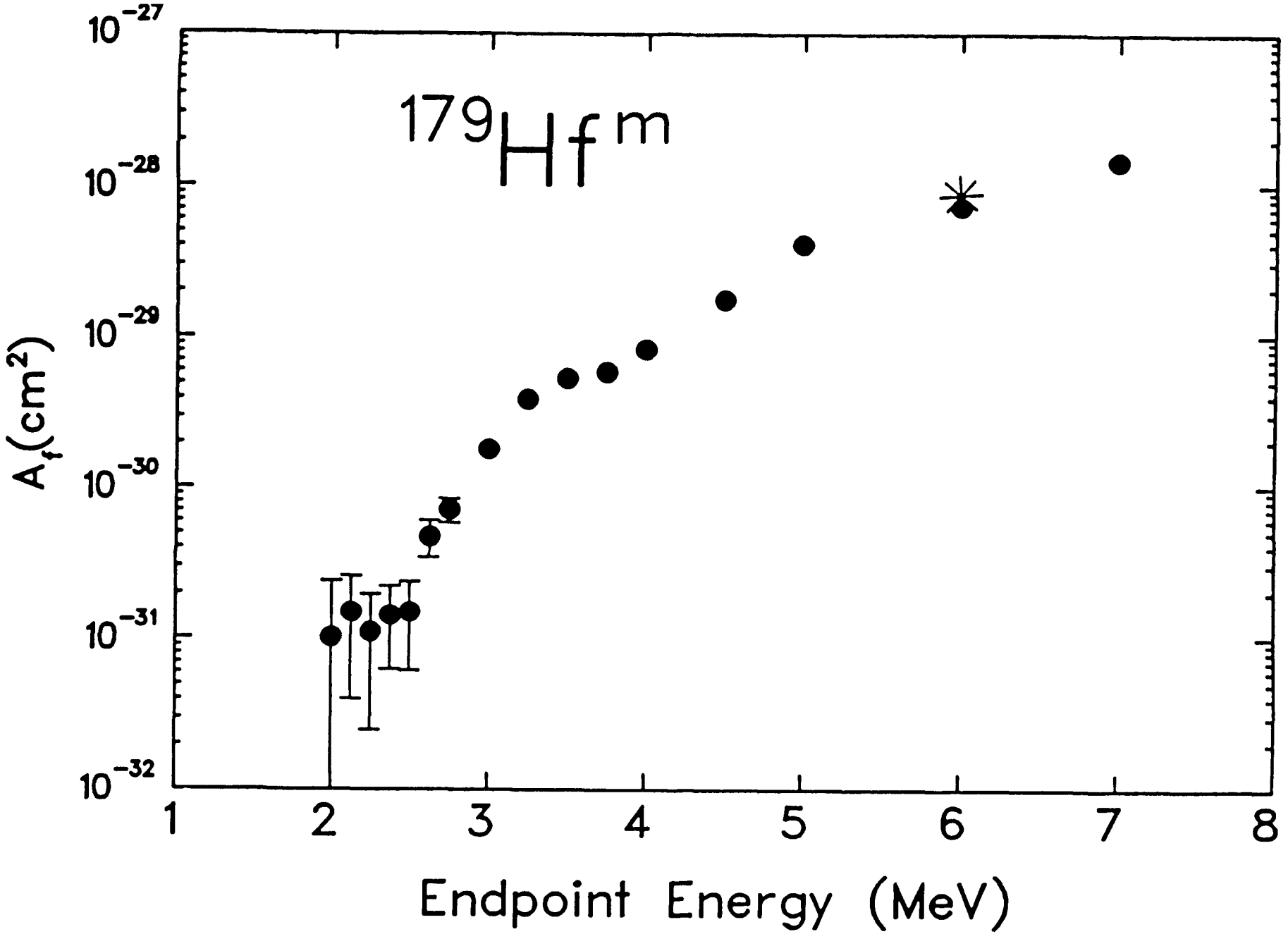
^{179}Hf^{m}
10^{-27}
10^{-28}
10^{-29}
10^{-30}
10^{-31}
10^{-32}
$A_f(cm^2)$
1
2
3
4
5
6
7
8
Endpoint Energy (MeV)

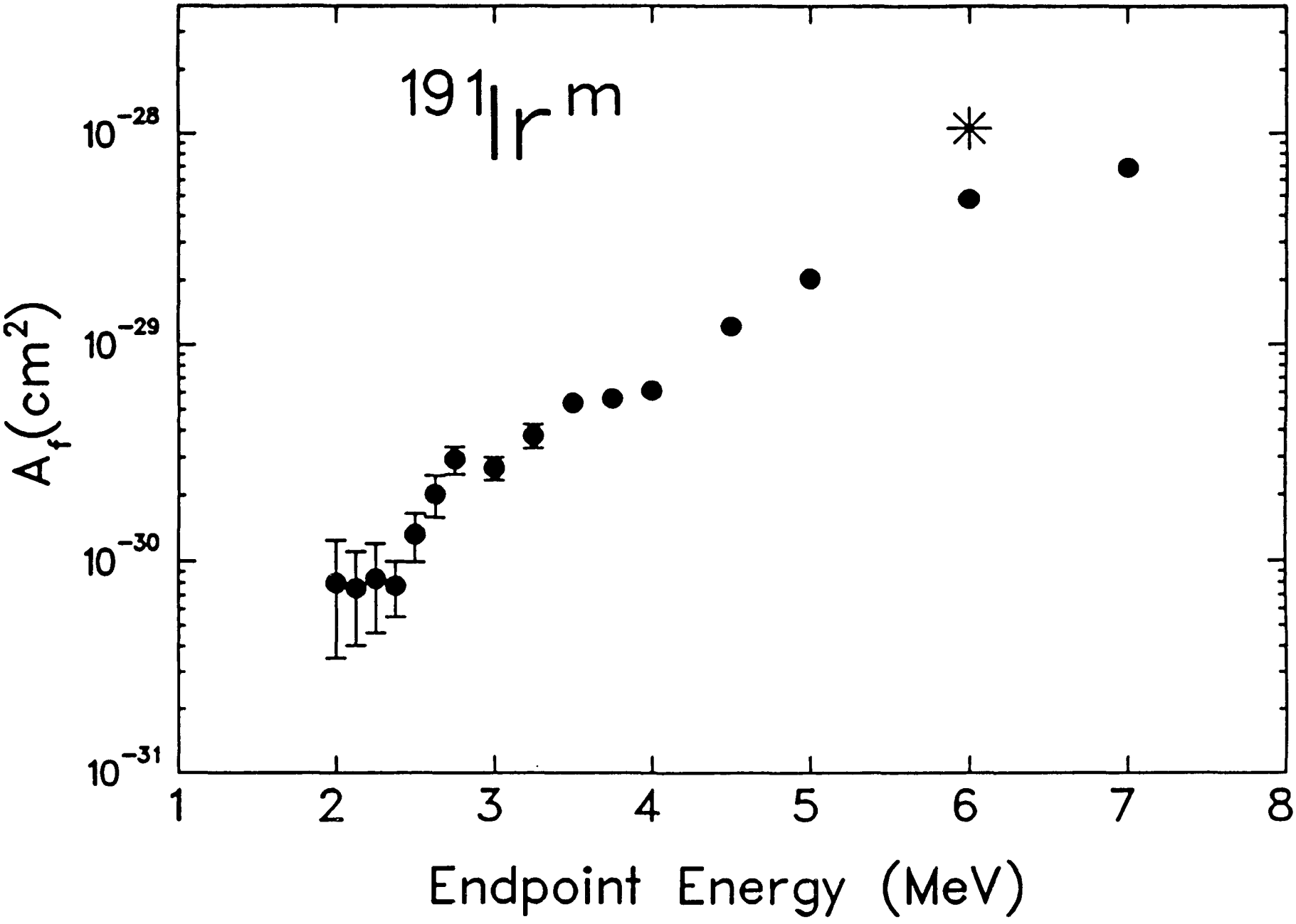
^{191}Ir^{m}
$A_f(cm^2)$
10^{-28}
10^{-29}
10^{-30}
10^{-31}
1
2
3
4
5
6
7
8
Endpoint Energy (MeV)

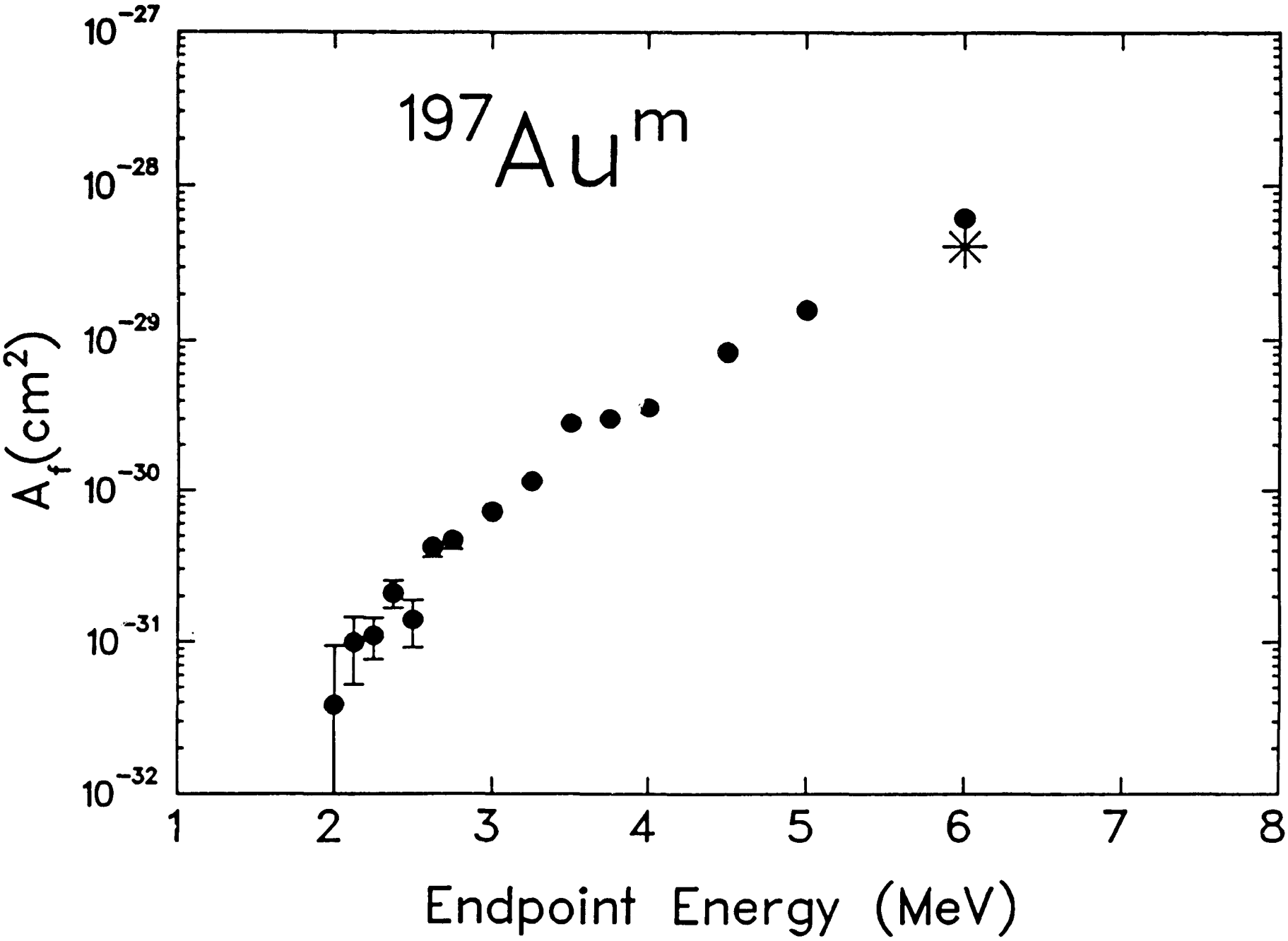
$^{197}Au^{m}$
$A_f(cm^2)$
10^{-27}
10^{-28}
10^{-29}
10^{-30}
10^{-31}
10^{-32}
1
2
3
4
5
6
7
8
Endpoint Energy (MeV)

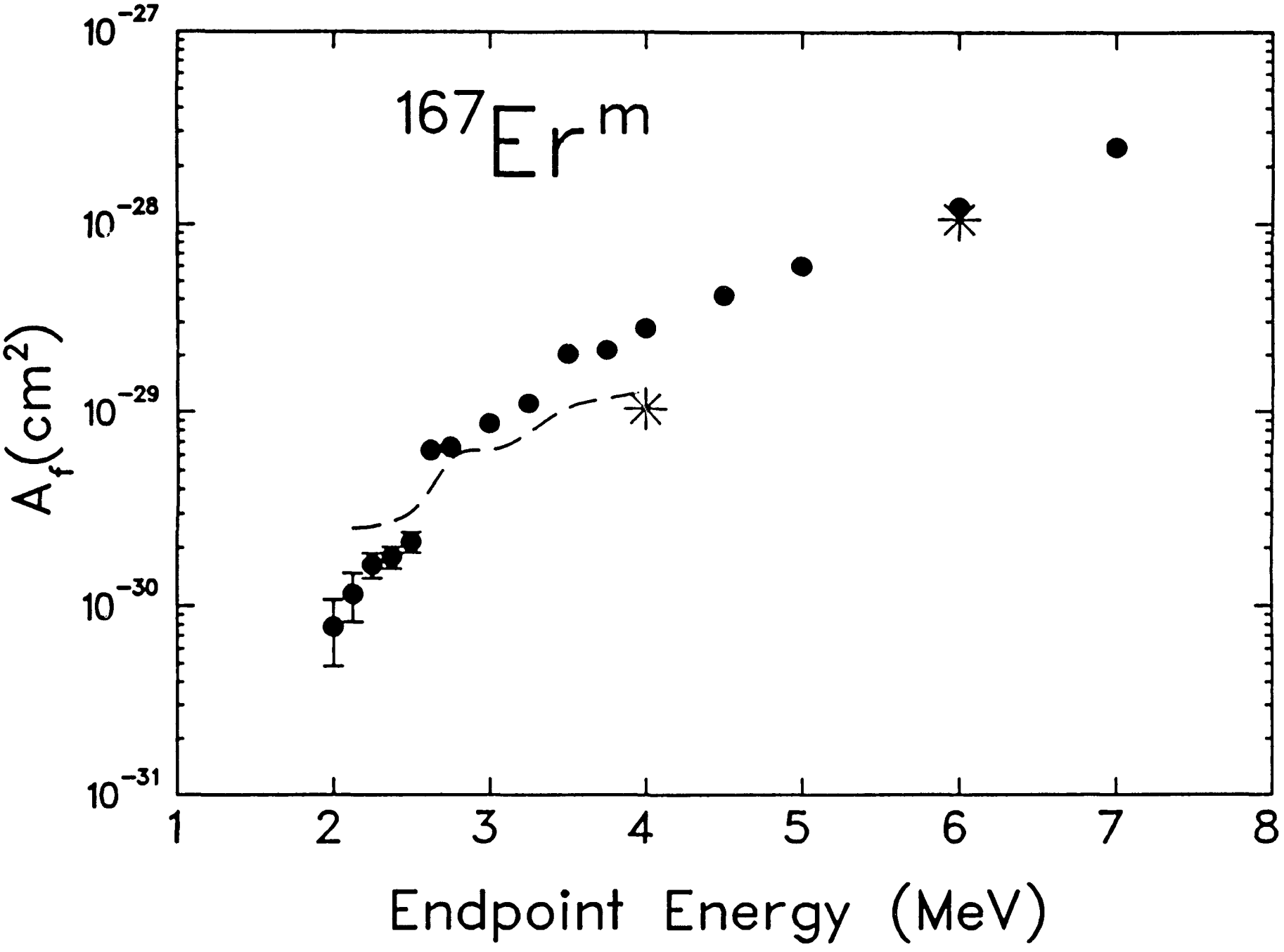
$^{167}Er^{m}$
$A_f(cm^2)$
10^{-27}
10^{-28}
10^{-29}
10^{-30}
10^{-31}
1
2
3
4
5
6
7
8
Endpoint Energy (MeV)

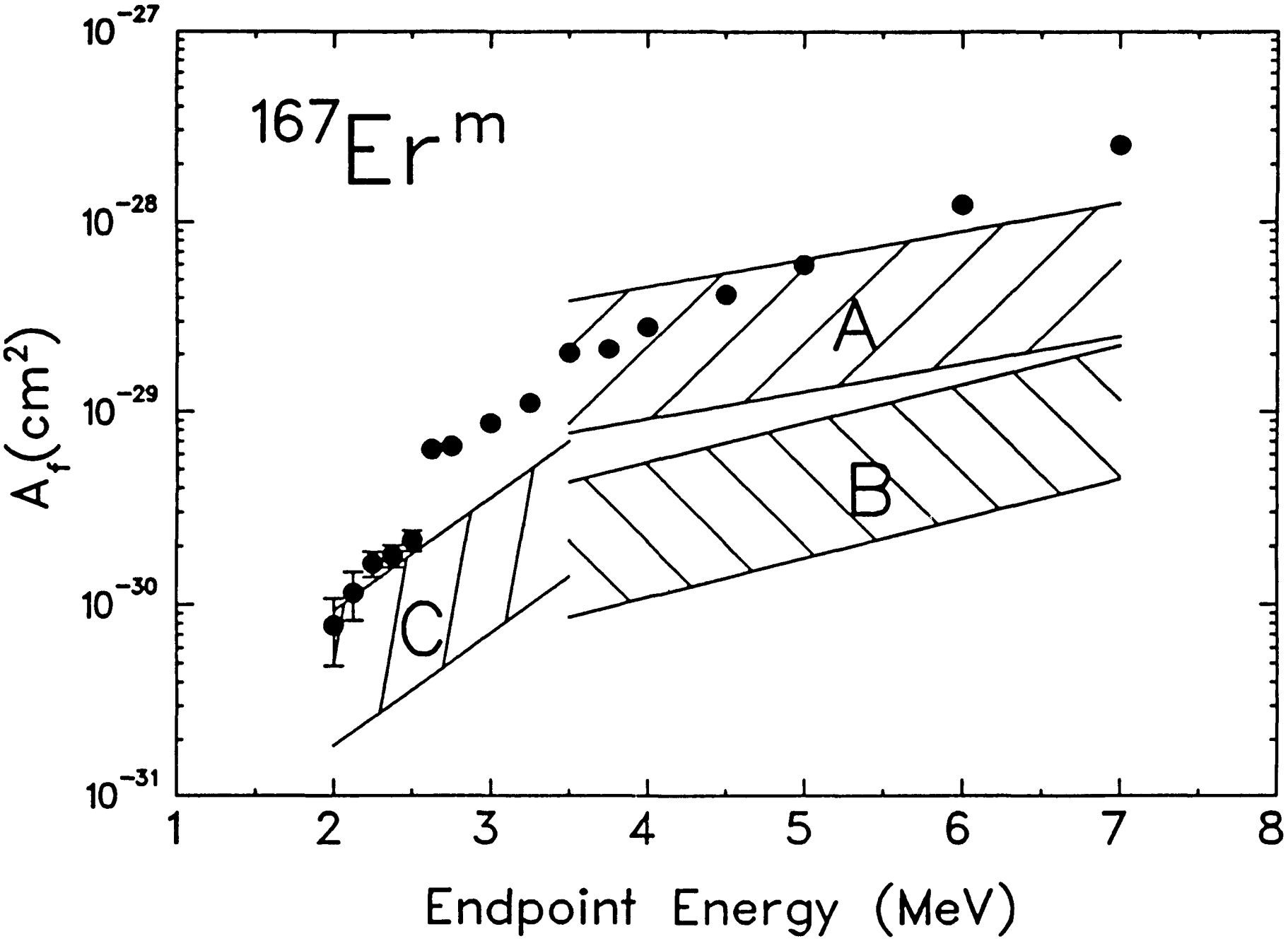
$^{167}Er^{m}$
10^{-27}
10^{-28}
10^{-29}
10^{-30}
10^{-31}
$A_f(cm^2)$
A
B
C
1
2
3
4
5
6
7
8
Endpoint Energy (MeV)

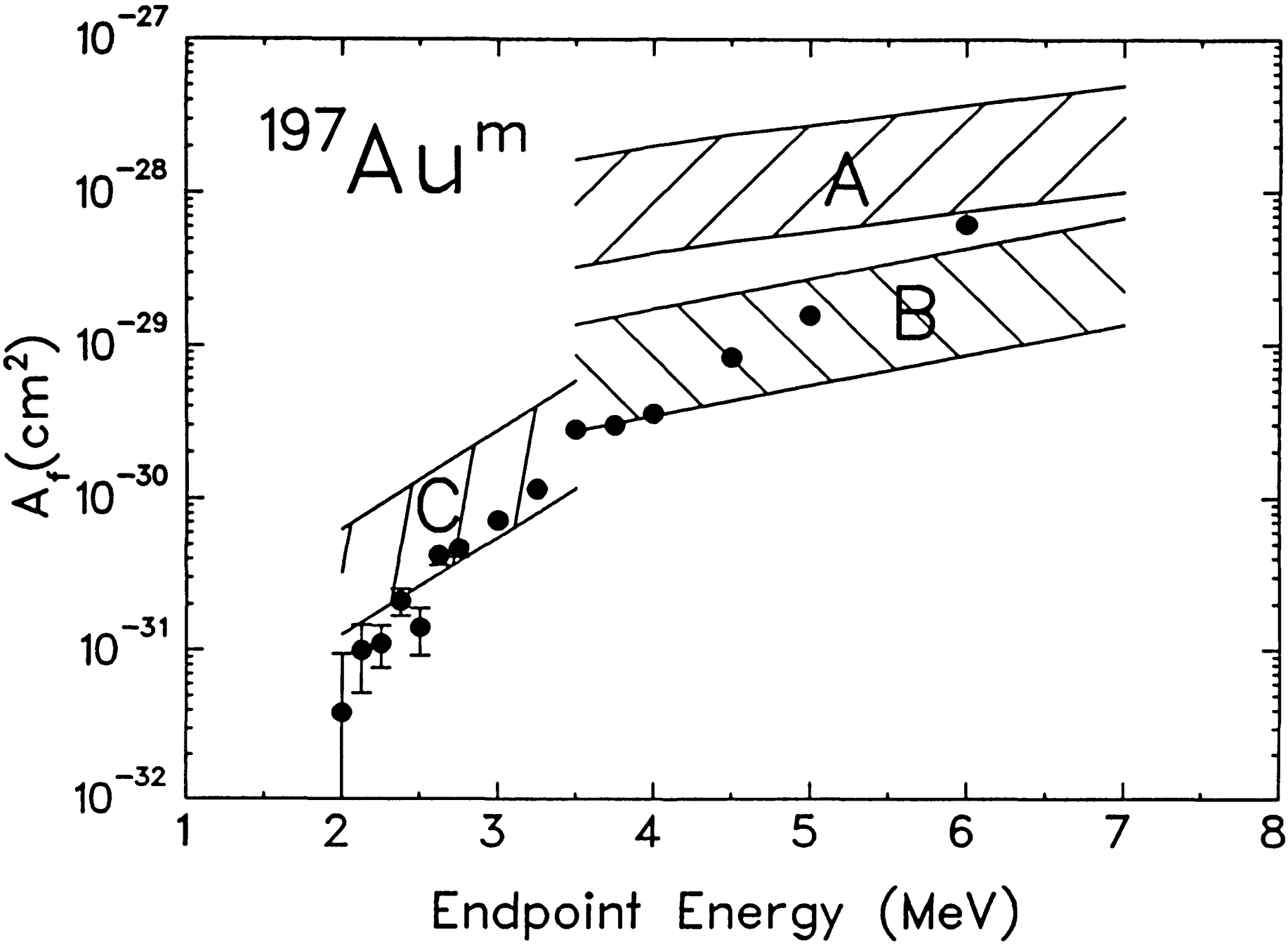
$^{197}Au^{m}$
A
B
C
$A_f(cm^2)$
10^{-27}
10^{-28}
10^{-29}
10^{-30}
10^{-31}
10^{-32}
1
2
3
4
5
6
7
8
Endpoint Energy (MeV)

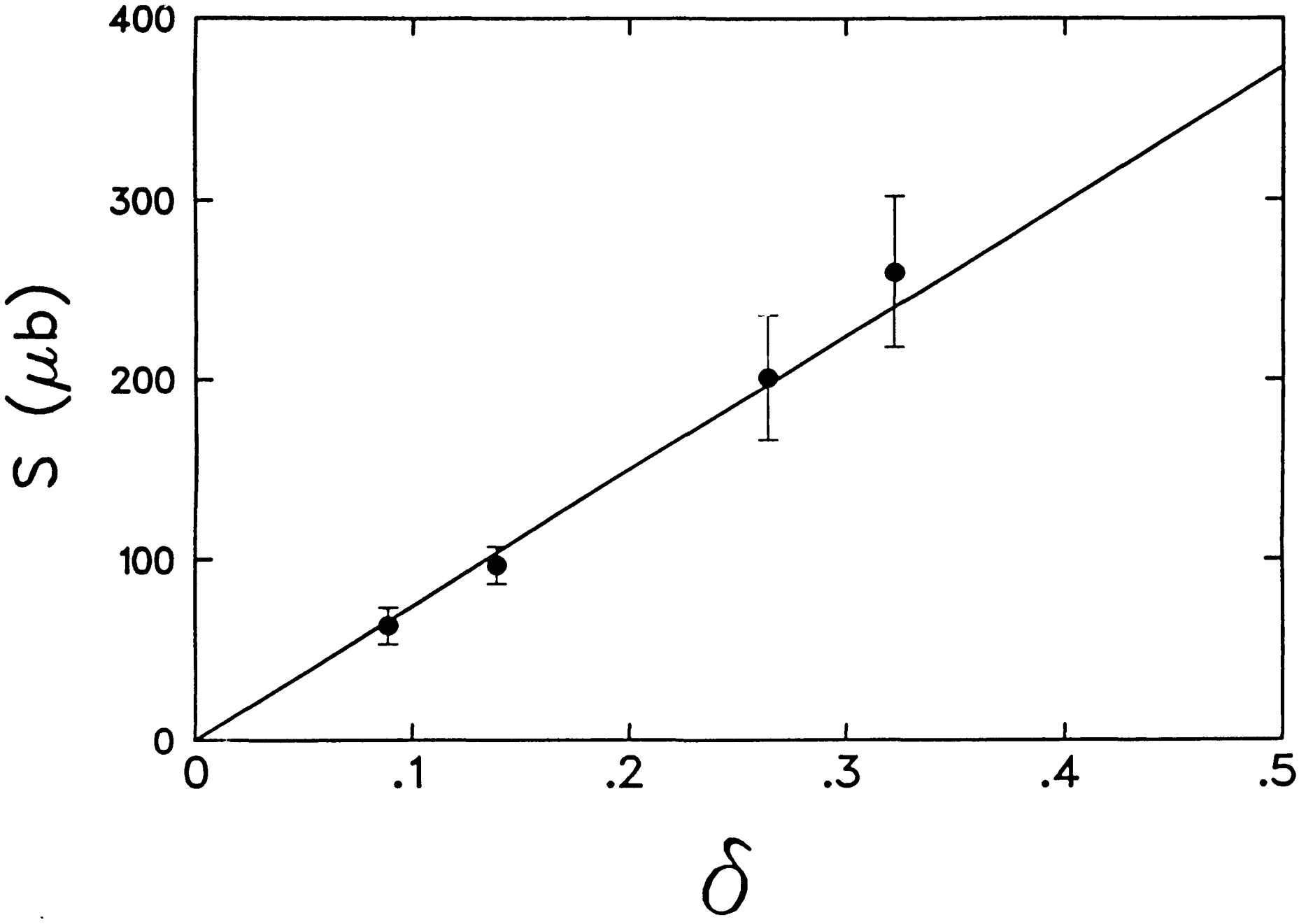
400
300
200
100
0
S (μb)
0
.1
.2
.3
.4
.5
δ

Experimental Preparations for the Excitation of Short-Lived Nuclear Isomers Pumped with the UTD-LINAC

by

K. N. Taylor, T. W. Sinor, J. D. Standifird, C. Hong,

J. J. Carroll, D. G. Richmond, and C. B. Collins

Center for Quantum Electronics

University of Texas at Dallas

P.O. Box 830688

Richardson, TX 75083

ABSTRACT

Experiments have been designed to populate Mössbauer levels of ^{57}Fe and ^{119}Sn by cascade from giant resonances pumped by bremsstrahlung radiation generated by the UTD-LINAC, the facility for which is currently under construction. In particular we have employed both resonant and non-resonant radiation transfer studies to aid in the design, construction, and characterization of a detection system for monitoring the signal electrons produced by the decay of the short-lived isomeric targets employed. Measurements utilizing conversion electron Mössbauer spectroscopy indicate that the detection system developed, convincingly approaches the level of performance considered mandatory for the harsh environment anticipated for the intended nuclear fluorescence experiments.

INTRODUCTION

Since 1986, gamma-ray laser research at the Center for Quantum Electronics has focused upon the photoexcitation of nuclei from their ground states to relatively long-lived metastable states. Current efforts have concentrated on extending the scope of this research to short-lived states. In particular, current experiments have been designed to populate the Mössbauer levels of ^{57}Fe and ^{119}Sn by cascade from giant resonances pumped by bremsstrahlung radiation generated by the UTD-LINAC. The UTD-LINAC facility is under construction and should be on-line in the spring of 1992.

In past experiments involving the photoexcitation of long-lived nuclear isomers pneumatic transfer systems were used to move the irradiated targets from the pumping environment to the detection systems. To study isomers with lifetimes less than 100 nsec, however, it will be necessary to develop experimental apparatus that allows nondestructive, in-situ detection of the fluorescence signal or some other emission proportional to it. The approach taken here to verify and measure the rate of population of the isomeric levels of the sample is to utilize it as a source of recoil-free radiation and Doppler modulate the energy of the Mössbauer emissions to pump a similar sample in an evacuated detector chamber. The second sample would then be monitored via conversion electron Mössbauer spectroscopy (CEMS) [1-6].

Research for the past six months has employed both resonant and non-resonant radiation transfer studies to aid in the design, construction, and characterization of the detection system needed to provide the capabilities for the measurements described above. Several phases of development and investigation have been involved in bringing the detection system to a level of maturity that closely approaches the design objectives. These goals include (1) an efficient transfer of resonance radiation from the external target, pumped by the bremsstrahlung radiation, to the sample, (2) an optimized collection/detector system for the signal electrons

emitted from the surface of the sample and (3) a *minimum* of scattering-induced background noise from the vacuum chamber and the components of the detection system within the chamber.

Extensive efforts were pursued to develop a system that optimized the transfer of the resonant radiation from the external target to the sample. To assure passage of the resonant γ rays into the target chamber a thin entrance window constructed of titanium was employed. This window had the added benefit of filtering many of the lower energy x rays that are products of the de-excitation process.

For a given solid angle, defined by the geometry of the external source, the sample and their separation, the next most significant factor affecting the efficiency of the resonant transfer process was the collimator. The collimator design that yielded the best performance for CEMS consisted of a lead plate having a circular aperture at its center. The aperture was shaped so that its diameter increased in the direction of propagation of the radiation. With the source located at the appropriate distance in front of the plate the desired collimation was achieved.

The significance of using the aperture-plate as opposed to a long mass of lead with a hole along its axis was that with the source backed away from the aperture, not only was the geometrical collimation defined (and therefore the scattering-induced background in the chamber limited) but a minimum of radiative scattering associated with the collimator itself occured. Due to the extremely narrow linewidths encountered in Mössbauer spectroscopy any resonant photons scattered off the sides of the collimator would be shifted out of resonance and thus become potential sources of noise inside the chamber.

Closely allied with the rationale for developing an optimized transfer of the resonance radiation from the irradiated target to the sample is that of developing an efficient detection system for the resonant γ rays entering the chamber. An ideal γ-ray detector would possess a high throughput for the signal and a correspondingly low throughput for the noise. Due to the

nature of the resonance phenomena involved in CEMS, one is in an advantageous position for developing a detector that possesses, to a significant degree, these properties. Such a resonant detector has been constructed and it consists of the resonant target, which converts the incoming γ rays to signal electrons, an electron collection system and an electron detector.

Various efforts have been pursued to separately investigate the photoelectric emission generated from the entrance and exit windows of the target chamber, the holder for the sample target, the effect of the target itself, the walls of the chamber and the electron lens assembly responsible for collecting the signal electrons emitted by the target. Radioactive samples external to the chamber served as calibration sources of radiation to produce the scattering effects required for these evaluations. The radiation emitted from the sources was collimated to define the beam geometry and its path through the chamber.

A dual microchannel plate (MCP) assembly configured in the chevron tradition was chosen as the electron detector. (See Figure 1 for the chevron configuration and biases typical of our experiments.) A microchannel plate is an array of approximately 10^6 parallel channels that serve as miniature electron multipliers. Nominal diameters of the channels range from 10 to 100 μm and have typical length-to-diameter ratios ranging from 40 to 100. The channels are either normal to, or biased at a small angle of approximately eight degrees to, the input surface of the MCP. In our research efforts we use a 25 mm diameter Galileo Electro-Optic chevron. In the chevron arrangement [7,8], two plates are oriented so that the channel bias angles provide a sufficiently large directional change at the interface to inhibit positive ions produced near the output of the rear plate (by electron-residual-gas collisions) from migrating to the input of the front plate where, upon collision with the channel wall, they might cause indistinguishable noise pulses. The plates are separated normally by approximately 50 to 150 μm. Typical detection efficiencies of chevrons for various kinds of primary radiation are summarized in Table 1 [9].

The electron collection system consisted of the target, an aperture lens designed with the aid of computer simulations and a Faraday cage structure integrated with the lens and target in such a way as to shield the lens elements from the ground potentials of the chamber walls. The lens was designed to focus and accelerate the electron emissions from the target to the electron detector. Post-emission acceleration of the electrons enhanced the focusing power of the lens and produced and increased the energy of the electrons to a level more compatible with the energy-response region of the electron detector.

OVERVIEW OF CONVERSION ELECTRON MOSSBAUER SPECTROSCOPY

Evaluation of the resonant detection system described in the previous section was most effectively obtained by performing CEMS with an external source of ^{57}Co and an enriched target of ^{57}Fe inside the target chamber. Use of the Mössbauer effect in this evaluation was of considerable value for two reasons: (1) The method of measurement in the experiment with the LINAC will involve the emission and absorption of resonance radiation. The early incorporation of the Mössbauer effect thus serves to simulate to some degree that expectation. (2) Its use also allows for the simultaneous evaluation of signal and noise production in the detection system. The Mössbauer effect makes possible a high resolution nuclear spectroscopic technique applicable to certain transitions having γ-ray energies from 10 - 100 keV. The lifetimes of the nuclear states are typically 10^{-8} seconds, which is approximately the same order of magnitude as optical transitions in atomic states. However, due to the higher energy of the gamma radiation the Q ($=\Delta E/\Gamma$) of the resonance is about 10^{12}. This ratio of the transition energy to the natural linewidth is a measure of the accuracy of the determination of relative frequency or energy changes of the system. Therefore, the Mössbauer effect allows an intrinsic resolving power much

greater than any other form of spectroscopy. It is only through the existence of Mössbauer transitions that a practical source of very narrow line radiation can be produced and detected.

A nucleus resonantly excited by the recoil-free absorption of a γ ray can decay in various ways, involving either the re-emission of a γ ray or the ejection of an atomic electron via internal conversion. Typically, low energy isomeric states are characterized by internal conversion coefficients between 1 and 100 so that the resonant scattering of Mössbauer gamma radiation is dominated by the conversion process. Since all synchronous radiation emitted after the resonant decay of a nucleus can be employed to record a Mössbauer spectrum, the detection of conversion electrons and the subsequently emitted Auger and secondary electrons, can provide a low noise spectroscopic signal for the study of the de-excitation of short-lived nuclear isomers. CEMS necessarily imposes a scattering geometry upon the experimental arrangement and therefore the emission spectrum one observes is seen as an increase in count rate in the detector.

It is significant to point out that since only those electrons emitted from the surface can be detected, this, in a sense, places a natural limit on the effective thickness of the absorber. This limit on effective absorber thickness removes any saturation effects that might be related to the severe dependence of the resonant absorption coefficient on the energy of the incoming gamma ray. Hence, the natural linewidth of the transition is observed. Typical ranges for both the 7.3 keV conversion electrons and 5.4 keV Auger electrons in iron are approximately 57 nm and 36 nm, respectively.

The decay scheme and energy level diagram of the nuclear emission for ^{57}Co and its daughter isotope ^{57}Fe are shown in Figure 2. The ^{57}Co source decays by electron capture into an excited state of ^{57}Fe, with the 3/2 $\rightarrow$ 1/2 Mössbauer transition leading to either the emission of a 14.4 keV γ ray or a conversion electron. The mean lifetime of the isomer, τ, is 1.4 X 10^{-7} seconds. From Heisenberg's uncertainty principle, $\Delta E = \Gamma = \hbar/\tau$, it can be shown that the natural

linewidth of the transition is $\Gamma = 5 \times 10^{-9}$ eV. For ^{57}Co prepared as a resonant, single-line source in a palladium lattice the 14.4 keV γ-ray emission can occur without recoil, or measurable loss of energy, in about 62-66% of the decays. Hence, in the majority of cases resonant absorption can occur since the nuclear energy levels of the source and absorber match.

With the frequency of the resonant photons so well defined, an optical Doppler shift accomplished by moving the source relative to the absorber can be easily used to tune the single emission line of the source into and out of resonance with the absorber (which may be either single-line or possess hyperfine structure). The relative velocity of the source and absorber necessary to scan a full width, 2Γ, of the resonance line is given by

$$E_D = (v/c)E_\gamma \cos\theta \quad , \qquad (1)$$

where E is the energy of the γ ray, v is the relative velocity between the source and absorber, c is the speed of light and θ is the angle between the source velocity and the direction of the γ-ray propagation.

As previously mentioned, the de-excitation of a resonant nucleus in the absorber can proceed through the emission of a Mössbauer quantum or by internal conversion, and for ^{57}Fe the total electron conversion coefficient is 8.2. The relative intensities of the conversion and Auger electrons [1] are: (1) for conversion electrons: K(7.3 keV, 79%), L(13.6 keV, 8%), and M(5.4 keV, 1%); and (2) for Auger electrons: KLL(5.4 keV, 60%) and LMM (0.5 keV, 6%). As a practical matter, insofar as actual emission from the absorber is concerned, it has been shown that 50% of the signal electrons ejected from the target have energies below 15 eV because of scattering and thermalization effects [10-12].

The sensitivity of CEMS is determined by many factors that depend on the nuclear, atomic and solid state properties of the source and scatterer. For a thin, single-line source and resonant

scatterer the maximum resonant effect to be expected is given by the ratio of the number of conversion electrons ejected from the absorber to the number of photoelectrons ejected [1,2]. The expression for calculating this figure is given by

$$\eta_{cems} = \frac{N_0 - N_\infty}{N_\infty} = \frac{na\delta f_s f_a \alpha \sigma_0 \Omega}{2n\delta\,(\alpha + 1)\,\sigma_{ph}\Omega} = \frac{a f_s f_a \alpha \sigma_0}{2\,(\alpha + 1)\sigma_{ph}\Omega} \quad , \qquad (2)$$

where N_0, N_∞ are the count rates on and off resonance, n is the number of target nuclei per cm^3, a is the isotopic abundance of resonant nuclei, δ is the thickness of the target (on the order of several mean-free-paths of the conversion electrons in the absorber), σ_0 and σ_{ph} are the cross-sections for the Mössbauer and photoeffect and Ω is the relative solid angle (normalized to 4π) for detection of electrons, f_s and f_a are the recoil-free fractions for the source and absorber, and α is the total internal conversion coefficient. In actuality, the observed magnitude of the effect is significantly smaller than the value calculated from Equation 2. One major reason is that in the experiment conducted here a single-line emitter is used for the source but the absorber exhibits a multiplicity in which six allowed transitions having line intensities in the approximate ratios of 3:2:1:1:2:3 are present. The percent effect of the transitions are reduced by the ratio of the area under the resonances. Therefore, CEMS for the first transition would be about 20 using the values $\sigma_0/\sigma_{ph} = 400$, $\alpha = 8.2$ and $f_S = f_a = 0.7$.

OVERVIEW OF DESIGN AND DEVELOPMENT

Several distinct phases of design and testing were involved in bringing the target chamber to its present level of performance. For the earlier stages of development and evaluation a 12 mCi source of ^{57}Co was used to supply non-resonant radiation to the vacuum chamber and its

contents in order to simulate the scattering conditions to be expected in the latter steps of the evaluation process. The final stage of studies involved utilizing the CEMS procedure to determine the efficacy of the resonant detection system. The same source of radiation was used for both the nonresonant and resonant studies.

The physical layout of the system consisted of mounting the MCP, sample, electric feedthrough connectors and the Faraday cage as an integral unit on a six inch vacuum flange. As indicated in Figure 3, this provided for the convenient mounting and removal of the entire assembly from the vacuum chamber. The angular position of the target assembly with respect to the direction of the γ rays could be changed by rotating it about a vertical axis.

Chamber Background

To determine the contributions of the chamber itself to the scattered radiation arriving at the input of the electron detector, the MCP was replaced with a thin-window NaI detector placed in a shielded, custom mount that was located in the exact location of the MCP. It was found that radiation scattering from the chamber could be minimized by providing a radiation exit window diametrically opposite the entrance window. This window was constructed of mylar to minimize backscattering of the radiation and had a diameter of four inches. With proper collimation of the ^{57}Co source, the beam size could be optimized to illuminate only the target while not expanding to a diameter greater than the output window.

Detector Assembly Background

One of the initial experiments conceived to optimize the detector arrangement consisted of measuring the photoelectric contribution of the detector assembly excited by the external radioactive source. In part, to prevent contamination of these measurements by photoelectrons

produced by incident radiation striking and scattering off the walls of the vacuum chamber the MCP target assembly was enclosed in a Faraday cage which served as an opaque barrier to all but the most energetic photoelectrons.

To verify a consistent performance of the MCP for these background measurements an unsealed ^{57}Co source with a nominal activity of 11.6 microcuries was mounted inside the target chamber. A lead disk coupled to a rotary vacuum feedthrough served as a selective filter to pass either electrons and photons, γ rays and x rays only, or to block all direct radiation from the MCP. Since this source was mounted outside the Faraday cage, the effectiveness of the Faraday electrostatic shield against the inward migration of electrons could also be observed.

The relative photoelectric and Compton contributions from components inside the Faraday cage were determined in a series of experiments in which materials having different Z-values were employed. The basic experimental arrangement contained a chevron (with an electron lens) and a static external $^{57}Co(Pd)$ source for exciting the chamber. Once the chevron was shown to be operating at nominal sensitivity the internal reference source was blocked by the radiation filter. The radiation from the external Mössbauer source was, of course, collimated to define the beam. Data were collected in this arrangement with various combinations of the detector components assembled. The configurations included: (1) null, (2) Faraday cage, and (3) Faraday cage with target holder. In the final configuration, 5 cm by 5 cm targets of mylar, aluminum, copper, and tantalum were used. The results of these experiments are summarized in Table 2. In all of the configurations above, the operating bias across the chevron was -1440 V, and the protection grid and Faraday cage biases were -2400 V.

Relative Background Contributions of Target/Target Holder

As indicated previously, a collimator was used to control the spatial extent of the radiation beam entering the chamber. The most effective configuration for the background measurement was found to be a cylindrical collimator 5.4 cm in diameter and 21.3 cm long cast out of lead with a 0.7 cm bore machined to obtain the desired collimating effects. This collimator produced a spot size at the target center of 1.2 cm diameter and expanded to 1.8 cm at the radiation escape window. Since only the non-resonant processes were of interest at this stage, the frequency downconversion characteristic of a long collimator was not detrimental. To take proper advantage of this high level of collimation the collimator was mounted on a gimbal and coupled to a micrometer which allowed the radiation to be scanned horizontally over the target assembly (no Faraday cage or lens being present). To measure the angular deviation of the source about the normal to the entrance window a mirror epoxied to the rear of the collimator was illuminated with a He-Ne laser normally incident to the mirror. The angular separation of the incident and reflected beam, 2θ, was measured geometrically.

By scanning the radiation across the target assembly the sensitivity and value of this approach was confirmed by the extent of the relative photoelectron contributions observed for the holder and target. Again, data were collected for mylar, tantalum and null targets. Representative data for the tantalum and null targets are shown in Figure 4. As can be seen from the figure, photoelectrons from the target holder, constructed out of teflon, are clearly visible to the detector. While this signal is much smaller than that from a tantalum target, it was soon determined that it could still contribute a significant background in a CEM spectrum. To circumvent this source of noise, a new target holder was constructed out of delrin, which is a low-Z polymer having excellent vacuum properties.

Electron Lens Design and Construction

To increase the total detection efficiency for signal electrons by the chevron, an electrostatic, aperture lens was constructed to effectively increase the solid angle between the electron detector and the target foil. With a 1.2 cm spot size on the target foil, a chevron with a diameter of 2.5 cm and a separation distance of 9.5 cm, a geometrical solid angle of 1.3 steradians was defined. Numerous computer simulations using plane-wave and point-source electron configurations have shown that the electrostatic lens gives an effective solid angle of almost 2π steradians for electrons having appropriately low energies.

The structure and dimensions of the lens can be seen in Figure 3. It exhibits a standard two-stage ring configuration constructed from copper mesh with the potential difference between the two rings acting as the primary electron accelerator. It has an outside diameter of 12.7 cm, and a length of approximately 15 cm. The two annuli making up the rings have successively smaller apertures as the MCP is approached. The first annulus has an inside diameter of 3.2 cm while the second has an inside diameter of 2.5 cm. This was done to allow the electrostatic fields generated by the annuli to penetrate into the region occupied by the target foil, and so that the inside diameter of the second annulus matched the diameter of the MCP. This aided in preventing oversteering of the electrons so that a greater fraction of them were incident upon the face of the MCP.

Each lens segment is surrounded by copper wire cloth, fashioned in a simple weave, so as to simulate a Faraday cage. The Faraday cage used in earlier experiments proved the value of such structures in shielding the MCP from noise electrons produced outside the cage. Most importantly, however, the Faraday cage here serves to shield the various lens elements from the ground potentials of the chamber walls that would grossly distort the focusing fields. A fine mesh

endcap with 81% open area was placed over the portion of the lens next to the chevron input to complete the shield assembly.

The choice of copper wire cloth for the lens material was made for several reasons. First, it was very important that the mass inside the chamber be kept to a minimum since any mass can potentially be a source of photoelectric and Compton noise. Secondly, a mesh was needed so that openings would exist for the external radiation source to illuminate the target foil. The field disturbances caused by using a mesh instead of a continuous sheet of metal can easily be shown to be negligible [13].

The copper mesh has a wire diameter of approximately 250 μm and about 6 weaves per cm. Using simple formulae, it can be shown that this material has 69 percent open area. To increase the percent open area in the direct path of the radiation, alternate wires in the region of the lens within the path of the external radiation were removed. This reduced the mass present in the path of the radiation and, correspondingly, the photoelectric and Compton noise. The lens elements were then shaped and mounted on the MCP-target assembly. An annulus constructed from a low-Z polymer separated the two lens elements.

Once construction of the lens was completed and initial experimentation begun, it was necessary to find optimum potentials for the various parts of the lens so that maximum focusing could be achieved without putting "bright spots" on the face of the MCP which could physically damage the detector. This was accomplished using the EGUN2c electron optics software package traceable to SLAC. Once the initial boundary configuration was entered it was possible to test a variety of voltage arrangements, and plot corresponding electron trajectories. A set of representative trajectories is shown in Figure 5.

As indicated previously, about 50% of the signal electrons leaving the target have energies at or below 15 eV. Using this energy, various electron emission configurations such as plane

waves and point sources were simulated with electrons starting just off the surface of the foil. The overriding concern in the optimization process was that in order for an electron to be appreciably accelerated through the lens, it must, of course, be exposed to progressively higher potentials as it traverses the lens. However, the target foil is biased slightly less negatively than the first lens element to assist electrons near the edges in escaping from the target foil (see Fig. 3). The primary constraints on the optimum voltage selections were due to the fact that the chevron grid was being operated at -1870 V, and that the power supplies readily available were not capable of producing more than -3000 V. Nonetheless, suitable biases were found to achieve an effective collection solid angle of almost 2π steradians.

After optimizing the lens biases using computer simulations, further experimental refinement was performed by analyzing the count rates in multichannel scaler (MCS) spectra collected at various lens bias settings. The optimum operating biases for the lens were found to be V_{R1} = -2817 V, V_{R2} = -1967 V, and V_{Target} = -2757 V when the chevron was operated at -1616 V, and with the MCP grid at -1866 V.

It was expected that a small fraction of the signal electrons from the target foil would have energies approaching 7.3 keV. At these energies, the lens is almost completely ineffective due to limitations on its size imposed by the vacuum chamber and by restrictions on its bias values. The geometrical collection efficiencies for these electrons, having an effective solid angle defined solely by the geometry, prevented the experimental signal-to-noise ratios from reaching the full theoretical value.

CEMS EXPERIMENTAL ARRANGEMENT FOR DETECTOR EVALUATION

A block diagram of the experimental arrangement is shown in Figure 6. The source-target-detector was in a typical scattering geometry. A ^{57}Co(Pd) source was mounted on a velocity

transducer to Doppler shift the energy of the source. The intensity of the scattered radiation (conversion, Auger and secondary electrons) was monitored as a function of velocity.

The Mössbauer spectrometer employed made use of a velocity sweep system with an electromechanical driver on which the source was mounted and which was swept periodically through the range of interest. The spectrum was recorded by storing counts in memory channels of a multichannel scalar, that were addressed sequentially and synchronized with the velocity. By monitoring the Doppler motion of the source with an interferometer, velocity information was multiplexed into every 16th channel of the MCS. During the subsequent data analysis, a channel number could easily be converted into velocity units. This form of data collection is usually called a constant acceleration mode since a range of velocities are swept through at a linear rate.

To optimize the counts per second registered by the detector, useful information was obtained by difference measurements performed at constant velocity. In general, the Doppler velocity of the source was chosen to coincide with one of the Mössbauer resonances, then some parameter of the experiment was changed and the counting rate, (CPS), recorded. The experiment was repeated off-resonance to determine the noise contributed to the spectrum. This technique was used in our calibration work to monitor the intensity of a selected resonant emission as a function of the lens bias configuration.

Vacuum Pumping System for CEMS

Up to this point, for non-resonant studies of the environmental influences on the signal noise, the vacuum requirements were satisfied by using a turbo molecular pump (TMP) to maintain the appropriate pressure in the target chamber. But now, after having identified and reduced the sources of noise due to photoelectrons and scattered radiation, it became appropriate to proceed with the more precise Mössbauer experiments in which both resonant and non-

resonant signals could be observed. Unfortunately, however, since the Mössbauer effect is easily destroyed by spurious vibrations, the TMP could no longer be used to produce the vacuum of 2 X 10^{-6} Torr necessary for proper MCP operation.

To provide for vibrationless pumping, a 140 l/s Varian diode Vaclon pump was employed. Such pumps operate by ionizing gas in a magnetically confined cold-cathode discharge. Several mechanisms typically combine to pump the myriad of gases present in a vacuum chamber. These include the trapping of electrons in orbits by a magnetic field, ionization of gases by collision, sputtering of the titanium anodes by ion bombardment, gettering of active gases by the titanium, and diffusion of hydrogen and helium into the titanium. For the noble gases, the basic pumping mechanism is burial in the pump walls. These mechanisms combine to form an extremely harsh environment inside the Vaclon pump. Unless proper precautions are taken, neutral and charged particles as well as radiation (hard UV) can escape from the pump and seriously degrade the performance of the detector. To prevent contamination from the Vaclon from entering the target chamber, a line of sight baffle was inserted between the pump and target chamber. The baffle consisted of six successive plates having staggered apertures serving as choking orifices for the pump feedback.

Unfortunately, by using the baffle to reduce the noise from the pump to a negligible level, the efficiency of the pump was reduced to such a point that it could no longer maintain the chamber at the required pressure of 2 μTorr. To overcome this problem, an additional, smaller, ion pump was added to the pumping system. In this manner the contamination of the signal was reduced below observable limits and pressures as low as 1 μTorr could be maintained.

CEMS Evaluation of Detection System

The final test of the electron lens assembly was to collect a CEM spectrum at the optimum bias potentials. Since resonant effects were being studied at this point in the development the aperture collimator was introduced. The target was a 5.0 cm by 5.0 cm by 2 μm iron foil with an enriched abundance of ^{57}Fe nuclei of 93.55 percent. Data were collected with the electron lens in the active mode at the optimum biases previously mentioned and in the passive mode with the Faraday shield bias at -1866 V. These data are shown in Figure 7. In Figure 7a, with the lens in a passive mode, only those electrons falling within the geometric solid angle subtended by the target and chevron were collected. With the lens in the active mode, Figure 7b, the effective solid angle approaches 2π. The signal-to-noise of the specrtum, $(N_0 - N_\infty)/N_\infty$, was found to be 8.1; over an 800 percent effect in the #1 transition!

The maximum percent effect reported in the literature is η_{CEMS} = 3600 percent [1]. However, this was for a single line source and absorber. Since approximately 25 percent of the total resonance was under the #1 transition in our data, we can multiply the literature value η_{CEMS} = 3600 percent by 0.25 to estimate what their percent effect would have been if they had used a split absorber. This gives η_{CEMS} = 900 percent. Our data gave a percent effect only 10 percent lower than the maximum ever reported in the literature!

CONCLUSIONS

The substantial effort that has been contributed to the design, development and characterization of the target chamber being prepared for use with the UTD-LINAC has yielded a detector system that convincingly approaches the level of performance considered mandatory for the harsh environment anticipated for the intended nuclear fluorescence experiments conducted under more

nearly laser-like conditions. Certainly room for further refinement exists and efforts will continue to take us in that direction. Efforts toward improving the collecting ability of the electron lens toward higher energy electrons can be pursued, further reduction of background noise can be addressed, reliability standards of the microchannel plates can be established, and efforts toward determination of the total detection efficiency of the detector can be completed.

TABLE I

Detection efficiency of a chevron microchannel plate for various types of incident radiation.

Type of Radiation	Range	Detection Efficiency (%)
Electrons	0.2 - 2 keV	50 - 85
	2 - 50 keV	10 - 60
U. V. photons	300 - 11 A	5 - 15
	1100 - 1500 A	1 - 5
Soft γ rays and x rays	0.5 - 2 A	5 - 15

TABLE 2

Counts per second for various component configurations inside the chamber with the internal reference blocked.

Component	CPS with external source	CPS without source
Null	30.23 ± 1.62	3.14 ± 1.49
Cage	36.65 ± 1.88	2.56 ± 0.56
Cage/Holder	43.90 ± 1.87	1.65 ± 0.35
Mylar	42.02 ± 2.22	2.39 ± 0.44
Aluminum	41.41 ± 1.94	1.54 ± 0.40
Copper	46.20 ± 1.85	1.57 ± 0.38
Tantalum	67.55 ± 2.44	1.56 ± 0.35

REFERENCES

1. J. A. Sawicki, Industrial Applications of the Mössbauer Effect, ed by G. J. Long and J. G. Stevens. (Plenum Press, New York, 1986), p.83.
2. Gerd Weyer, Mössbauer Effect Methodology, Vol. 10, ed by I. J. Gruverman and Carl W. Seidel, p. 301 (1976).
3. K. R. Swanson and J. J. Spijkerman, J. Appl. Phys., 41, 3155 (1970).
4. R. Oswald and M. Ohring, J. Vac. Sci. Technol., 13, 40 (1976).
5. J. J. Spijkerman, Mössbauer Effect Methodology, Vol. 7, ed by J. Gruverman, p. 85 (1971).
6. J. A. Sawicki, Nucl. Instrum. and Meth., B16, 483, (1986).
7. R. W. Airey, T. T. Norton, B. L. Morgan, J. L. A. Fordham, D. A. Bone, and J. R. Powell, Electron Image Tubes and Image Intensifiers, SPIE 1243, 140 (1990).
8. O. H. W. Siegmund, K. Coburn, and R. F. Malina, IEEE Trans. Nucl. Sci., NS-32, 443 (1985).
9. P. Schagen, Advances in Image Pick-up and Display, Vol. 1. (Academic Press, New York, 1974), p.1
10. J. S. Zabinski and B. J. Tatrchuk, Nucl. Instrum. and Meth., B42 379 (1989).
11. W. Jones, J. M. Thomas, R. K. Thorpe, and M. J. Tricker, Appl. Surf. Sci. 1, 388 (1978).
12. J. A. Sawicki and T, Tyliszczak, Nucl. Instrum. and Meth., 216, 501 (1983).
13. R. P. Feynman, R. B. Leighton, and M. Sands, The Feynman Lectures in Physics, Vol II, (Addison-Wesley, Reading Massachusetts, 1964), p. 7-10.

CAPTIONS

Figure 1: Energy level diagram for ^{57}Co source and ^{57}Fe target showing (a) the emission process for the 14.4 keV gamma ray and (b) the nuclear Zeeman splitting of the nuclear energy levels due to the large internal magnetic fields in a ferromagnetic iron foil. Note: In (b) the energy scale is about 10^{13} smaller than in (a).

Figure 2: Schematic diagram of the experimental apparatus. For Mössbauer studies, the source-target-detector are in a backscatter geometry.

Figure 3: Circuit diagram of the supporting electronics for the chevron microchannel plate assembly electron detector.

Figure 4: Sweep data collected by scanning a highly collimated radiation beam across the target holder assembly containing (a) tantalum and (b) null targets. The contribution from the target holder is clearly seen in (c) after chamber background counts have been removed.

Figure 5: Drawing of the two-element electron lens. The steering of the electrons is performed primarily by the potential gradients established between R_1 and R_2.

Figure 6: The EGUN2c computer program was used to design the electron lens used in CEMS. In (a) the calculated electron trajectories for electrons emitted from a point source at the geometric center of the target are shown. A "plane-wave" of electrons emitted uniformly from the face of the target is shown in (b).

Figure 7: Conversion electron Mössbauer spectra for a 93.55% enriched ^{57}Fe target: (a) Lens in a passive mode possessing no focusing or accelerating properties and (b) Lens in a focusing or active mode.

Figure 1

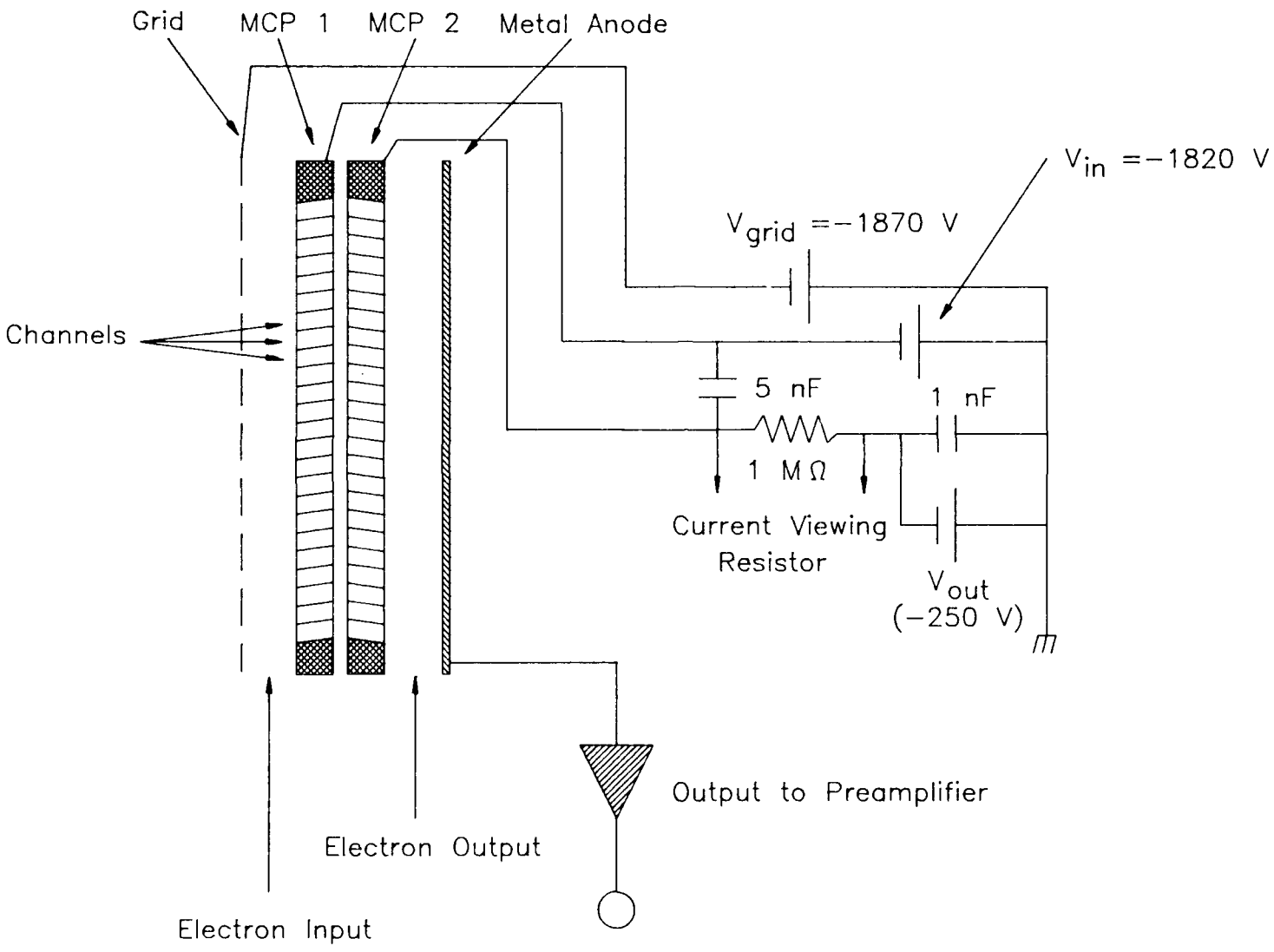

Chevron and Biasing Arrangement

Figure 2

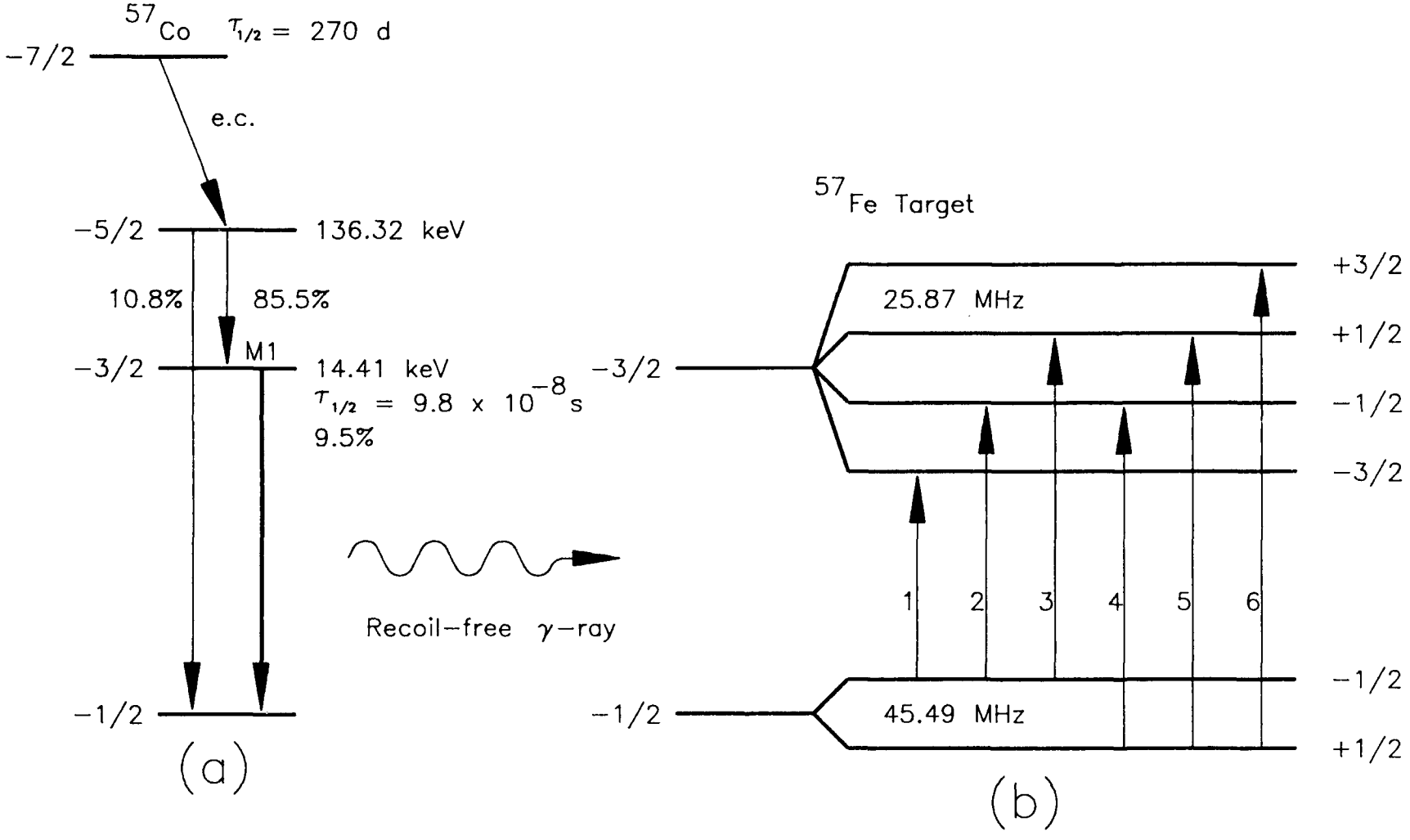
^{57}Co $\tau_{1/2}$ = 270 d
−7/2
e.c.
−5/2
136.32 keV
10.8%
85.5%
M1
−3/2
14.41 keV
$\tau_{1/2}$ = 9.8 x 10^{-8} s
9.5%
−1/2
(a)
Recoil−free γ−ray
^{57}Fe Target
+3/2
25.87 MHz
+1/2
−3/2
−1/2
−3/2
1
2
3
4
5
6
−1/2
−1/2
45.49 MHz
+1/2
(b)

Figure 3

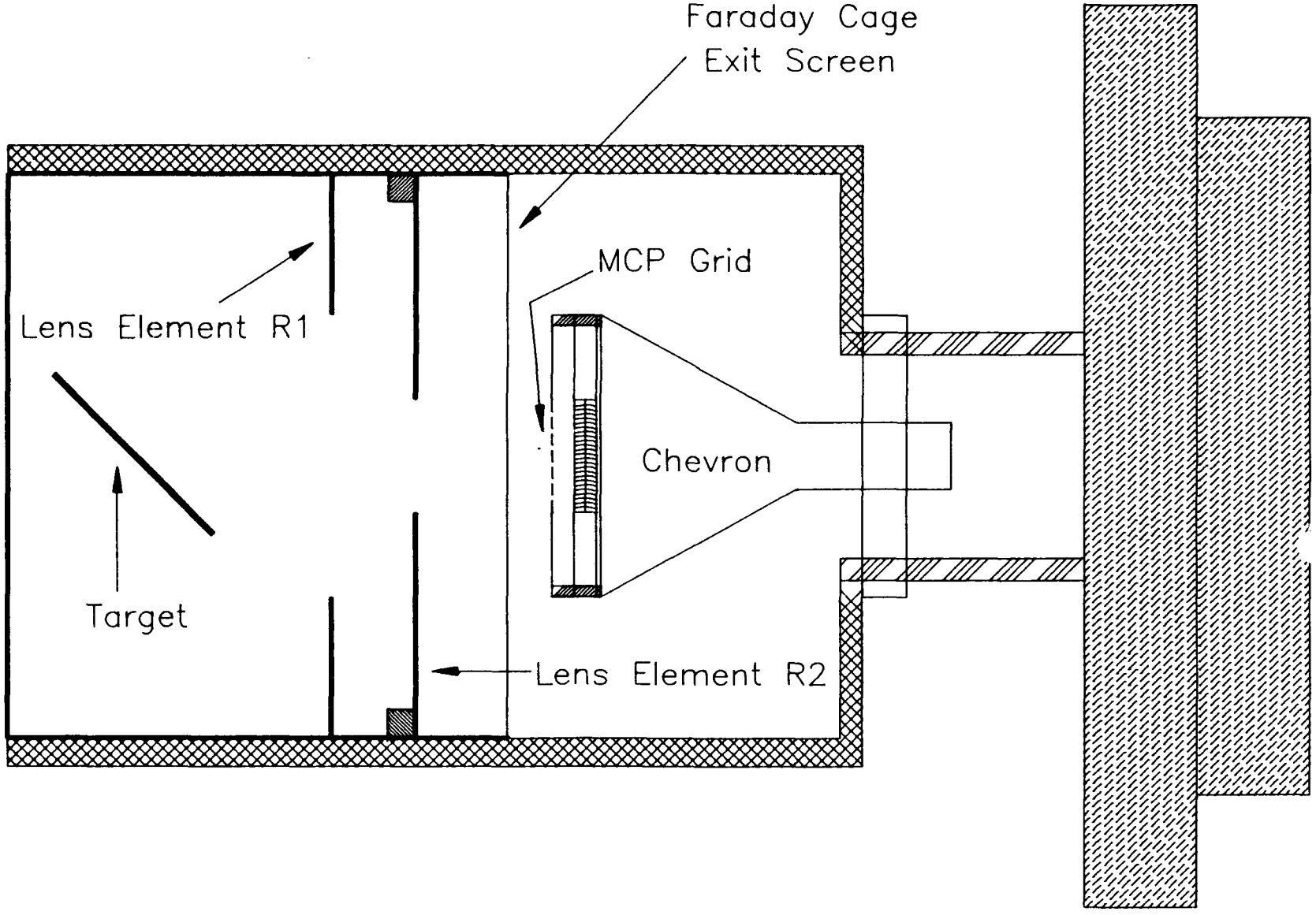
Faraday Cage
Exit Screen
MCP Grid
Lens Element R1
Chevron
Target
Lens Element R2

Figure 4

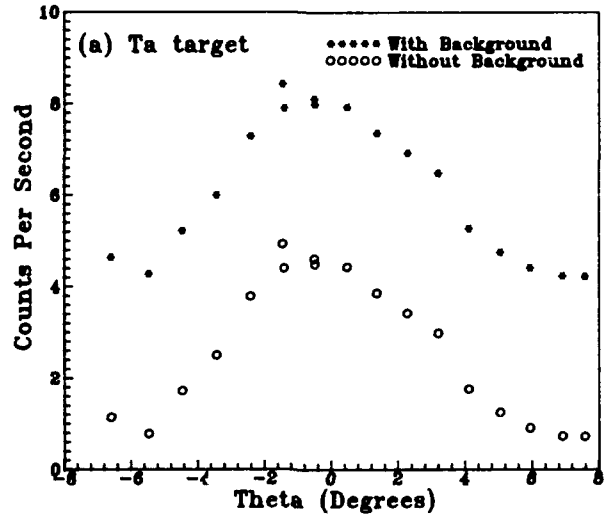
(a) Ta target
••••• With Background
ooooo Without Background
Counts Per Second
Theta (Degrees)

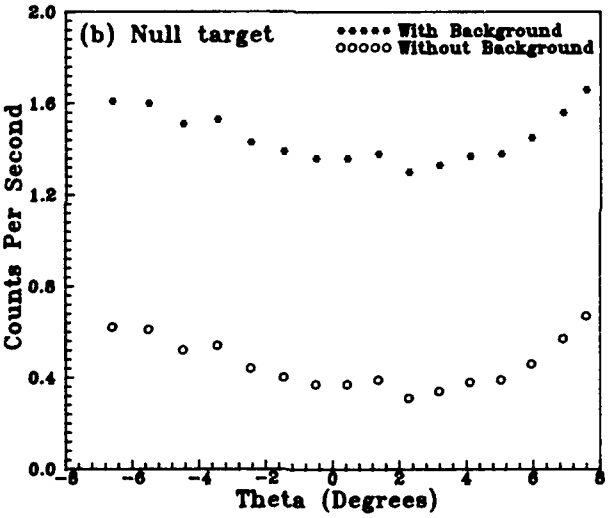
(b) Null target
••••• With Background
ooooo Without Background
Counts Per Second
Theta (Degrees)

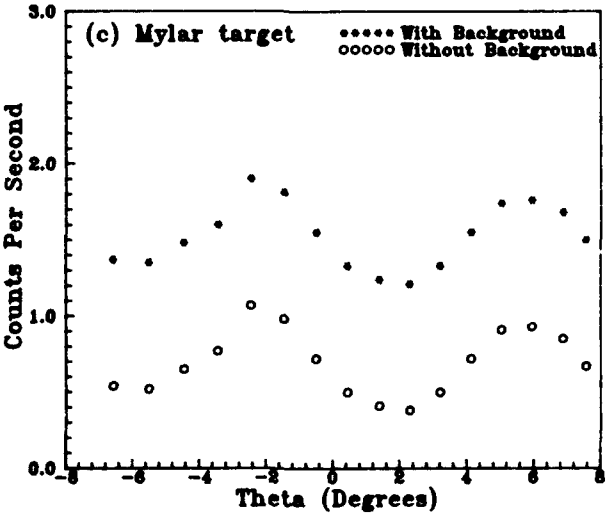
(c) Mylar target
••••• With Background
ooooo Without Background
Counts Per Second
Theta (Degrees)

Figure 5

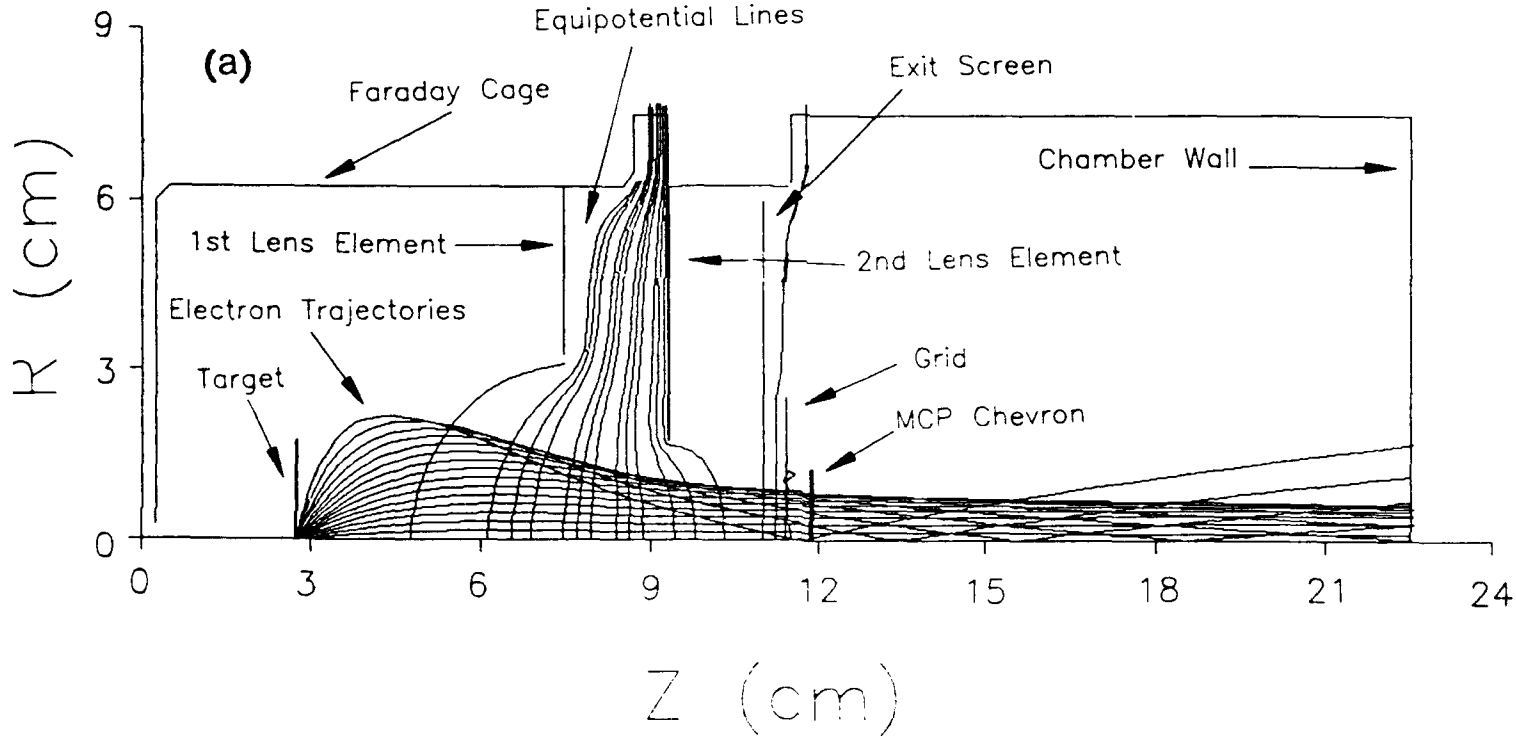
(a)
Equipotential Lines
Faraday Cage
Exit Screen
Chamber Wall
1st Lens Element
2nd Lens Element
Electron Trajectories
Target
Grid
MCP Chevron
R (cm)
Z (cm)
0
3
6
9
12
15
18
21
24

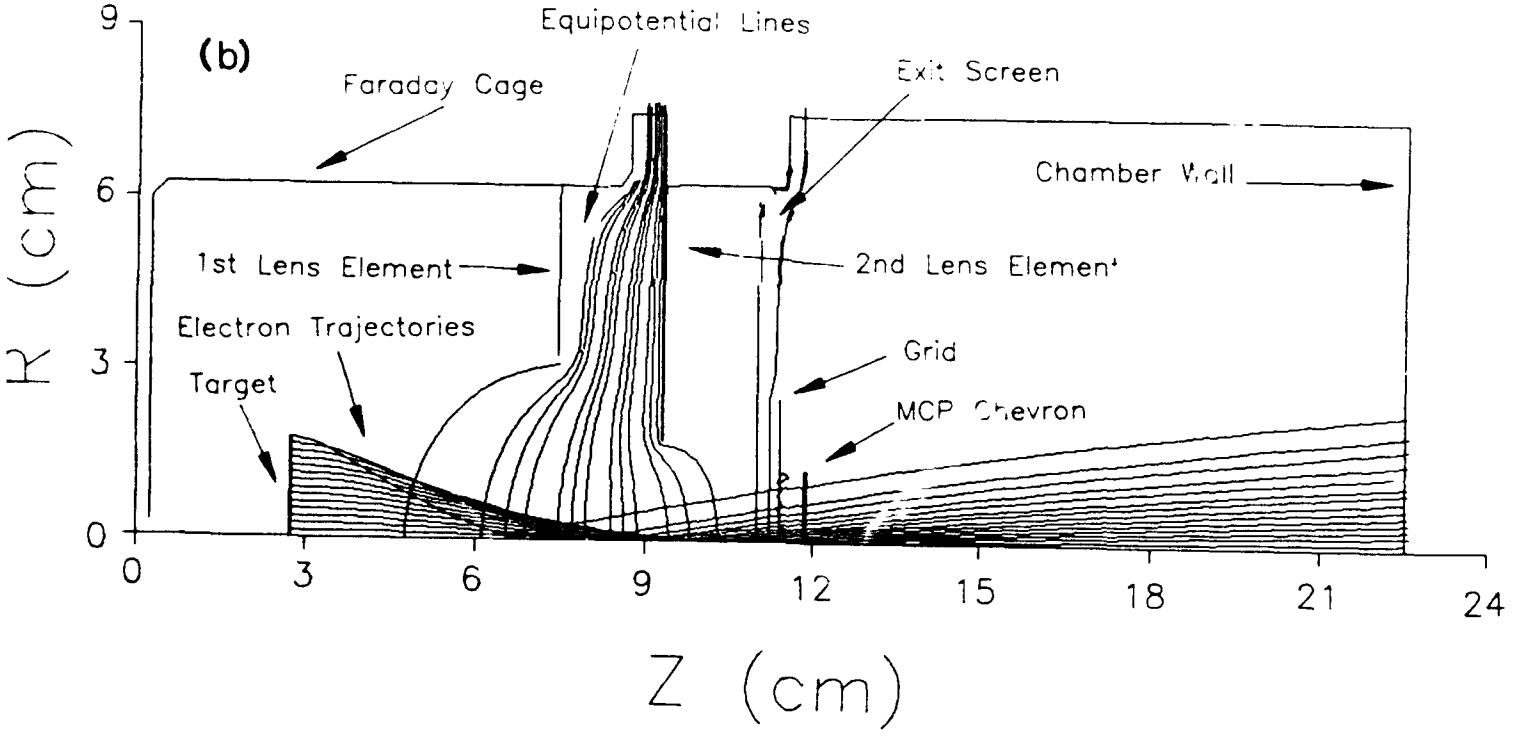
(b)
Equipotential Lines
Faraday Cage
Exit Screen
Chamber Wall
1st Lens Element
2nd Lens Element
Electron Trajectories
Target
Grid
MCP Chevron
R (cm)
Z (cm)
0
3
6
9
12
15
18
21
24

Figure 6

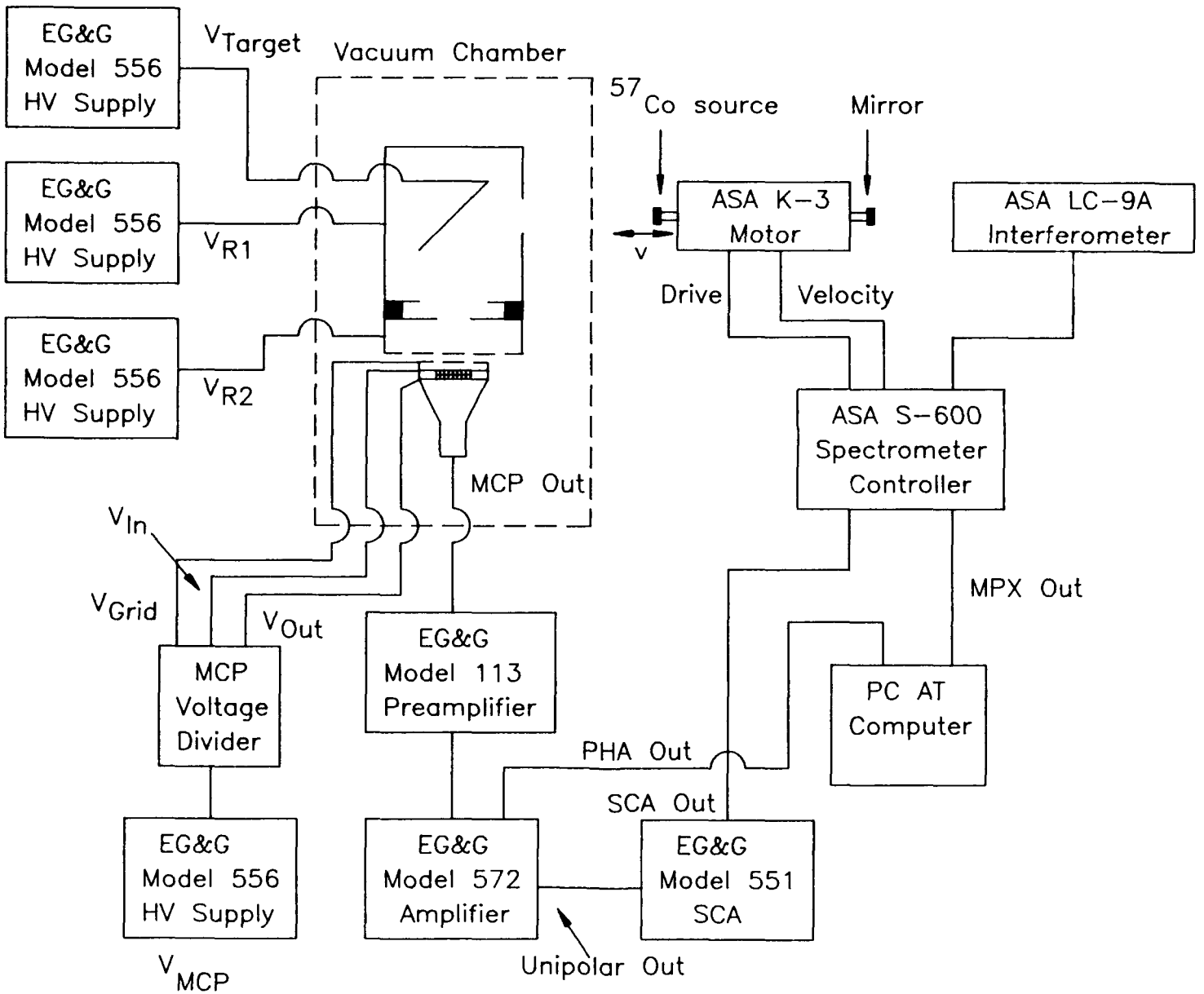
EG&G Model 556 HV Supply
V_{Target}
Vacuum Chamber
^{57}Co source
Mirror
EG&G Model 556 HV Supply
V_{R1}
ASA K-3 Motor
ASA LC-9A Interferometer
v
Drive
Velocity
EG&G Model 556 HV Supply
V_{R2}
ASA S-600 Spectrometer Controller
MCP Out
V_{In}
V_{Grid}
V_{Out}
MPX Out
MCP Voltage Divider
EG&G Model 113 Preamplifier
PC AT Computer
PHA Out
SCA Out
EG&G Model 556 HV Supply
EG&G Model 572 Amplifier
EG&G Model 551 SCA
V_{MCP}
Unipolar Out

Figure 7

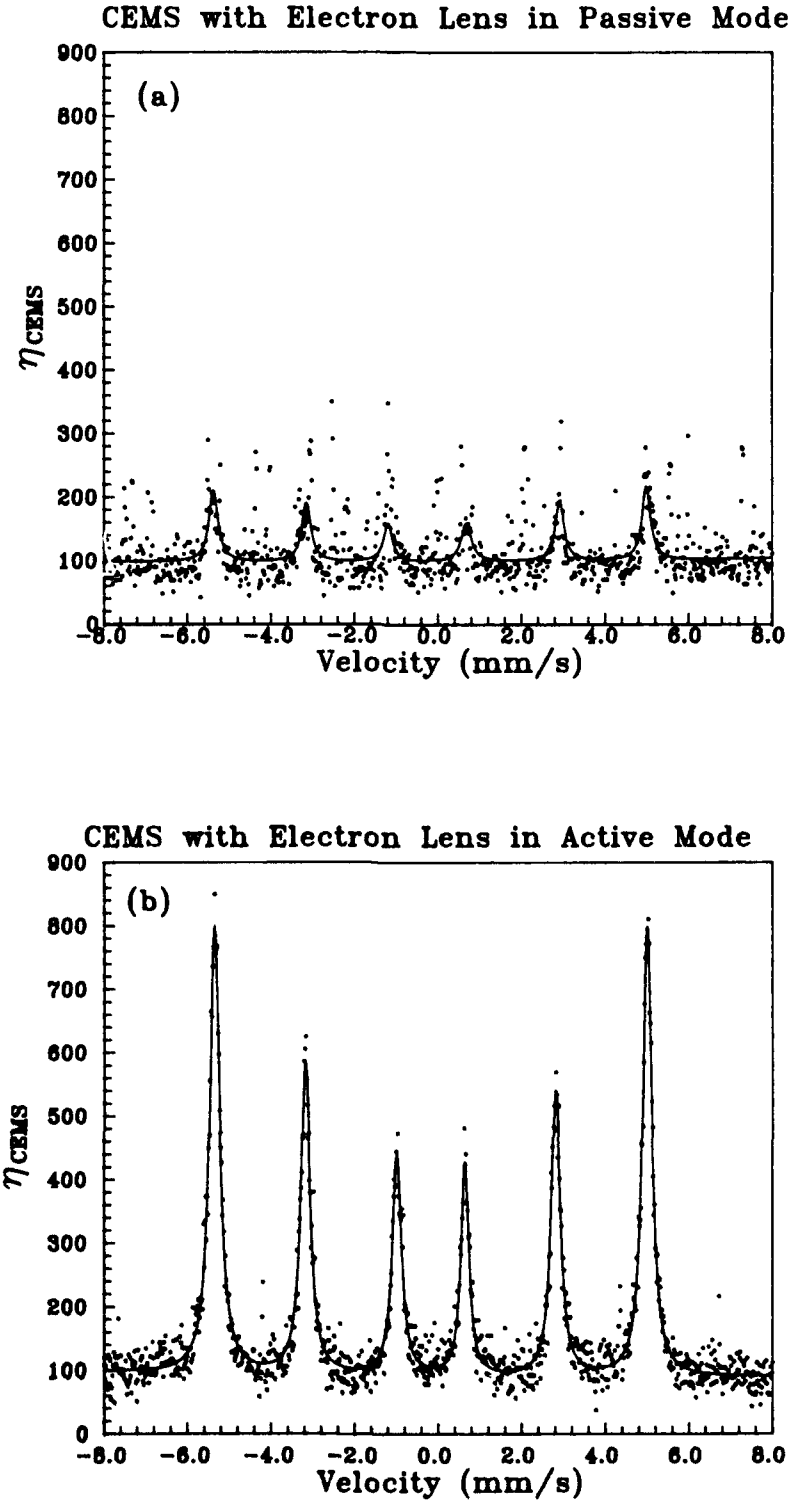
CEMS with Electron Lens in Passive Mode
(a)
η_{CEMS}
900
800
700
600
500
400
300
200
100
0
-8.0
-6.0
-4.0
-2.0
0.0
2.0
4.0
6.0
8.0
Velocity (mm/s)
CEMS with Electron Lens in Active Mode
(b)
η_{CEMS}
900
800
700
600
500
400
300
200
100
0
-8.0
-6.0
-4.0
-2.0
0.0
2.0
4.0
6.0
8.0
Velocity (mm/s)